AD-A162 163 HIGH-TEMPERATURE THERMAL SIMULATOR(U) SCIENCE 1/2
APPLICATIONS INTERNATIONAL CORP MCLEAN VA
J A SIMMONS ET AL. 28 FEB 85 SAIC-84/1715 DNA-TR-84-312
UNCLASSIFIED DNA001-83-C-0224 F/G 20/13 NL

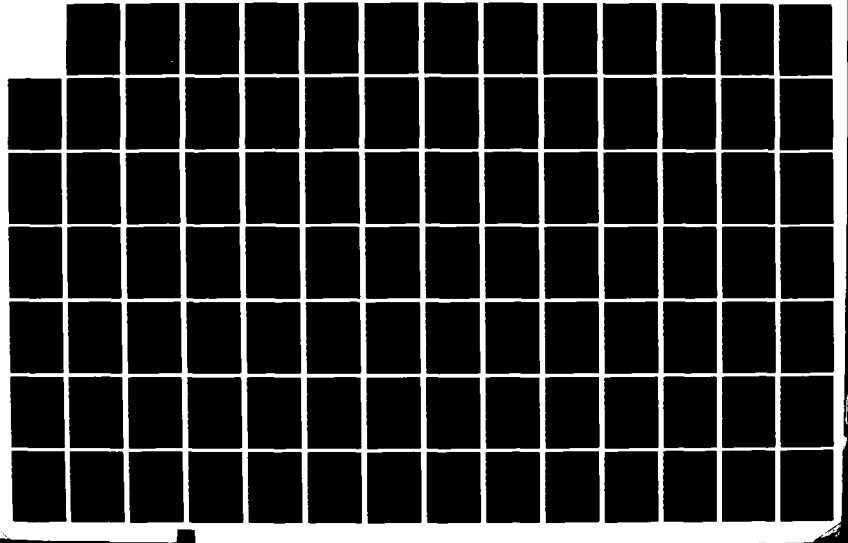

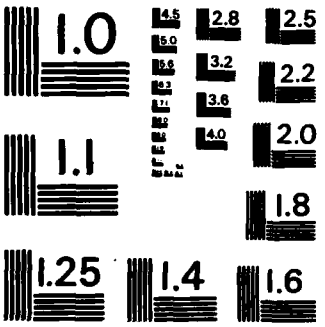

E301844

AD-A162 163

DNA-TR-84-312

HIGH-TEMPERATURE THERMAL SIMULATOR

Phase 1

Science Applications International Corporation
P.O. Drawer 1303
McLean, VA 22102-1303

28 February 1985

Technical Report

CONTRACT No. DNA 001-83-C-0224

Approved for public release;
distribution is unlimited.

THIS WORK WAS SPONSORED BY THE DEFENSE NUCLEAR AGENCY
UNDER RDT&E RMSS CODE B345083466 G55AMXGR00014 H2590D.

Prepared for
Director
DEFENSE NUCLEAR AGENCY
Washington, DC 20305-1000

Destroy this report when it is no longer needed. Do not return to sender.

PLEASE NOTIFY THE DEFENSE NUCLEAR AGENCY, ATTN: STTI, WASHINGTON, DC 20305-1000, IF YOUR ADDRESS IS INCORRECT, IF YOU WISH IT DELETED FROM THE DISTRIBUTION LIST, OR IF THE ADDRESSEE IS NO LONGER EMPLOYED BY YOUR ORGANIZATION.

UNCLASSIFIED
SECURITY CLASSIFICATION OF THIS PAGE

AD-A162 163

REPORT DOCUMENTATION PAGE

Form Approved
OMB No. 0704-0188
Exp. Date: Jun 30, 1986

1a. REPORT SECURITY CLASSIFICATION UNCLASSIFIED	1b. RESTRICTIVE MARKINGS
2a. SECURITY CLASSIFICATION AUTHORITY	3. DISTRIBUTION/AVAILABILITY OF REPORT Approved for public release; distribution is unlimited.
2b. DECLASSIFICATION/DOWNGRADING SCHEDULE N/A since UNCLASSIFIED	
4. PERFORMING ORGANIZATION REPORT NUMBER(S) SAIC-84/1715	5. MONITORING ORGANIZATION REPORT NUMBER(S) DNA-TR-84-312
6a. NAME OF PERFORMING ORGANIZATION Science Applications International Corporation 6b. OFFICE SYMBOL (If applicable)	7a. NAME OF MONITORING ORGANIZATION Director Defense Nuclear Agency
6c. ADDRESS (City, State, and ZIP Code) P.O. Box 1303 McLean, VA 22101	7b. ADDRESS (City, State, and ZIP Code) Washington, DC 20305-1000
8a. NAME OF FUNDING/SPONSORING ORGANIZATION 8b. OFFICE SYMBOL (If applicable)	9. PROCUREMENT INSTRUMENT IDENTIFICATION NUMBER DNA 001-83-C-0224
8c. ADDRESS (City, State, and ZIP Code)	10. SOURCE OF FUNDING NUMBERS PROGRAM ELEMENT NO: 62715H; PROJECT NO: G55AMXG; TASK NO: R; WORK UNIT ACCESSION NO: DH006965

11. TITLE (Include Security Classification)
HIGH-TEMPERATURE THERMAL SIMULATOR
Phase 1

12. PERSONAL AUTHOR(S)
John A. Simmons and Michael D. McDonnell

13a. TYPE OF REPORT	13b. TIME COVERED	14. DATE OF REPORT (Year, Month, Day)	15. PAGE COUNT
Technical	FRO 1 830815 TO 840915	1985, February 28	116

16. SUPPLEMENTARY NOTATION
This work was sponsored by the Defense Nuclear Agency under RDT&E RMSS Code B345083466 G55AMXGR00014 H2590D.

17 COSATI CODES			18. SUBJECT TERMS (Continue on reverse if necessary and identify by block number)
FIELD	GROUP	SUB-GROUP	Thermal Radiation Simulation Metal-Oxygen Combustion Flame Radiation
20	13		
14	2		

19. ABSTRACT (Continue on reverse if necessary and identify by block number)

This report describes the results of a study whose purpose was to determine how and to what extent the radiative output of DNA's Thermal Radiation Simulator (TRS) could be increased. Another purpose was to recommend a program for realizing that higher level of output. This study constituted the first phase of a program whose goals are to create a High Temperature Radiation Simulator (HTRS) producing:

- A radiative flux exceeding 160 cal/cm^2 - sec
- A radiation color temperature effectively greater than 4000^{0}K.

The study consisted of an examination of the pertinent literature and some theoretical analyses. The literature examined dealt primarily with the fundamental features of the combustion of metals with oxygen and the radiative and optical characteristics of metal-oxygen combustion products. The theoretical analyses focused on calculation of tempera-

20. DISTRIBUTION/AVAILABILITY OF ABSTRACT ☐ UNCLASSIFIED/UNLIMITED ☒ SAME AS RPT. ☐ DTIC USERS	21. ABSTRACT SECURITY CLASSIFICATION UNCLASSIFIED
22a. NAME OF RESPONSIBLE INDIVIDUAL Betty L. Fox	22b. TELEPHONE (Include Area Code) (202) 325-7042 22c. OFFICE SYMBOL DNA/STTI

DD FORM 1473, 84 MAR

83 APR edition may be used until exhausted
All other editions are obsolete.

SECURITY CLASSIFICATION OF THIS PAGE
UNCLASSIFIED

19. ABSTRACT (Continued).

ture and energy released from the combustion of various fuels with oxygen, estimation of radiation from a cloud of hot particulates, determination of the approximate relationships between radiative flux and flame height versus flame velocity, particle size and flame thickness, interpretation of combustion data to determine the burning rates of metal particles, and a qualitative analysis of the fluid dynamic and temperature structure of the present TRS's aluminum-oxygen flame. Based on the results, a set of techniques was defined which could lead to the attainment of the HTRS goals. Additionally, a program of experimental research was outlined to explore, develop and implement these techniques.

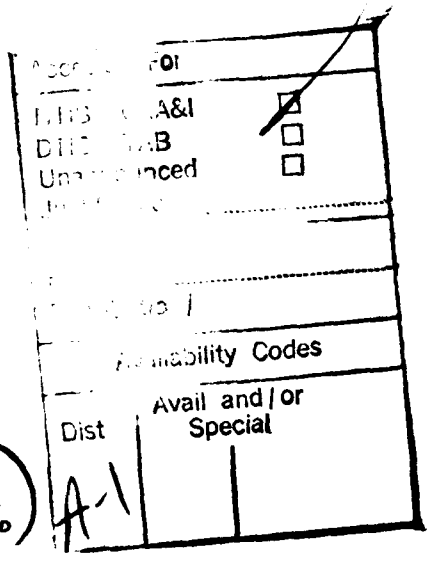

TABLE OF CONTENTS

TABLE OF CONTENTS (Continued)

LIST OF ILLUSTRATIONS

LIST OF ILLUSTRATIONS (Continued)

LIST OF TABLES

SECTION 1
INTRODUCTION

This report describes the results of a study whose purpose was to determine how and to what extent the radiative output of DNA's Thermal Radiation Simulator (TRS) could be increased. Another purpose was to recommend a program for realizing that higher level of output. This study constituted the first phase of a program whose goals are to create a radiation simulator producing:

- A radiative flux exceeding 160 cal/cm^2-sec
- A radiation color temperature effectively greater than 4000^{o}K

A simulator with these levels of performance has been referred to as a High-Temperature Radiation Simulator or HTRS. The study was performed under Contract DNA 001-83-C-0224 during the period of August 1983 through September 1984.

1.1 The Rationale for the Study

The need for an HTRS stems from the requirements that certain military equipment must be capable of surviving the thermal effects of a nuclear burst. At the minimum distances of interest, the incident radiant thermal flux from a nuclear burst on a target may be as high as a few hundred cal/cm^2-sec with a comparable deposition of thermal energy. Moreover, the color temperature of the thermal radiation approximates that of a black body at about 5000 to 6000^{o}K. DNA's current TRS only produces thermal radiation having a color temperature of about 2800^{o}K and maximum flux of about 60 cal/cm^2-sec.

The current TRS utilizes a highly exothermic chemical reaction, the combustion of aluminum with oxygen, as the source of the radiation. The HTRS program continues to emphasize exothermic combustion processes. The reason for this is practicality. Combustion is a means of rapidly releasing a very large amount of energy over a large area from materials which can be stored in a small space. The equipment required to perform

the combustion is relatively inexpensive and is easily transported to different test sites.

1.2 The Scope of the Study

The study consisted of an examination of the pertinent literature and some theoretical analyses. The literature examined dealt primarily with:

- The fundamental features of the combustion of metals with oxygen and
- The radiative and optical characteristics of metal-oxygen combustion products.

The theoretical analyses focused on:

- Calculation of temperature and energy released from the combustion of various fuels with oxygen and fluorine oxidizers,
- Estimation of radiation from a cloud of hot particulates,
- Determination of the approximate relationships between radiative flux and flame height versus flame velocity, particle size and flame thickness,
- Interpretation of combustion data to determine the burning rates of metal particles, and
- A qualitative analysis of the fluid dynamic and temperature structure of the present TRS's aluminum-oxygen flame.

Based on these results, a set of techniques was defined, which could lead to the attainment of the HTRS goals. Additionally, a program of experimental research was outlined to explore, develop and implement these techniques.

1.3 Principal Conclusions

Theoretical calculations of chemical equilibria show that the combustion of aluminum, zirconium, beryllium and titanium with oxygen can produce flames which will equal or exceed the HTRS goals. The theoretical flame temperature of a stoichiometric mixture of aluminum and oxygen is 3977°K and the heat available in the combustion products above 3300°K (the radiant flux from a black-body at this temperature is 160 cal/cm^2-sec) is 4956 cal/g-Al. The corresponding values for zirconium are 4279°K and 2036 cal/g-Zr. The study emphasized only the combustion of aluminum and zirconium because beryllium and its oxide are toxic and the performance of titanium is expected to be similar to but not as good as zirconium.

Measurements of the color temperature and the output of visible light from commercial photoflash bulbs further support the conclusion that the HTRS goals can be met with aluminum and zirconium. The radiation produced by these bulbs is similar to that of a black body with an effective color temperature of about 4100 and 4400°K, respectively. The energy radiated at these temperatures is approximately 3000 and 1600 cal/g of metal, respectively. Additional radiation is produced as the metal oxide combustion products cool to lower temperatures.

Aluminum powder burns in oxygen by a vapor diffusion process in which the temperature of the aluminum particle does not exceed its boiling temperature, 2766°K. Nearly all of the energy for radiation is released only when the oxide, $Al_2O_3(l)$, condenses from the vapor phase.

Zirconium powder burns in oxygen mainly by the reaction of oxygen at the surface of the particle. The temperature of the burning particle is limited by the boiling temperature of the oxide, 4279°K (calculated) or 4300°K (measured for a single particle). About one-half the energy for radiation is generated in the burning particle; the other half is generated by the condensation of oxide, $ZrO_2(l)$, from the vapor phase.

Condensation from the vapor phase tends to produce particles of oxide usually characterized as a smoke, i.e. particles about one micron or less in diameter. Experimentally, smoke-size particles are observed in burned photoflash bulbs and in the residues from single particles burning in a cold oxygen atmosphere. The optical mean free path in these smokes is predicted to be very short, only a few centimeters.

Calculations of the radiation from a metal-oxygen flame, using a one-dimensional model, show that radiation can develop very steep temperature gradients at the periphery of the flame. The steepness of the gradients depends inversely on the optical mean free path. Therefore the maintenance of high radiative flux at the surface of the flame is favored by relatively large-size particulates which allow a long optical mean free path. Consequently, in order to obtain a flame that is tall and has a high level of radiant flux, the particulates in the flame should be relatively large, larger than is characteristic of "smokes", provided the thickness of the flame exceeds the optical mean free path. The adverse effects of smoke-size particulates can be compensated for by increasing the velocity of the flame and the turbulent mixing in the flame. The latter tends to reduce the temperature gradients.

The periphery of the flame can be cooled by non-radiative processes such as mixing with cold ambient air. The same one-dimensional calculations of radiation also showed that such cooling will markedly reduce the level of radiant flux.

The flame of the present (in 1983) TRS is believed to be very "smoky" and therefore it has a very short optical mean free path. Most of its radiation occurs from a vertical segment of the flame which is about four meters high and which can be characterized, fluid dynamically, as a turbulent jet. Between this segment and the nozzle of the TRS is a short segment of rapid, pressure-driven expansion. Significant entrainment of cold air is expected in these segments and hence the periphery of the flame consists of an optically thick sheath of relatively cold oxide particles. This blocks-out the radiation from the hotter core of the flame, and is believed to be the main reason why the present TRS cannot

achieve its potentially high level of radiative performance. Mixing with ambient air must be minimized in an HTRS.

The emissivity of aluminum oxide, and hence the radiation from aluminum-oxygen flames, may be sensitive to impurities and the presence of free metal. Additionally the presence of small amounts of moisture, carbon dioxide and nitrogen in the combustion gases appears to affect the characteristics of aluminum-aluminum oxide surfaces. These materials could have a beneficial effect on the emissivity of aluminum oxide as well.

1.4 Recommended Development of Techniques to Enhance Radiative Performance

The findings of this study suggest six techniques which have the potential of achieving the HTRS goals.

(1) Cold Gas Envelope. The TRS flame would be encircled by a stream of air or oxygen whose velocity matches the velocity of the flame. This will minimize mixing with cold air and result in a thinner sheath of cold particles. The height to which such protection of the flame can be extended depends on the width of the envelope.

(2) Hot Gas Envelope. A fuel gas such as propane or cyanogen would be burned in the envelope to heat it to between 2000 and 4500°K. This can virtually eliminate non-radiative losses of heat from the flame.

(3) Zirconium Powder Fuel. Zirconium powder rather than aluminum would be used as the fuel. The resulting flame should have a color temperature of close to 4400°K and a correspondingly high level of radiative flux. A cold or a hot gas envelope probably would be required as well.

(4) Fuel Rich Mixtures. Mixtures which have less than the stoichiometric amount of oxygen would be burned in the flame.

This technique may result in an increased emissivity of the metal oxide particles. Also, it is a technique that might be successful in controlling the optical mean free path of zirconium-oxygen flames.

(5) Additives. Iron or nickel, which form black oxides, and/or water, nitrogen or carbon dioxide would be added in small quantities to the fuel. These could increase the emissivity of the particles in the flame.

(6) Powder Particle Size. A metal powder with a range of sizes would be burned. For the aluminum TRS, in particular, this could allow the growth of larger particles of oxide, which, in turn, would improve the optical properties of the flame.

As a first step, it is recommended that the effectiveness of these techniques be explored with a laboratory-scale burner. Powders of aluminum and zirconium would be burned at rates between 20 and 200 g/sec with gaseous oxygen. The radiative properties of the flames produced would be studied with calorimeters to measure flux and spectrometers to measure color temperature. Flux and color temperature would be determined as a function of the width, velocity and temperature of a gaseous envelope, and of the metal particle size, stoichiometry, flow velocity, thickness of the flame and additives.

With the data obtained, existing TRS units may be modified to improve the characteristics of their radiative output. Also the data are expected to suggest new HTRS designs which then would be tested in prototype versions.

SECTION 2
THE HTRS GOALS AND PROGRAM

There is a growing and pressing need to obtain high-fidelity simulation of the nuclear environment for weapons testing. The thermal pulse from a nuclear explosion is a key part of that environment, and its "correct" simulation is essential. New tests (e.g. DNA's series of high-explosive shots) and new facilities (e.g. the Army's proposed Large Blast Thermal Simulator) are being designed with great pains taken to provide for simulation of thermal effects.

Towards this purpose Science Applications International Corporation, under the sponsorship of DNA, has developed thermal simulation techniques based on the combustion of aluminum with oxygen as the source of thermal radiation. These techniques have evolved over a period of approximately nine years, culminating in the current Thermal Radiation Simulator, or TRS. This device burns a partially premixed, two-inch jet of aluminum powder and liquid oxygen.

Unfortunately the simulation provided by the TRS is not as good as desired. Its spectral temperature is only about 2800°K verses 5000 to 6000°K for a nuclear fireball. Additionally the maximum radiative thermal flux from the surface of the aluminum-oxygen jet flame is only about 60 cal/cm^2-sec. Testing of many new weapon systems requires 200 cal/cm^2-sec of thermal flux delivered on a target. On the other hand the present TRS has important advantages, including the ability to irradiate large targets (e.g. 20 feet wide by 16 feet high) and to be used both in the field and at fixed locations.

In August 1983, DNA launched a new program to correct the deficiencies in performance while retaining the existing advantages. A new type of TRS, a High-Temperature Thermal Radiation Simulator, HTRS, is to be developed. This device has the following performance goals:

- A color temperature exceeding 4000°K
- A flame-surface flux exceeding 160 cal/cm^2-sec
- A high level of reliability
- Retention and utilization of a maximum of the TRS's hardware

This report describes the results of the first phase of this program. The objectives of this first phase were:

- Understand the mechanism of the present TRS
- Understand the combustion mechanisms and thermal radiation potential of fuels and oxidizers for HTRS
- Recommend modifications of the TRS which will reach the HTRS performance goals
- Plan a development program for the HTRS.

The scope of this phase included a literature search for data on the combustion mechanism of potential HTRS fuels and on the optical properties of the combustion products, and theoretical calculations to predict the performance of selected HTRS fuels. One key output of this phase is the considerable evidence indicating the potential of combustion of metal powder fuels with oxygen for meeting the HTRS performance goals. Other key outputs are the conceptualization of techniques for realizing this potential and the formulation of an experimental approach for testing the techniques at a small scale. It is believed that these experiments will constitute a fruitful second phase of the HTRS program.

SECTION 3
CHEMISTRY OF RADIATIVE FLAMES

This section presents a discussion of the thermodynamics and chemistry of combustion systems. Based on the evidence available it is concluded that metal powders can burn with oxygen at high flame temperatures and a major fraction of the combustion energy can be released at temperatures near to or exceeding 4000°K. Moreover, the flames contain condensed-phase combustion products which can serve as a source of continuum radiation at the flame temperature. Although they burn by quite different mechanisms, aluminum and zirconium appear to have the best potentials as fuels for a HTRS.

3.1 Fundamental Criteria for a HTRS

At the beginning of this phase of work, it was immediately recognized that to achieve the HTRS performance goals, a combustion system (a given combination of fuel and oxidizer) must:

1) Have a high flame temperature; this is attained through highly exothermic and stable combustion products

2) Have a high emissivity; this is provided by particulate combustion products

3) Have a high heat capacity at a high temperature; this is provided by condensation of liquid or solid combustion products from their vapors.

Additional requirements include highly reliable hardware and a minimum of fire, explosion, and toxicity hazards. Also the HTRS should have a low operational cost and utilize the existing TRS hardware a to maximum extent.

Because of their position in the Periodic Table of the elements, elemental oxygen and flourine, and certain compounds containing these elements, are generally recognized as the most energetic of all oxidizing materials. Indeed, liquid oxygen, nitrogen oxides and perchlorates have received continuing use as oxidizers in common rocket propellant systems. In that application, the ability to generate a large amount of energy per unit weight of material is an important selection criteria. This criteria is consistent with that of generating high combustion temperatures. On the other hand, high-energy fluorine-containing oxidizers presently are little used in rocket propellant systems primarily because of their general instability and corrosive nature. Nevertheless, the combustion of fluorine with hydrogen and lithium, especially, are popularly known as combustion systems with the highest flame temperature.(1) However, the combustion products, hydrogen fluoride and lithium fluoride are gases above 2000°K. In fact all fluorides, that might be the basis of a combustion system for attaining high flame temperatures, are gases at 3000°K or lower.(2) Hence it appears that fluorine combustion systems cannot meet the last two criteria listed above.

However, it was thought that fluorine-oxidized systems could be made to satisfy those criteria by including a source of carbon, which in the absence of oxygen would condense into an amorphous solid and serve as a source of continuum radiation. The flame temperature and heat capacity of several such combustion systems were calculated with the NASA equilibrium thermochemical computer program.(3) The combustion systems considered included:

- Lithium and tetrafluoroethylene
- Aluminum and tetrafluoroethylene
- Boron and tetrafluoroethylene
- Magnesium and tetrafluoroethylene.

The equilibrium composition of formulations, which were stoichiometric to the metal fluoride, had solid carbon in the combustion products, but the flame temperature was less than 3650°K. Also the heat content above 3300°K (theoretical blockbody radiation at this temperature is 160 cal/cm^2-sec) was low (e.g. 2460 cal/g for aluminum) compared with oxygen combustion systems (see below). Furthermore the results of the calculations indicated that the sublimation of carbon together with the endothermic dissociation of the metal fluorides limited the flame temperature of these types of systems to relatively low levels.

The rationale for the use of tetrafluoroethylene was that it simultaneously provides carbon and fluorine. Clearly a more energetic fluorine oxidizer (e.g. elemental fluorine) could be used as the oxidizer, but then the combustion system would require a third component, a source of carbon. Although a somewhat higher flame temperature might be obtained by using fluorine, it was reasoned that the flame temperature would still be limited to a level less than 3700°K by the endothermic sublimation of carbon.

Therefore combustion systems containing fluorine were not given further consideration. This decision also is supported by practical considerations for the TRS. Fluorine and all "high-energy" fluorine compounds (e.g. ClF_3, NF_3, etc.) are toxic and corrosive, and are therefore difficult to handle.

In contrast, combustion systems using oxygen oxidizers do meet the three basic selection criteria. Many metal powders burn easily in oxygen with flame temperatures ranging from 3300 to 4300°K and yield condensed-phase combustion products. The metals giving the best theoretical performance are those in the Periodic Table located in the first two rows of groups II A and III A and group IV B. These same periodic groups of metals also are known to be high-energy fuels for rocket propellants. The flame temperature of the combustion of these metal powders with oxygen is the boiling temperature of the metal oxide, which in a TRS will be the normal atmospheric boiling temperature.(5) A major fraction of the metal's combustion heat is stored in its partially

vaporized oxide. As radiative cooling proceeds, the oxide vapors condense (or recondense) with a large exothermic heat effect.

With these considerations in mind it was concluded to focus the research in Phase I on combustion systems consisting of a metal powder and oxygen.

3.2 Chemical Thermodynamics of Oxygen-Metal Powder Combustion

This section describes the results of a thermochemical analysis of oxygen metal powder combustion systems. The analysis shows, based on thermodynamics alone, that aluminum, zirconium, titanium, and beryllium are fuels having the potential of meeting the HTRS goals. However, beryllium and its oxide are toxic and is therefore unsuitable for most expected applications of a HTRS.

Table 1 lists the metal fuels, whose combustion with oxygen were evaluated theoretically. The fuel-oxygen mixtures, which yield a high combustion temperature, also produce a condensed-phase combustion product. The table includes several pertinent properties of the fuels and their oxides. The first of these is the boiling temperature of the metal. As discussed in subsequent subsections, fuels with boiling temperatures well below the boiling temperature of their oxide will burn with vapor diffusion flames (e.g., Mg and Al). When the reverse is true, combustion occurs via direct oxidation on the surface of the fuel particle (e.g., Zr). The third item listed is the boiling temperature of the oxide. This also is the upper limit of the combustion temperature because vaporization of the oxide is highly endothermic especially since most metal oxides dissociate to gaseous sub-oxides and atoms in the vapor. The next two items, the heat of combustion of the metal and the ratio of this heat to the sensible heat of the oxide at a minimum desired temperature, in this case 3300°K, are indicative of the energy potentially available for conversion into radiant power. The temperature of 3300°K was selected as a base for comparison because a blackbody at that temperature produces a radiant heat flux of 160 cal/cm^2-sec.

Table 1. Some combustion - related properties of metals and their oxides

PERIODIC GROUP AND METAL		T_B OF METAL (^oK)	FORMULA	PROPERTIES OF THE OXIDE T_B (^oK)	HEAT OF COMBUSTION (CAL/G OF METAL)	QUOTIENT OF HEAT OF COMBUSTION AND SENSIBLE HEAT OF OXIDE AT 3300^oK
GROUP IA:	Na	1177	Na_2O	2223	2392	-
GROUP IIA:	Be	2757	BeO	4204	15877	2.64
	Mg	1378	MgO	3432	5909	2.52
	Ca	1767	CaO	3914	3787	2.54
	Ba	2122	BaO	3361	954	2.25
GROUP IIIA:	B	3931	B_2O_3	2300	14031	-
	Al	2766	Al_2O_3	3977	7419	3.25
GROUP IVA:	C_2N_2	-	CO(g)	-	2435	1.69 (70% C_2N_2 with O_2)
	Si	3492	SiO_2	3180	7681	-
GROUP IB:	Cu	2573	CuO	460	592	-
GROUP IIB:	Zn	1180	ZnO	2500	1273	-
GROUP IIIB:	Y	2773	Y_2O_3	4570	2550	3.3

T_B Boiling Temperature

Data From Reference 3 and 4 and Brewer, L., "The Thermodynamic Properties of the Oxides and their Vaporization Processes," Chem Rev. 52, 1 (1953); National Bureau of Standards Technical Notes 270-3, 270-4, 270-5, 270-6, 270-7 and 270-8.

Table 1. Some combustion - related properties of metals and their oxides (continued)

PERIODIC GROUP AND METAL		T_B OF METAL (^oK)	FORMULA	PROPERTIES OF THE OXIDE T_B (^oK)	HEAT OF COMBUSTION (CAL/G OF METAL)	QUOTIENT OF HEAT OF COMBUSTION AND SENSIBLE HEAT OF OXIDE AT 3300^oK
RARE EARTHS:	La	2073	La_2O_3	4470	3086	3.1
ACTINIDES:	Th	3000	ThO_2	4670	1263	3.7
GROUP IVB:	Ti	3591	Ti_3O_5	4004		
			Ti_4O_7			
			TiO_2		4399	3.07
	Zr	4777	ZrO_2	4279	2875	3.43
GROUP VB:	V	3273	VO	3300	2026	1.73
GROUP VIB:	Cr	2473	Cr_2O_3	3300	2710	-
	Mo	4919	MoO_3	1530	1171	-
GROUP VIIB:	Mn	2173	MnO	3400	1676	-
GROUP VIII:	Fe	3145	FeO	3404	1164	1.26

T_B Boiling Temperature

Data From Reference 4 and Brewer, L., "The Thermodynamic Properties of the Oxides and their Vaporization Processes," Chem. Rev. 52, 1 (1953); National Bureau of Standards Technical Notes 270-3, 270-4, 270-5, 270-6, 270-7 and 270-8.

Table 1 includes the metals of Groups II A, III A, and IV B. Cyanogen, a gas, also is included for comparative purposes and because its combustion with oxygen yields one of the highest flame temperatures known for any combustion system, 4854°K. Unfortunately the mixture of cyanogen and oxygen which burns at this temperature does not yield a condensed-phase combustion product. A mixture containing 70 percent cyanogen does produce condensed carbon (soot), but the flame temperature of this mixture is only 3550°K.

The table indicates that there are a large number of metals with heats of combustion exceeding 2000 cal/g, but a relatively few whose oxide does not boil or dissociate at temperatures below 4000°K. These latter include Zirconium beryllium, Yittrium, Thorium, and Lanthanum. Aluminum and calcium are two metals whose oxides boil above 3900°K, which is close to the goal of 4000°K. Of the remaining metals, the oxides of most boil below 3000°K. These include boron, the Group VIII metals (with the exception of iron), Groups I B and II B (as represented by copper and zinc) the alkali metals (as represented by sodium) and tungsten. The oxides of a few other metals have intermediate boiling temperatures, 3000 to 3800°K. These include all the alkaline earths (except calcuim), chromium, manganese and iron.

Zirconium has the highest ratio of the heat of combustion to the sensible heat of the oxide, 4.17, and this together with the high boiling point of its oxide, 4279°K, indicates a high potential for meeting the HTRS goals. Other metal oxides with a high boiling temperature and a heat ratio above three include the oxides of aluminum, beryllium, titanium, yittrium, lanthanum, and thorium. Calcium's heat ratio is less than three.

Yittrium and lanthanum are rare earths and their use in large quantities as fuels would be very costy. Thorium is radioactive as well as costly, and it too is not desirable for an HTRS. Calcium is a very soft metal and is not available as a powder. Moreover, calcium corrodes rapidly in air and therefore would be difficult to handle. Hence, calcium too, appears to be an unsuitable fuel for an HTRS at this time. Finally, beryllium and its oxide are toxic, and hence this metal, too, would be

unsuitable for HTRS applications. However there could be applications in the future in which the combustion products would be contained, and then beryllium would be a suitable fuel.

With these considerations the selection of fuels for an HTRS narrows down to aluminum, beryllium, titanium and zirconium. The thermodynamic potential of these fuels therefore was examined further using the above-mentioned NASA computer program for chemical equilibria. (3) The program was used to compute the flame temperature, the heat content of the combustion products as a function of temperature, and other properties of the equilibrium combustion of these metals with oxygen. Table 2 summarizes the computed results, listing the flame temperature and the combustion heat available above 3300°K. Plots of the heat content verses temperature for burned stochiometric and oxygen-rich mixtures containing aluminum, beryllium, zirconium and titanium are presented in Figures 1, 2, 3, and 4, respectively.

The results in these exhibits confirm and enlarge those presented in Table 1. The highest temperature, 4279°K, is reached by burning a stoichiometric mixture of zirconium and oxygen, and the heat available above 3300°K is 2036 cal/g of zirconium, which is 71 percent of its heat of combustion. As predicted by Table 1 and demonstrated in Table 2 this is the the highest percentage of combustion heat for all of the fuels listed.

Burning beryllium metal is predicted to yield the next highest flame temperature, 4204°K, and as also shown in Table 2, 9403 cal/gm of metal, or 59 percent of the combustion heat, is available above 3300°K. Beryllium fuel yields the most heat per unit weight of metal.

Aluminum fuel has the second highest yield of available heat per unit weight, 4956 cal/g for a stoichiometric mixture with oxygen. The flame temperature, 3977°K, is only slightly less than the HTRS goal. Combustion of titanium with oxygen also should yield a flame temperature close to the HTRS goal. However, the yield of heat above 3300°K is less than that of aluminum.

Table 2. Thermodynamics of metal fuels burned with oxygen stoichiometric to the metal oxide

METAL	BOILING POINT (°K)	OXIDE	BOILING POINT (°K)	HEAT AVAILABLE ABOVE 3300° CAL/G METAL	% OF METAL COMBUSTION HEAT
Al	2766	Al_2O_3	3977	4956	67
Be	2760	BeO	4204	9403	59
Ti	3591	Ti_3O_5	4000	2700	66
Zr	4777	ZrO_2	4279	2036	71

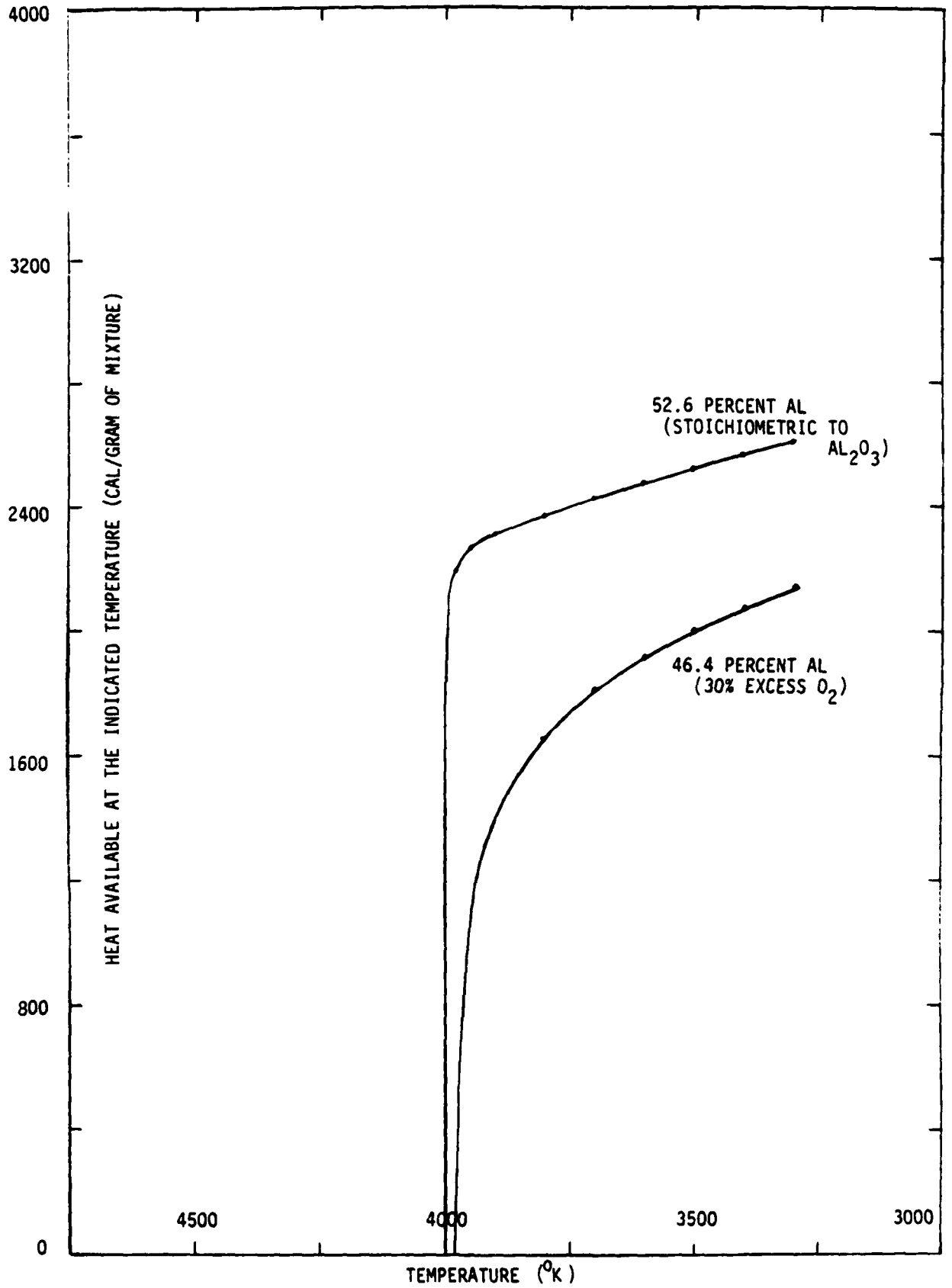

Figure 1. Heat content of aluminum-oxygen combustion products at temperatures below the adiabatic flame temperature

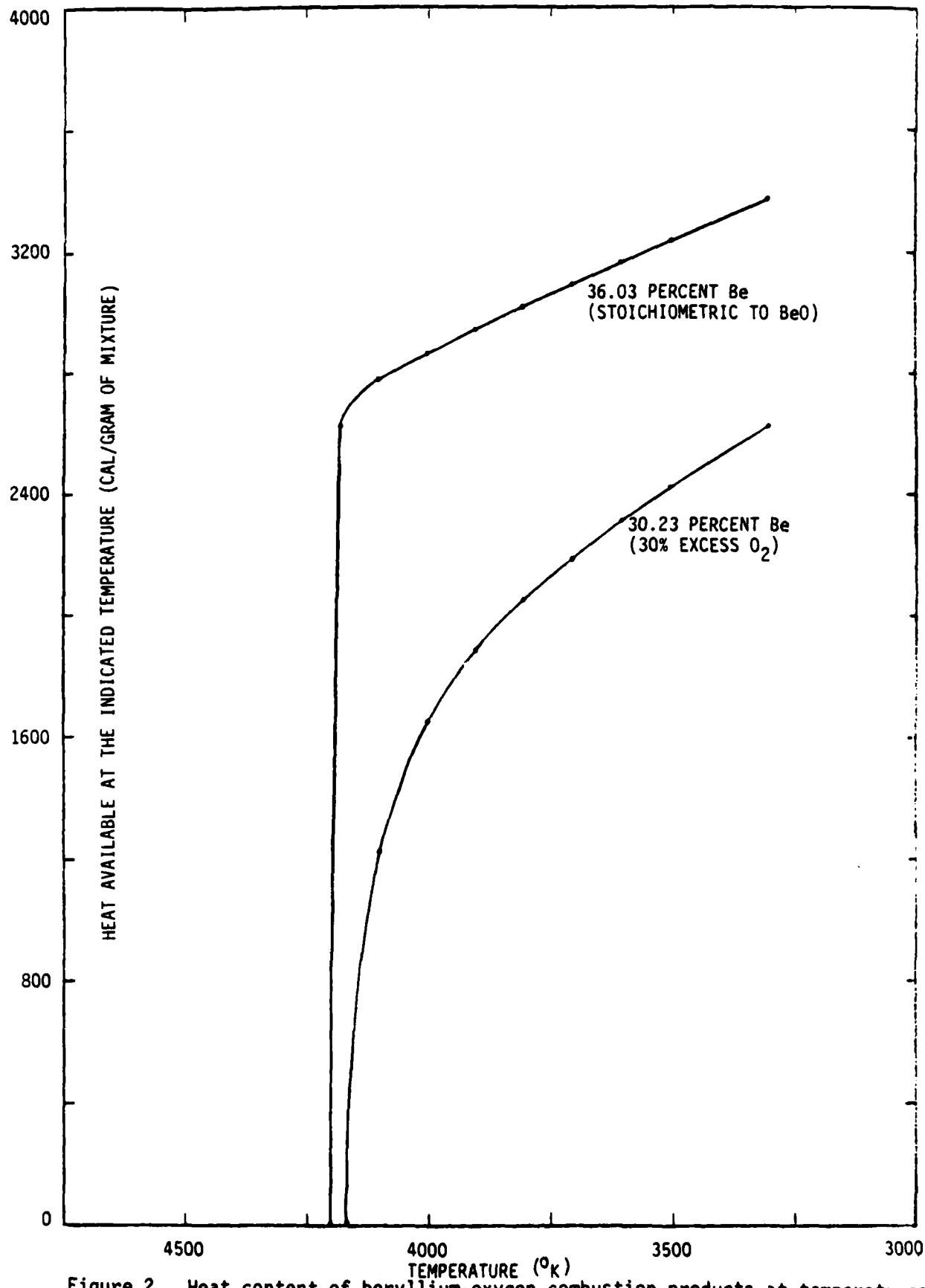

Figure 2. Heat content of beryllium-oxygen combustion products at temperatures below the adiabatic flame temperature

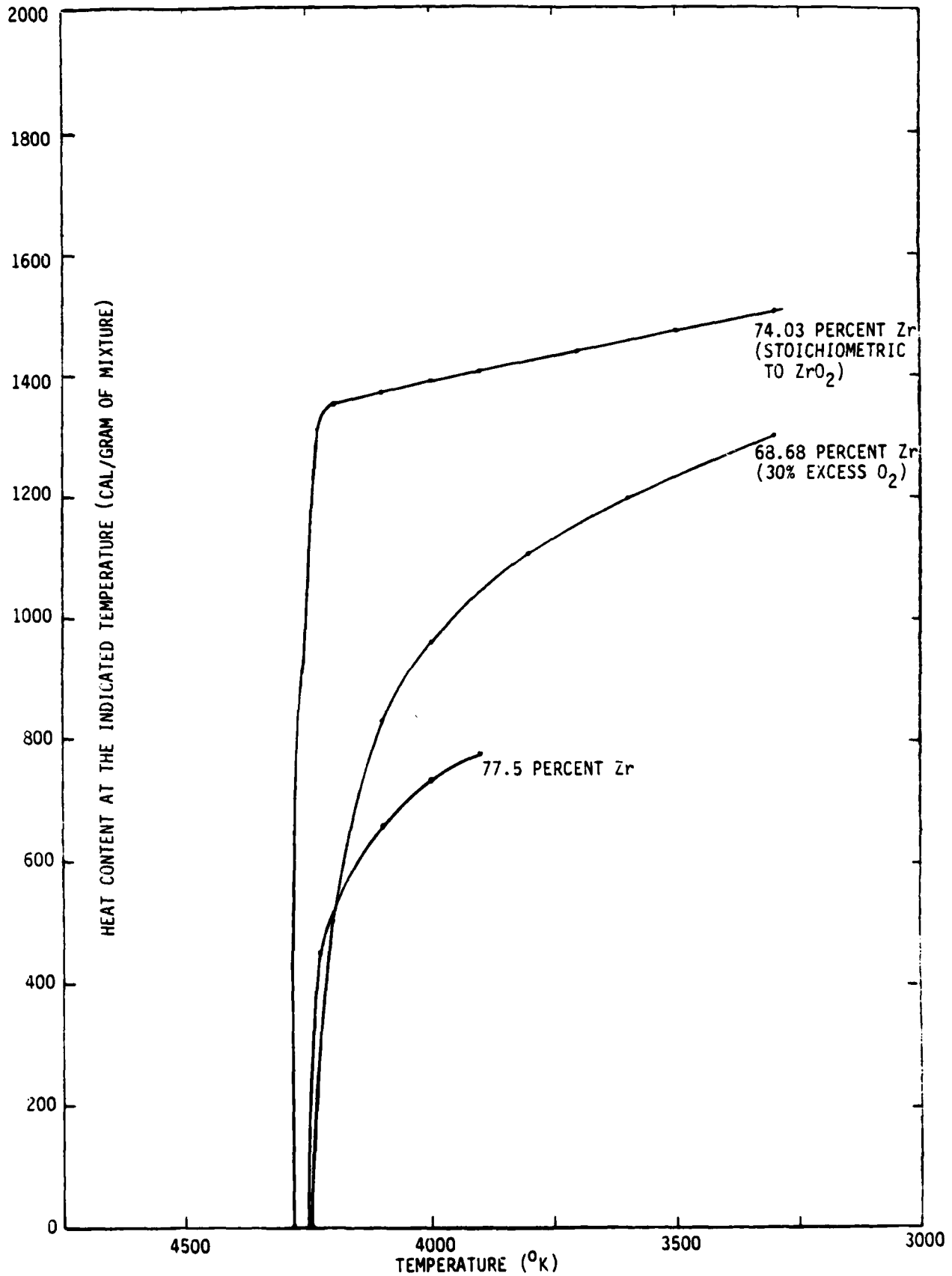

Figure 3. Heat content of zirconium-oxygen combustion products at temperatures below the adiabatic flame temperature.

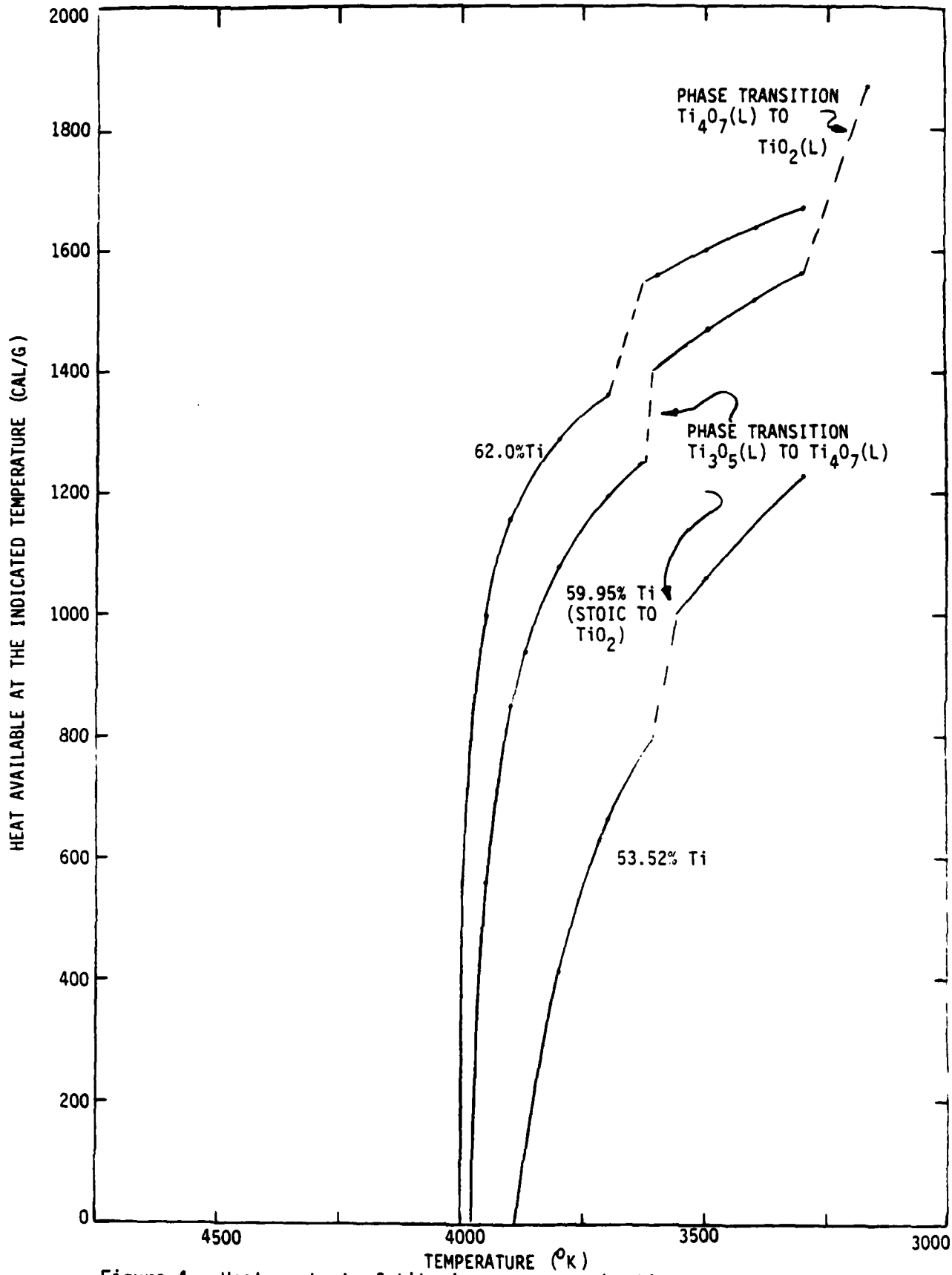

Figure 4. Heat content of titanium-oxygen combustion products at temperatures below the adiabatic flame temperature

The plots of available heat as a function of temperature in Figures 1, 2, 3, and 4 illustrate an important point. Currently the present aluminum-fueled TRS burns a mixture which nominally contains oxygen in 30 percent excess of the stoichiometric amount. This is done because the extra amount is believed to be necessary to ensure complete combustion. However, as shown in the exhibits, this tends to reduce the amount of heat available at the highest temperature compared with a stoichiometric mixture. Considering a stoichiometric aluminum-oxygen mixture (Figure 1) approximately 3800 cal/g, or 51 percent of the heat of combustion, is available at the flame temperature, about 3977°K. Similarly for zirconium (Figure 3) approximately 1600 cal/g, or 56 percent of the heat of combustion, is available near the flame temperature, 4279°K. This may be compared with oxygen-rich mixtures in which the same amount of heat is available only over a range of lower temperatures. The reason for this is somewhat obscure, but it stems from the fact that the total pressure of gaseous metal oxide species above the liquid oxide is primarily a function of temperature. The presence of a diluent, either reactive as is oxygen or inert as is argon, results in a higher fraction of vaporized oxide, compared with the stoichiometric case at the same temperature. Also, because of the heat capacity of the diluent, the flame temperature of the stoichiometric mixture is always greater relative to the mixture containing diluent. Thus the amount of available heat above a given temperature when excess oxygen is used is always less than the stoichiometric case.

Therefore, based on equilibrium thermodynamics alone, the maximum availability of heat for radiation at the highest temperature is obtained from mixtures which are stoichiometric to the oxide. However as will be discussed in subsequent sections, a stoichiometric mixture may not necessarily provide a flame with a maximum radiative flux.

3.3 Combustion Characteristics of Aluminum and Similar Metals

This section reviews the state of knowledge about how powders of such metals as aluminum and beryllium burn in oxygen. The basic combustion mechanism is described, together with how the burning is affected by particle size and gaseous impurities. However, there are few data on how

these characteristics affect the radiative properties of a metal powder-oxygen flame. Some insight, however, is provided by a "first principles" analysis.

3.3.1 The Vapor Phase Combustion Mechanism

Virtually all the information about the combustion mechanisms of these metals derives from experiments with single particles and small-diameter rods ignited and burned in cold gaseous atmospheres. With one exception, there are no studies of larger metal-oxygen flames, i.e. flames which are orders of magnitude larger than the fuel particles. The observations appearing in the literature on the combustion of solid propellants are not especially relevant because of the vastly different environment, high pressures and complex gaseous mixtures, as compared with a TRS.

Based on the results of the single-particle experiments, aluminum, beryllium, calcium, magnesium and many other metals burn as a vapor diffusion flame. (5) The essential criteria for this type of combustion is that the boiling temperature of the metal be lower than the boiling temperature of the oxide. Thus combustion heat vaporizes metal from a burning particle and the vapors diffuse away and eventually react with oxygen to form gaseous oxides. Subsequently as conditions permit, metal oxide condenses exothermically as a smoke of fine particles at some distance from the burning particle. Heat and reactive species diffuse back to the metal particle to supply energy for vaporization.

This reaction mechanism is illustrated schematically in Figure 5. This mechanism is characteristic of combustion in atmospheres with a high concentration of oxygen, in which the rate of combustion is high. When the oxygen is diluted with inert gases or when other oxidizing species are involved, the rate of combustion may be less, temperatures lower and condensation of oxide may occur on the surface of the burning particle. (6)

These features are based on substantial experimental evidence. During the combustion of aluminum and magnesium, the spectral lines of the metal atoms often are observed in absorption against a continuum (from

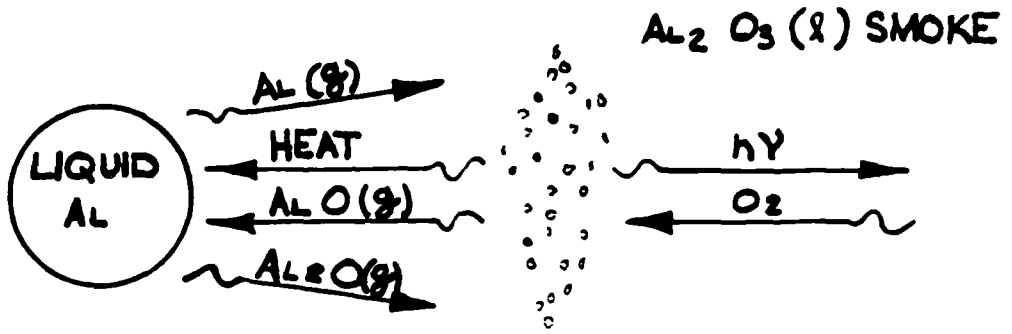

Aluminum: A smoke of $Al_2O_3(l)$ particles forms exothermically from reaction of gaseous oxides, such as AlO and Al_2O, with O_2. This produces thermal radiation. Also Al(g) reacts with O_2 to form AlO(g). Heat diffuses back to the liquid particle causing evolution of Al(g) and AlO(g) also diffuses back towards the particle and reacts exothermically with Al(g) to form $Al_2O(g)$.

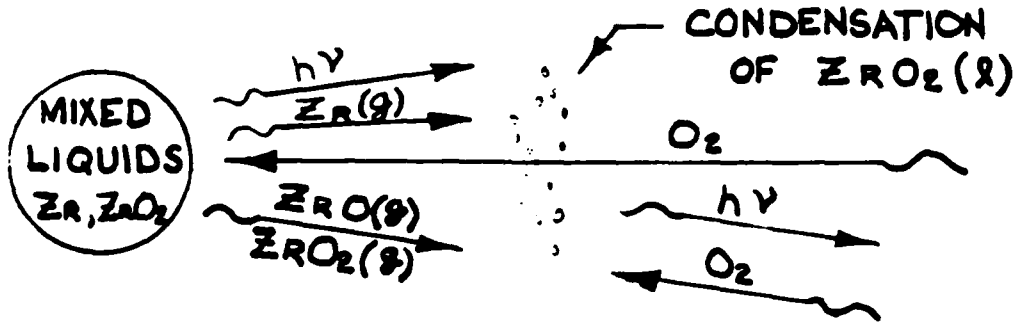

Zirconium: Oxygen diffuses to liquid Zr particle and reacts exothermically to form $ZrO_2(l)$ which dissolves in the particle. Heat is radiated from the particle. ZrO(g) and $ZrO_2(g)$ vaporize from the particle and condense exothermically away from the particle generating additional radiation.

Figure 5. Approximate combustion mechanisms of aluminum and zirconium in pure oxygen

condensing oxides). (5) This indicates that the atomic metal vapor is in the coldest part of the flame. On the other hand, spectral lines of AlO (a gaseous oxide intermediate) are found to be brighter than the continuum indicating that this species forms in the hottest part of the flame.(5)

In cold atmospheres with a high oxygen content, the condensed oxide formed is a smoke consisting of particles less than 5 microns in diameter.(6,7) Single burning particles quenched on a glass slide show a halo of fine particles surrounding the metal particle. (7) Highly magnified photographs of burning aluminum particles show a strongly luminous sphere centered around an inner luminous sphere. (6,8) The inner sphere is the burning particle and the outer sphere is the condensing particles of liquid oxide. As the oxygen content of the atmosphere increases, the luminosity of the outer sphere also increases and the burning particle becomes hidden. (8)

In analogy with the combustion of droplets of liquid hydrocarbons, a consequence of this "vapor diffusion" combustion process is that the theoretical burning time of a metal particle should be proportional to the square of the original diameter of the particle. (9) It is well established that the rate of diffusion of heat or mass to a small particle, per unit area of its surface, for which the particle's Nusselt number is constant (about 2), is inversely proportional to the diameter of the particle. (9) On the other hand, the mass of metal to be burned is proportional to the cube of the diameter. Hence the burning time, which is the quotient of the total mass and the rate, is proportional to the square of the diameter. Data in Wilson and Williams' paper confirms this estimate. (8) Figure 6, showing a logarithmic plot of the burning time of aluminum particles versus their initial diameter, is taken from their paper. The data plotted are those obtained by many investigators, and they cover a range of diameters from 20 to nearly 500 microns. Also, the data apply only to atmospheres with oxygen contents of 10 to 31 volume percent. The data fall between two curves of the form:

$$t_b = \frac{d^2}{\beta} , \qquad (1)$$

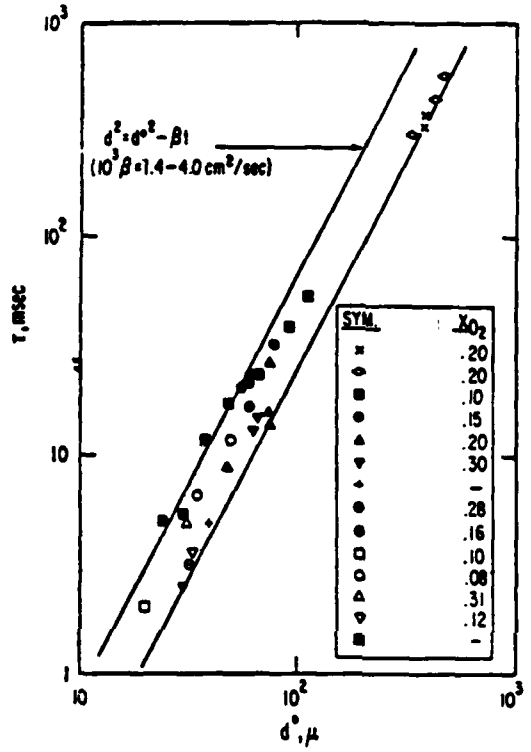

Source: Reference 8

Figure 6. Combustion of Al particles in O_2-laden gases: survey of previous measurements

where t_b is the burning time (τ in the paper), d the initial diameter, and β a constant depending on the oxygen concentration in the combustion atmosphere. The two curves correspond to two values of β: 1.4×10^{-3} and 4.0×10^{-3} cm^2/sec.

The burning time also is a strong function of oxygen content. Examples are presented in Figure 7 which show the measured burning times of 250 micron aluminum particles in cold oxygen-argon and oxygen-nitrogen atmospheres at a total pressure of 700 torr. The data are taken from Reference 6. For oxygen-argon atmospheres, the burning time is nearly inversely proportional to the oxygen partial pressure, which is an intuitively expected result. Burning time has a stronger dependency on oxygen content in oxygen-nitrogen atmospheres. This suggests a different mechanism, which, in view of the observations to be described subsequently, is not surprising. The data in Reference 6 also indicate that saturating the cold atmosphere with water vapor produces a small decrease in burning time.

3.3.2 The Effects of Diluents on the Combustion Mechanism

In several papers Prentice and others have criticized the "d^2" law. There are two basic reasons for this. The first is that, over a limited range of particle sizes, the burning time dependency often appears to be linear (eg. See plots of data in References 6 and 10). However there are data which justify particle diameter burning time exponents ranging from 1.0 to 2.4 . (6,8)

Second, alumium particles burning in atmospheres containing nitrogen or water vapor undergo a variety of erratic behavior. (6,7,10) In single-particle combustion experiments in air and atmospheres containing nitrogen, aluminum oxide condenses both as a smoke and in the form of a globule on the burning metal particle. Near the end of combustion the globule has grown to contain about a third of the original quantity of the aluminum in the particle. Apparently, the condensation of oxide on the molten aluminum droplet is enabled by the presence of nitrogen; a complex Al-N-O phase is formed which permits molten oxide to "stick" to the metal.

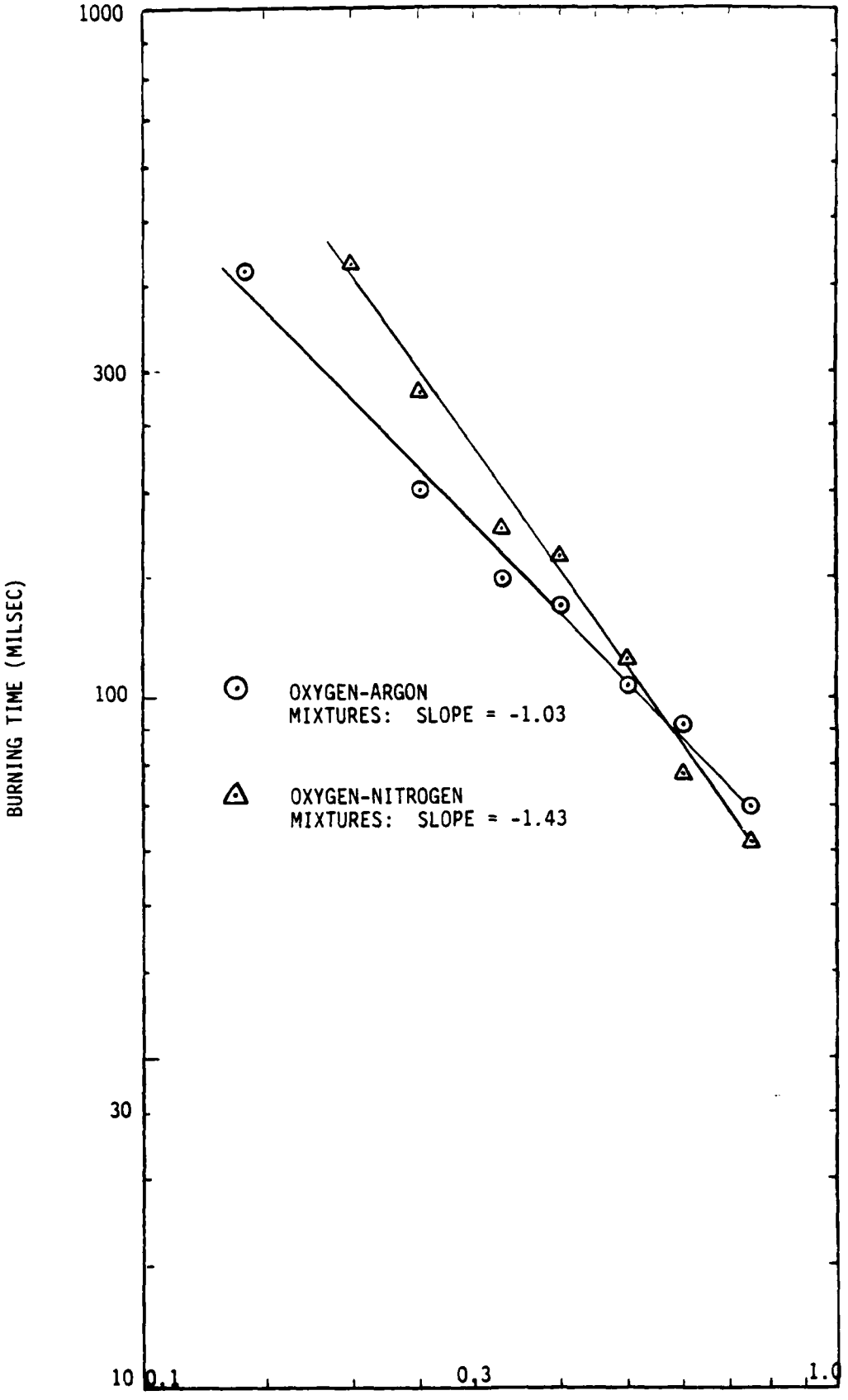

Figure 7. Effect of oxygen concentration on burning time of aluminum particles

No such globules are formed during combustion in atmospheres of pure oxygen or in mixtures of oxygen and argon. However, the addition of 5 to 10 percent of nitrogen in argon-oxygen atmospheres, permits the formation of the oxide globules. With more than 10 percent nitrogen, the globules and metal fragment explosively as combustion nears completion. The globule, apparently because of surface forces, grows as a "cap" on one side of the particle. This results in vaporization of aluminum only from the opposite side, as shown clearly in photographs of quenched burning drops. The assymmetry of the vaporization also is evident in time-lapse photographs, in which the burning droplets are observed to spin at high rates. (6, 10)

When water vapor is present, the burning particle is encased inside a hollow sphere of molten oxide. (6,7) Particle spinning also is observed. (6,7) Similarly, during combustion in CO_2, condensation of the oxide on the burning aluminum particle is observed, and this is believed to be enabled by the formation of a complex Al-C-O phase. (10)

Eruptions from and fragmentation of the burning particle also occur in atmospheres containing nitrogen, water vapor and carbon dioxide. (6,7) The eruptions are believed to be gas driven, the result of a phase change with the sudden evolution of nitrogen, carbon oxide or hydrogen (see the description of zirconium combustion in Section 3.4). (6) During burning, the particle may undergo one or more eruptions, and a larger violent eruption (explosion) usually terminates combustion. (6)

Condensation of oxide on the burning metal particle, assymmetric vaporization, and eruptions do not occur in pure oxygen and oxygen diluted with argon (6, 8, 10,).

These erratic processes also dramatically affect the size and shape of the oxide particulates produced. Photographs of aluminum particles, 20 to 350 microns in diameter, burning in pure oxygen and oxygen-argon mixtures, show oxide condensing in a sphere of smoke at a distance of 3 to 5 particle radii. (8, 10, 11) As mentioned above, these particles are very small, being less than 5 microns in size. When water vapor, carbon

dioxide or nitrogen are present, both smoke and much larger particles are formed. At first, larger accumulations of oxide are formed via condensation on the burning aluminum particle. Subsequently, these accumulations are fragmented by the several eruptions and the terminal explosion. In dry nitrogen-oxygen mixtures, the explosions generate solid oxide particles which are smaller than the original aluminum particle. In the presence of water vapor, hollow oxide spheres (oxide balloons) and a few solid oxide spheres are produced. Table 3 (from Reference 6) summarizes the types of aluminum oxide particulate matter formed in the various types of oxygen containing atmospheres.

3.3.3 The Source of Thermal Radiation During Aluminum Combustion

Thermal and visible radiation from the combustion of powders of aluminum and similar metals has been investigated experimentally to some extent. This will be discussed in Section 4 in detail. Here, the above-described combustion data will be used to show that a negligible fraction of aluminum's combustion energy can be radiated from small aluminum particles, 15 microns in diameter and smaller, burning in oxygen, and instead essentially all of the radiation can only be generated as the oxide condenses.

The energy radiated, Q_r, by one gram of burning aluminum particles is:

$$Q_r = j_r \, n \, A_p \, t_b \, , \qquad (2)$$

where n is the number of aluminum particles in one gram, A_p is the time-average area of an aluminum particle during burning, t_b is the burning time defined by Equation (1), and j_r is the radiant flux emitted by the particle. The number of aluminum particles in one gram is simply:

$$n = \frac{6}{\rho_m \, \pi \, d^3} \, , \qquad (3)$$

Table 3. Residue from the combustion of single aluminum particles
SOURCE: REFERENCE 6

OXIDIZER	WATER VAPOR CONTENT	FORM AND SIZE OF THE ALUMINUM OXIDE RESIDUE[a]
OXYGEN-NITROGEN	DRY	SMOKE (1 TO 2 MICRONS), SOLID SPHERES ($0.2d_o$)
	SATURATED	SMOKE (1 TO 2 MICRONS), SOLID SPHERES ($0.4 - 0.7d_o$), HOLLOW SPHERES ($0.2 - 0.8d_o$)
OXYGEN-ARGON	DRY	SMOKE (1 TO 2 MICRONS)
	SATURATED	SMOKE (1 TO 2 MICRONS), SOLID SPHERES ($0.75-0.85d_o$)
OXYGEN-CARBON DIOXIDE	DRY	SMOKE (1 TO 2 MICRONS), SOLID SPHERES ($0.2 - 0.4d_o$), BALLOONS (40 TO 50 MICRONS)
	SATURATED	SMOKE (1 TO 2 MICRONS), BALLOONS (40 TO 50 MICRONS)

a d_o IS THE DIAMETER OF THE ORIGINAL ALUMINUM PARTICLE.

ρ_m is the density of aluminum and d is the diameter of the particle. Since according to Figure 6, d^2 is approximately linear in time during burning, the time-averaged area of a particle is:

$$A_p = \frac{\pi d^2}{2} , \tag{4}$$

Finally, if it is assumed that the emissivity of a burning aluminum particle is unity, then the maximum radiant flux it can emit is :

$$j_r = \sigma T_b^4 , \tag{5}$$

where T_b is the boiling temperature of aluminum metal, 2766°K (see Table 1) and σ is the Stefan-Boltzmann constant, 1.355×10^{-12} cal/cm^2-sec-°K^4. Substituting these expressions into Equation (2) yields:

$$Q_r = \frac{3 \sigma T_b^4 d}{\rho_m \beta} , \text{ cal/g} \tag{6}$$

which shows that the radiation emitted during burning is directly proportional to the diameter of the burning particle. In pure oxygen, the minimum value of β is estimated to be $4 \times 1.4 \times 10^{-3} = 5.6 \times 10^{-3}$ cm^2/sec. With d = 15 microns and $\rho_m = 2.7$ g/cm^3 the total heat radiated by an aluminum particle burning in pure oxygen is estimated to be 24 cal. This is less than one percent of the heat available for radiation above 3300°K (see Table 2).

The above calculation shows that a neglegible quantity of energy is radiated by an aluminum particle burning in pure oxygen. The calculation presented below shows that it is the condensation of liquid oxide from the vapor phase which generates essentially all the energy available for radiation. Vapor phase combustion of aluminum produces a number of gaseous sub-oxides such as AlO, Al_2O, AlO_2, and Al_2O_2. As shown in Figure 5, some of these oxides can diffuse back to the aluminum

particle where they may react exothermically and provide heat for vaporization. For example:

$$AlO+Al(l) = Al_2O, \Delta H = -60.8 \text{ kcal/mol.} \quad (7)$$

Also, the gaseous sub-oxides may diffuse away and ultimately condense on nuclei of liquid aluminum oxide. Figure 8 shows the temperature, enthalpy and composition of the combustion of aluminum with oxygen which is 30 percent in excess of the amount stoichiometric to Al_2O_3. (This is the nominal aluminum-oxygen composition of the current TRS flame.) The figure shows that under adiabatic conditions, the combustion of aluminum to form gaseous oxides alone (condensation assumed not to occur) is sufficiently exothermic to vaporize and consume the aluminum particle. The temperature, 3010°K, is almost 250°K above the normal boiling temperature of aluminum metal (2766°K). However, the enthalpy difference between the gaseous oxide products and the equilibrium composition, in which condensation has occurred isothermally, is about 5,000 cal/g of aluminum. This is about 76 percent of the total heat of combustion of aluminum with oxygen (as seen by comparison with the data in Table 1).

The main conclusion to be drawn is that it is the condensation of gaseous aluminum oxides which will supply the energy for thermal radiation. The amount and intensity of the radiation, which is derived from the condensation, therefore will depend on the temperature of the oxide particles as they form. This in turn will depend on the rate of condensation (ie. the rate of heat release) versus the rate of heat loss both by radiation and by non-radiative processes. The latter, for example, includes the dissipation of heat by mixing with cold ambient air, a mechanism which undoubtedly was operative in the single particle experiments and likely is a problem with the current TRS. If the non-radiative dissipation processes can be minimized, it is believed that the temperature of the oxide particles will be at a maximum, and a corresponding maximum of radiative flux can be achieved.

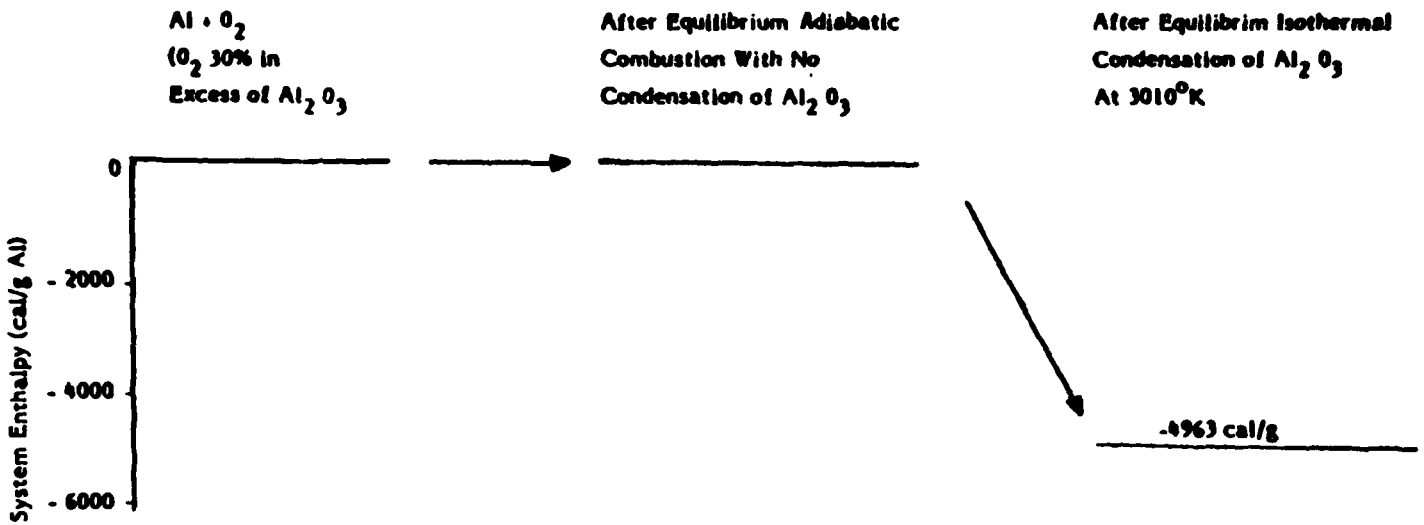

Temperature (°K)		298	3010	3010
Combustion Products, g-mol/gAl:				
AlO	(g)	-	2.5×10^{-3}	0
AlO_2	(g)	-	9.6×10^{-3}	0
Al_2O	(g)	-	1.8×10^{-3}	0
Al_2O_2	(g)	-	10.7×10^{-3}	0
O	(g)	-	2.6×10^{-3}	1.0×10^{-3}
O_2	(g)	-	12.4×10^{-3}	7.8×10^{-3}
Al_2O_3	(l)	-	0	18.6×10^{-3}

a Calculations based on data from Reference 2

Figure 8. Heat release from the condensation of liquid aluminum oxide in combustion conditions

No existing data on the kinetics and rate of condensation of aluminum oxide during combustion, which would be applicable to a TRS, were found in the literature. The only data available relate to combustion in solid propellant rocket motors which have conditions vastly different from a TRS (eg. combustion at 500 to 1000 psi). Nevertheless as will be discussed in Section 4.4, the rate of condensation of aluminum oxide can be high.

3.4 Combustion Characteristics of Zirconium and Titanium

This section describes the state of knowledge of how powders of metals like zirconium burn. An important feature is that much of the burning proceeds by surface oxidation. This is expected to have significant effects on the radiative properties of zirconium-oxygen flames. The effects of impurities on combustion is described, and combustion data are analyzed to derive a relationship between particle diameter and the time during which the radiation from a burning particle is at a maximum.

3.4.1. The Surface Oxidation Combustion Mechanism

As may be noted from the data in Table 1, zirconium's boiling temperature is higher than that of the oxide. One consequence of this is that much of the oxidation during combustion occurs on the surface of the metal. Although the boiling temperature of titanium is lower than that of its oxides, it is still high (almost 3600^{o}K), and surface oxidation also is a dominant mechanism in the combustion of this metal. This is in direct contrast with the situation for aluminum, berylium, magnesium and calcium, in which the oxidation reaction occurs in the gas phase.

Most of the existing knowledge of the combustion characteristics of zirconium and titanium has been developed from experiments with single particles. The bulk of these experiments have been with zirconium. Metal particles ranging in size from approximately 200 to 600 microns in diameter have been burned in atmospheres of air, helium-oxygen, argon-oxygen and pure oxygen. (10,12) Under the conditions encountered in these experiments, the combustion of these metals involved the highly exothermic absorption of oxygen at the surface of the particle. In air,

exothermic absorption of nitrogen was involved as well. It is well known that both oxygen and nitrogen are soluble in these metals. Thus an important fraction of the heat of combustion was generated in the burning particle itself and it became a high-temperature radiator.

Figure 9, which is taken from a paper by Nelson, shows the weight gain experienced by a series of zirconium particles, initially 525 microns in diameter, burning in pure oxygen. (13) Each particle was quenched in liquid argon after varying periods of combustion, and then the residue was weighed. The data indicate a linear absorption of oxygen at a rate of 0.11g O_2/cm^2-sec up to a time of 175 milsec. Assuming ZrO_2 (1) is the product, this rate of oxygen absorption implies a chemical heat flux of about 800 cal/cm^2-sec. This heat is absorbed, and is conducted and radiated away such that at about 80 milliseconds the temperature of the burning particle has peaked at about $4300^{o}\pm124^{o}K$, as determined by two-color pyrometry. (14) This peak temperature also corresponds to the peak in the intensity of radiation at 0.85 microns from the burning particle. During the 80-millisecond period preceding this peak, the intensity is greater than or equal to about 70 percent of the peak intensity. (14) At about 40 milsec following the peak, the intensity falls-off to appreciably below the maximum level. (14) Thus the temperature of the burning zirconium particle remains high, above about $3800^{o}K$, over a period corresponding to about 70 percent of its total burning time.

3.4.2. Oxide Vaporization and Condensation During Combustion

Surface oxidation heating a burning zirconium particle to a high temperature only describes a part of the combustion mechanism. Substantial vaporization of the oxide must occur as well, a conclusion which is easily inferred from the rapid uptake of oxygen (see Figure 9). As stated above, in pure oxygen the rate for a 525-micron particle is equivalent to a heat release rate of 800 cal/cm^2-sec. However, not all of this heat can be dissipated from the burning particle by radiation. Even if the emissivity of the particle were unity, the maximum radiative heat flux at the particle's temperature of $4300^{o}K$ is only 463

The "explosion" zone is discussed in Section 3.4.4 and is caused by contamination with gases such as nitrogen. The "spearpoint" zone is a short period of intense radiation from particle caused by the freezing of liquid ZrO_2 at 2950 K.

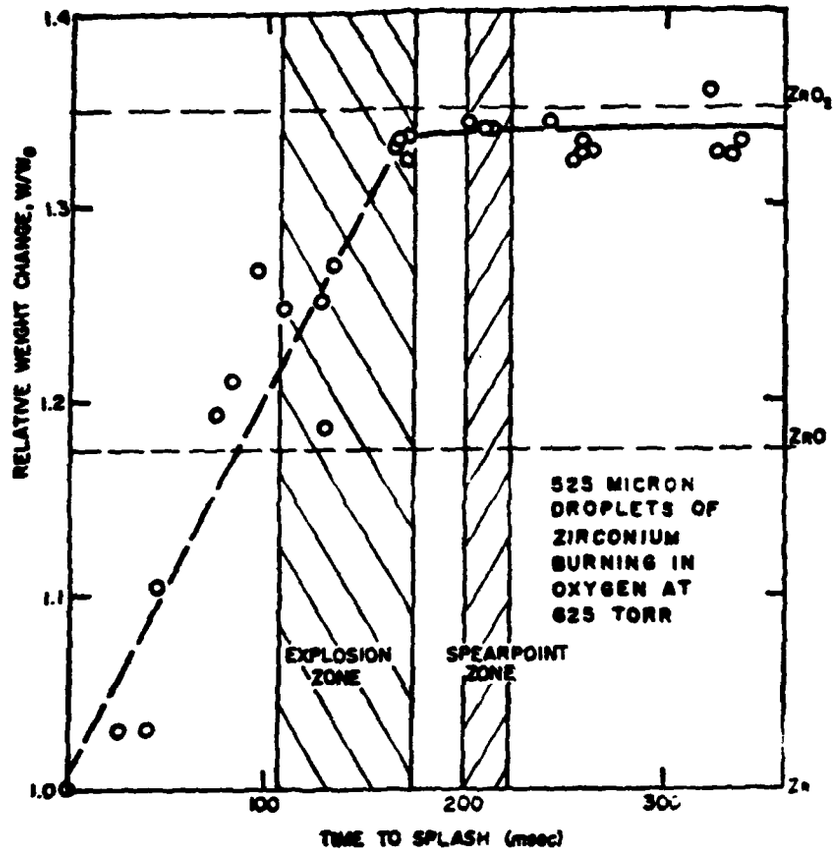

Source: Reference 13

Figure 9. Relative weight change of burning zirconium droplets as a function of time

cal/cm^2-sec. Part of the difference, at least 337 cal/cm^2-sec, likely is absorbed via the very endothermic heat of vaporization (to the equilibrium composition at 4279°K):

$$ZrO_2(l) = 0.537\ ZrO_2(g) + 0.462\ ZrO(g) + 0.462\ O(g), \qquad (8)$$
$$\Delta H = +2352\ cal/g\ of\ Zr.$$

Additionally, it is likely, too, that some of the oxidation occurs in the vapor phase. The calculated equilibrium vapor composition indicates the presence of ZrO(g). This is confirmed by spectroscopic data obtained during combustion. (12, 14, 15). Although a substantial concentration of zirconium atoms is not indicated by the equilibrium calculations, the spectroscopic data shows their presence as well. (12, 14, 15) Hence, some of the heat of combustion of zirconium must be released by partial oxidation and condensation of oxide external to the burning particle, a feature which is similar to aluminum combustion.

Thus the data presented in Figure 9 are somewhat misleading. In more fully instrumented experiments, Nelson and his coworkers and Charagundla et.al. showed that there is a substantial vaporization of the oxide and, due to the aerodynamic factors associated with these single particle experiments, nearly all of the vaporized oxide is reabsorbed at a later time on the parent particle. (11,12)

That vaporization does occur is evident from the observation of condensed oxide around the burning particle. (11, 12) Photographs have shown the existence of a "fog" of oxide particles in a spherical cloud surrounding the parent particle. Larger particles of oxide grow at the perimeter of the cloud, and these circulate up the sides to the top. (The zirconium particle is in free fall as it burns.) Usually a large oxide "follower" drop forms by agglomeration and follows the parent zirconium particle. Apparently it is held in place close to the parent particle by aerodynamic forces.

After reaching a size, which may correspond to an appreciable fraction of the parent patricle, the "follower" drop touches and coalesces with it. This process of growth and coalescence of oxide drop with the parent particle may occur several times during a zirconium particle's combustion. These detailed observations explain the steady gain in weight indicated in Figure 9.

The detailed photographs also show that upon coalescence of a "follower" drop of oxide, the spherical cloud collapses and coalesces with the parent drop as well. (11, 12) The likely explanation for this is that the oxide droplets are relatively cool (a result of radiation and conduction into the cold oxygen atmosphere used in the experiments.) Hence, their coalescence causes a momentary cooling of the parent particle and, consequently, a momentary interruption of vaporization of oxide and zirconium atoms. This then results in the collapse and coalescence of the fog as well. Immediately after this, there is little resistance to continued diffusion of oxygen to the surface of the particle, and hence vigorous oxidation resumes. Thus the rate of burning, and the temperature of the particle is oscilatory, as observed (see the discussion in the next subsection).

It is pertinent to contrast the combustion of single particles with a known, practical zirconium-oxygen combustion system. Very fine zirconium foil is burned with oxygen in several types of commercial photoflash bulbs. High-speed movies (Fastex Camera) of the combustion and analysis of the combustion products for M-3 flash bulbs have been made. (5) The movies showed the bulb to be filled with burning particles in violent motion. This was contrasted with aluminum-filled flash bulbs in which, when fired, no burning particles could be seen; the illumination was homogeneous. This is consistent with the burning mechanisms described.

Examination of the zirconium combustion products showed 10 to 200 micron particles stuck to the glass of the flash bulb's envelope. The larger particles had streaks of a white "smoke" around them. There also were loose spheres in the bulb: a few hollow spheres about 700 microns in

diameter and a much larger number 150 to 300 micron spheres. The occurrence of "smoke" about what must be quenched burning particles is consistent with the fog of oxide particles observed in the single particle experiments. The hollow spheres probably arise due to contamination of either the zirconium or the oxygen with nitrogen. This will be discussed further in Section 3.4.4.

3.4.3. Radiation from Burning Zirconium Particles

The relative intensity of radiation at selected frequencies and the apparent temperature of burning single zirconium particles has been measured. (11, 12) Intensity of luminosity varies during combustion as shown in Figure 10. This figure is a record of the intensity of the lunminosity of a 350 micron particle burning in a pure oxygen atmosphere at 300 torr (0.395 atm). (11) Following ignition, the luminosity rises steeply, within 10 milsec, to a plateau. At about 35 milsec after ignition, the luminosity decreases slowly until, at about 85 milsec after ignition it again rises steeply to another plateau, slightly higher than the first. As mentioned above this sudden increase in luminosity was shown to coincide with the coalescence of the "follower" drop and the momentary collapse of the fog of oxide particles. (11, 12) Subsequently the luminosity again decreases slowly until at about 130 milsec the luminosity begins an approximately exponential decrease. This decrease is believed to be associated with a change in the mechanism of oxidation in which the rate becomes controlled by the diffusion of oxygen within the molten particle. The reduced rate of oxidation results in a lowering of the burning particle's temperature. At about 240 milsec the burned particle undergoes the "spear point" phenomena, which is a small increase in luminosity caused by the onset of freezing of liquid zirconium dioxide.

Similar results were observed at higher pressures of pure oxygen (up to 0.82 atm). However the peaks in luminosity were greater and the same events occurred in a shorter time. Additionally more than one oscillation in luminosity may occur because of the repeated coalescence of oxide droplets with the burning particle.(12)

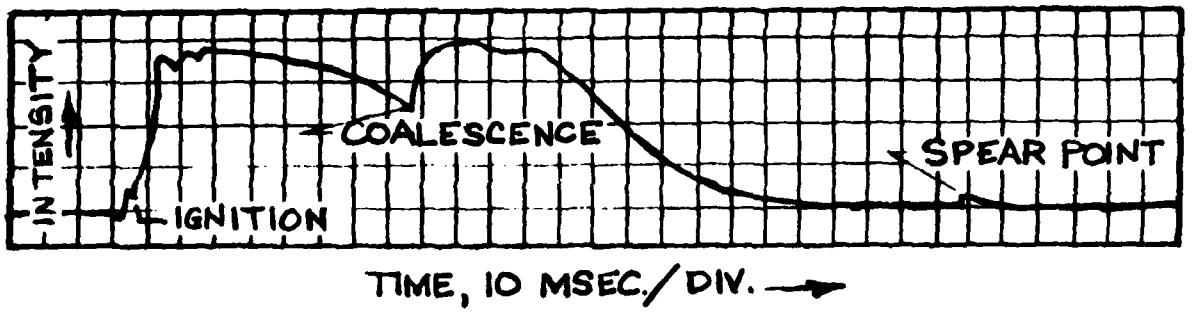

Figure 10. Luminosity record of a 350-micron zirconium particle burning in pure oxygen at 300 TORR

Through measurement of the relative intensity of luminosity at selected wave lengths, the temperature of a zirconium particle burning in pure oxygen at 0.82 atm has been measured to range between 3800 and 4300°K. The temperature of the fog of oxide particles has not been measured. However the fog is much less luminous and therefore is believed to be at a lower temperature than the burning particle for the reasons stated above.

The visible spectrum of burning zirconium particles also has been observed. (12, 14, 15) Besides the continuum, a strong banded spectra of ZrO(g) together with the lines of Zr(g) were observed. These spectral lines are strongest just after ignition. Subsequently, their intensity decays and fades away completely at about the time of the burning particle's peak luminosity, and just before the luminosity begins its final exponential decrease.

The combustion of zirconium particles apparently provides two sources of energy for radiation. One is the burning particle itself; the other is the condensation of oxide from the vapor phase. As mentioned in the preceding subsection, radiation from the burning particle accounts for approximately half of the combustion heat liberated, up to 463 cal/cm^2-sec. The balance is liberated in the smoke.

3.4.4. Effect of Diluents on Combustion

Generally the effect of diluents is to reduce the rate of combustion (increase the burning time), lower the temperature and reduce the intensity of radiation from the burning particle. The presence of nitrogen, even in very small amounts, results in the "explosion" of burning particles near the completion of their combustion (see Figure 9).

Figure 11 shows the burning times of 525-micron zirconium particles in helium-oxygen and argon-oxygen atmospheres at a total pressure of 625 torr (data from Reference 12). In this exhibit, burning time is defined as time of the onset of the exponential decay of luminosity (see Figure 10). The burning time in the helium mixtures is approximately inversely

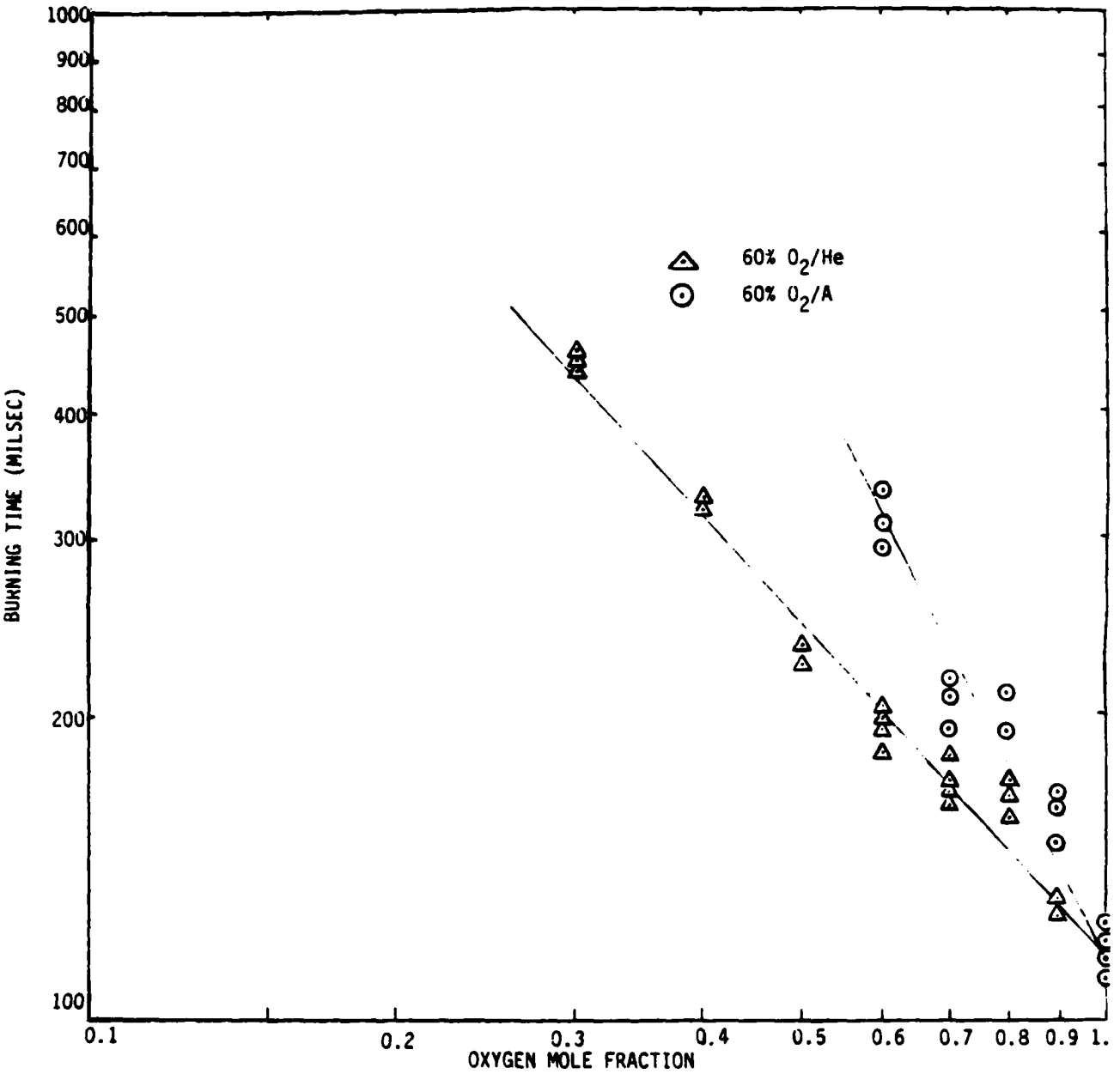

Figure 11. The burning time of 525-micron zirconium particles in oxygen containing helium and argon at 625 TORR

proportional to the mole fraction of oxygen in the mixture. This is the intuitively expected behavior based on an external diffusion, rate-controlled process. Surprisingly, however, the burning time is inversely proportional to the square of the oxygen mole fraction when argon is the diluent. There are no corresponding data for mixtures containing nitrogen. The reason for this difference in the effect of helium and argon on burning time is not understood, however, part of the difference may have been a difficulty in interpreting the time of on-set of exponential decay in luminosity.

Table 4 (from Reference 12) illustrates the effect of diluents on the maximum measured temperatures of burning zirconium particles. The temperatures were based on ratio pyrometry with calibration against a carbon arc at 3800°K and the assumption that the particle radiates as a grey body at all temperatures. Compared with combustion in pure oxygen, in which the maximum temperature is about 4300°K, the maximum temperature in 30/70 oxygen-helium is only about 3200°K. The lower temperature is intuitively correct, considering that the lower oxygen concentration results in a correspondingly slower rate of oxidation.

Figure 12 (from Reference 14) illustrates the effect of a diluent on the intensity of radiation from the burning particle. The exhibit consists of a set of traces of the intensity at 0.83 microns versus time for a series of helium oxygen mixtures. The most obvious effects of dilution with helium is the lowering of the maximum intensity of the radiation and the spreading-out in time of the radiation. These effects are consistent with the lowering of the maximum temperature and the slower burning rates as noted above.

Also, examining the details of the traces shows that at concentrations of oxygen above about 40 percent (mole basis) the radiation intensity oscillates and the frequency of oscillations increase as pure oxygen is approached. As explained in Section 3.4.3 these oscillations result from the repeated buildup and collapse of the fog of oxide particles. The coalescence of oxide droplets with the burning particle is a phenomenon

Table 4. Estimate of maximum burning temperatures by ratio pyrometry (initial droplet diameter: 525 M; total pressure: 625 TORR)

SOURCE REFERENCE 12

Diluent	Oxygen Mole Fraction	(°K)
None	1.00	4390
	1.00	411C
	1.00	4390
Helium	0.90	4310
	0.90	3650
	0.90	4160
	0.80	3830
	0.80	3830
	0.80	3700
	0.80	3830
	0.80	3830
	0.70	3900
	0.70	3750
	0.70	4480
	0.70	3650
	0.70	4160
	0.60	3560
	0.60	3860
	0.60	3580
	0.60	3790
	0.50	3740
	0.50	3480
	0.50	3500
	0.40	3290
	0.40	3640
	0.40	3290
	0.30	3260
	0.30	3070
	0.30	3290
Argon	0.80	3900
	0.80	3790
	0.80	4020
	0.60	3640
	0.60	3400

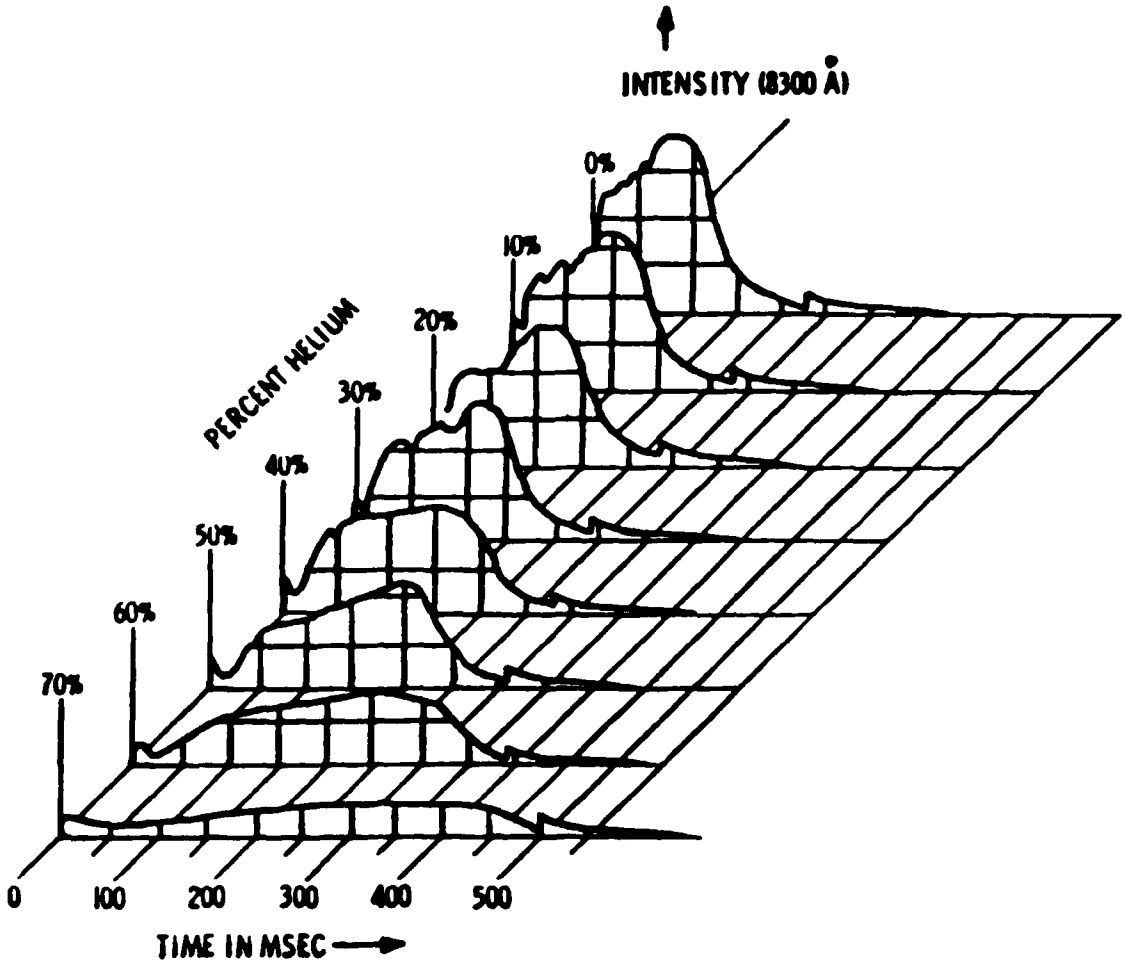

Source: Reference 14

Figure 12. Variation of luminosity-time traces with helium percentage. Initial droplet diameter was 525 microns; total gas pressure 625 ± 5 TORR. Photomultiplier (S-1 surface) was covered with a narrow band-pass filter with transmission at 8300 ± 50 Å

dependent on the concentration of oxygen: below an oxygen partial pressure of about 200 to 300 torr, it does not occur. (11, 12)

Although not discussed in the literature, the above described dilution effects on combustion with oxygen probably apply at least in a general way to nitrogen. However, the lowering of maximum temperature and radiation intensity may not be as severe as it is for helium because nitrogen can react exothermically with zirconium:

$$Zr(s) + 1/2\ N_2(g) = ZrN(s), \Delta H_{298} = -956\ cal/g\text{-}Zr. \qquad (9)$$

This heat of reaction is about one-third of that with oxygen.

One phenomenon caused by nitrogen has received some attention in the literature. When nitrogen is present, and especially in air, the combustion of a zirconium particle is terminated with an "explosion": the burning particle is fragmented into many much smaller particles. (10) In a series of remarkable experiments, Meyer and Nelson showed that the cause of the "explosions" were the growth and rupture of micro balloons of molten zirconium oxide. (15) They showed that nitrogen was the gas filling the micro balloons. The effect occurs when the nitrogen content is as low as 2.5 percent (mole basis). The balloons were collected by carefully timed quenching of burning zirconium particles. Zirconium particles 525 microns in diameter produced micro balloons up to 1730 microns in diameter. Nitrogen was shown to be the inflating gas by mass spectrometric analysis of crushed micro balloons.

3.4.5 The Effect of Particle Size on the Burning Rate

Burning time as a function of particle size for zirconium particles, 300 to 600 microns in diameter, in pure oxygen and in 60/40 mixtures of helium-oxygen and argon-oxygen, is shown in Figure 13, which is taken from Reference 12. The data for burning in pure oxygen suggest a linear relationship, whereas in impure atmospheres the relationships appear to have a slight upward concavity. In this figure, the measure of burning time is the "spear point" time defined in Figures 9 and 10. This is a

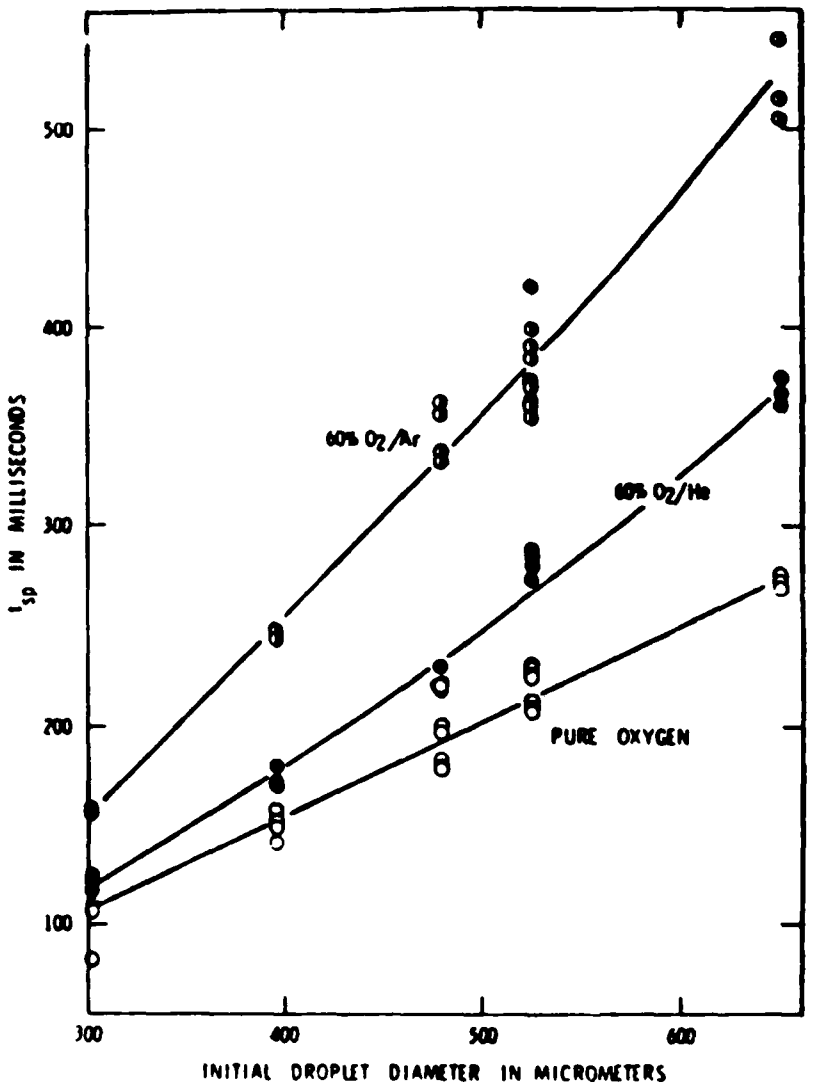

Source: Reference 12

Figure 13 Plots of burning time of zirconium droplets versus initial size in 60% O_2-Ar, in 60% O_2-He and in undiluted oxygen. Each atmosphere has a total pressure of 625 ± TORR

somewhat longer time than the period of maximum radiation and luminosity as discussed in the preceding subsections (see Figures 10 and 12). For an HTRS, the period of maximum radiation is a more useful measure; this was the measure used in constructing Figure 11, which showed the effect of oxygen concentration on the burning time of 525-micron particles.

As is, Figure 13 is not very useful for predicting the burning times of smaller particles. For an HTRS, burning times of less than 100 millisec and particles somewhat smaller than 300 microns are of interest. Aside from their not-too-useful definition of burning time, the pure-oxygen data in Figure 13 predict a zero burning time for a particle approximately 80 microns in diameter.

The burning times of single zirconium particles, 266 to 388 microns in diameter, in air was measured by Prentice and his coworkers.(10) In this case, burning time was defined as the time-to-explosion, the phenomena discussed in the previous subsection. Prentice found experimentally that this burning time was quite reproducible. These data also show a linear dependence on particle size.

In spite of its short-comings, the data for the "spear point" time in Figure 13 can be interpreted to estimate the maximum-luminosity burning time of both large and small zirconium particles. All that is needed are three reasonable assumptions. The first assumption permits scaling the maximum-luminosity burning time with the "spear point" time. As shown by the data in Figure 10 (which is typical) the difference between the two is the period of exponential decay of the luminosity and temperature of the particle. Intuitively, the time constant, τ, for this decay should be directly proportional to the mass of the particle and inversely proportional to the product of the particle's surface area and the heat flux from it:

$$\tau \propto \frac{\pi d^3 \rho}{6\pi d^2 j} \propto \frac{d}{j}, \qquad (10)$$

where d is the particle diameter, ρ is the density and j is the surface heat flux. The surface heat flux consists of two components: radiation and convection. The former is independent of particle diameter whereas the latter is inversely proportional to particle diameter. Here, for simplicity, it is assumed that the cooling is governed by convective heat transfer and therefore the time constant for cooling is directly proportional to the square of the particle diameter:

$$\tau \propto d^2 . \tag{11}$$

Table 5 compares the theoretical convective (Nusselt number = 2.0) and radiative heat fluxes from different sizes of particles at two temperatures, 3300 and 4000°K. Although convective heat transfer is the dominant mode for small particles ($\leq$100 microns), it is not for larger particles. Nevertheless it exceeds the radiant flux, and thus as a convenient approximation it is assumed to be the major mode.

In References 12 and 14 Nelson presented data which indicated that for a 525-micron zirconium particle, the maximum-luminosity burning time was about 120 millisec, whereas the "spear point" time was about 225 millisec. Therefore with the Proportionality (11), a relationship between the maximum-luminosity burning time and the "spear point" time can be derived:

$$t_b = t_{sp} - \frac{0.105d^2}{(0.0525)^2} = t_{sp} - 38.1d^2 , \tag{12}$$

where t_b is the maximum-luminosity burning time in seconds and t_{sp} is the "spear point" time in seconds and d is in centimeters.

The second major assumption is that the transition from the maximum-luminosity period to the period of exponential decay is governed by a critical distribution of the concentration of oxygen. As suggested by Figure 9, little free zirconium exists in the particle at this time and

Table 5. Comparison of the theoretical rates of heat transfer from burned zirconium particles to a cold atmosphere

Particle Diameter (Microns)	Convective Heat Transfer[a] (cal/cm^2-sec) At Particle Temperature		Radiative Heat Transfer (cal/cm^2-sec) At Particle Temperature	
	4000°K	3300°K	4000°K	3300°K
30	9965	6750	347	161
100	2990	2028	347	161
300	997	675	347	161
600	498	339	347	161

a Based on thermal diffusivities, 0.00404 @ 4000°K and 0.003379 @ 3300°K, in cal/cm^2-sec-°K, calculated by the NASA Computer Program, Reference 3.

most of this probably is near the center of the particle. The concentration of oxygen would vary in the opposite manner.

During the period of maximum luminosity, there is a flux of oxygen to the surface of the particle. The oxygen dissolves, reacts with zirconium metal, and diffuses towards the center. Whether or not the oxygen is free or combined with zirconium as it diffuses makes little difference since only the net concentration of oxygen is of interest. For a molten spherical particle with an external flux of oxygen, F_o, to its surface, the concentration of oxygen (expressed as weight fraction) can be described mathematically by the equation: (16)

$$\frac{\rho\, Dw}{d\, F_o} = \frac{6Dt}{d^2} + \frac{1}{4}\left[\left(\frac{2r}{d}\right)^2 - \frac{3}{5}\right]$$

$$- \frac{1}{(r/d)} \sum_n f_n\left(\frac{2r}{d}\,,\ \exp\left(-\frac{4Dt}{d^2}\right)\right), \qquad (13)$$

where:
- D is the diffusivity of oxygen in the molten metal,
- ρ is the density of the particle,
- w is the weight fraction of oxygen at r,
- d is the diameter of the particle,
- F_o is the external flux of oxygen, to the particle
- t is time,
- r is the variable radius.

Near the end of maximum-luminosity, the value of the quantity $4\ Dt/d^2$ is expected to be much greater than unity and the summation term vanishes. This is a consequence of the fact that the particle has absorbed nearly the stoichiometric quantity of oxygen and therefore w varies little with r.

The third assumption is that the flux of oxygen, F_o, to the particle is constant in time. This is a reasonable assumption in view of Figure 9. However in view of the discussion in Section 3.4.3, the flux of oxygen is only approximately constant. The assumption of a constant flux is one of convenience. Additionally the particles themselves are assumed not to change significantly in size, since oxygen atoms easily fit into the intersticies between zirconium atoms.

With these ideas in mind Equation (13) is rewritten:

$$\frac{t_b}{d^2} = \frac{\rho w_b}{6dF_o} - \frac{1}{24D} - \left[\left(\frac{2r}{d}\right)^2 - \frac{3}{5}\right], \qquad (14)$$

where t_b is now the time at the end of the maximum-luminosity period. For a particle of a given size at this time, the right side of Equation (14) is a constant, with w_b a fixed function of $2r/d$.

The question now arises as to how t_b varies with particle size, d. This in turn depends on how the external oxygen flux, F_o, varies with d. If F_o is controlled by a gas phase diffusional process, $F_o \propto 1/d$ is expected. (In the experiments, the diffusion Nusselt number was a constant at a value of nearly 2.) Then the right side of Equation (14) will be a constant which is independent of d, implying that t_b/d^2 is also a constant.

The data for "spear point" times in Figure 13 were converted to values of t_b, using Equation (12). Table 6 lists these values and the corresponding values of t_b/d^2. These later values are not constant, and therefore the assumption of $F_o \propto$ to $1/d$ appears to be incorrect.

On the other hand F_o could be independent of d, a situation that, for example, could be a result of the flux being controlled by the rate of collisions of oxygen molecules (or atoms) with the particle's surface. In this case Equation (14) may be multiplied by d, giving:

Table 6. The maximum-luminosity burning time of zirconium particles in oxygen

PARTICLE DIAMETER (MICRONS)	MEASURED SPEAR POINT TIME (MILSEC)	CALCULATED[a] MAXIMUM LUMINOSITY TIME, t_b (MILSEC)	t_b/d DATA (SEC/CM)	AVERAGE VALUE (SEC/CM)	t_b/d^2 DATA (SEC/CM^2)	AVERAGE VALUE (SEC/CM^2)
303	109	74	2.443	2.410	80.62	79.53
	107	72	2.377		78.44	
393	142	83	2.116	2.351	53.84	59.83
	151	92	2.345		59.67	
	153	94	2.396		60.96	
	159	100	2.548		64.85	
478	180	93	1.945	2.164	40.68	45.28
	184	97	2.028		43.43	
	197	110	2.300		48.12	
	201	114	2.383		49.87	
524	209	104	1.992	2.208	38.02	42.14
	210	105	2.011		38.38	
	214	109	2.088		39.84	
	226	121	2.317		44.21	
	231	126	2.412		46.03	
	232	127	2.431		46.39	
647	270	111	1.708	1.760	26.40	27.20
	273	114	1.754		27.16	
	277	118	1.816		28.07	

a Equation 12

$$\frac{t_b}{d} = \frac{\rho w_b}{6F_o} - \frac{d}{24D}\left[\left(\frac{2r}{d}\right)^2 - \frac{3}{5}\right] . \quad (15)$$

In this case t_b/d is predicted to have a linear dependence on d. The calculated values of t_b/d also are listed in Table 6 and are plotted in Figure 14. The latter exhibit includes both the average values and the actual data for each particle size. The data seem to fit the predicted linear dependence on d. Hence it is concluded that the oxygen flux F_o, is independent of particle size, and that therefore the maximum-luminosity burning time, t_b, is a linear function of particle diameter.

The correlations of t_b for burning zirconium in oxygen as illustrated in Figure 14 may be represented analytically:

$$t_b = d(3.03 - 18.17d), \text{ seconds}, \quad (16)$$

where d is in centimeters.

This prediction of the burning time of small particles of zirconium, based on data only for large particles, must be accepted with caution. The experience with aluminum illustrates the potential danger. The combustion of aluminum particles has been studied by many experimenters, each considering only a relatively narrow range of particle sizes. Their results indicated that burning time depended on d_o (d_o is initial particle diameter), with each experimenter's value of n lying between one and two. However, as shown in Figure 6, if all experiments are combined, n = 2 seems to be the best choice.

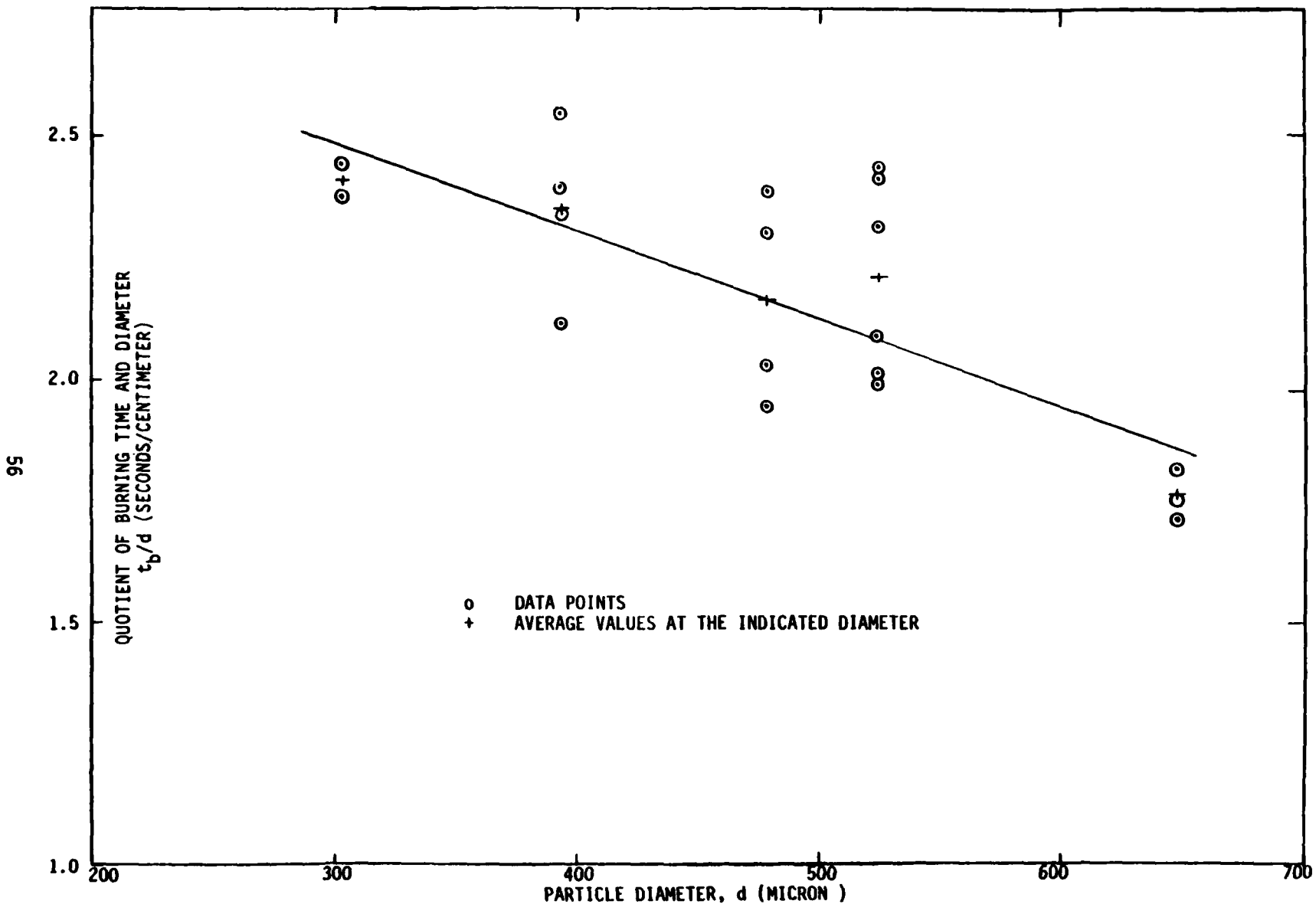

Figure 14. Correlation of maximum-luminosity burning times for zirconium particles in pure oxygen

SECTION 4
METAL POWDER-OXYGEN FLAMES

This section presents a description of the aluminum-oxygen flame of SAI's TRS as it was configured in 1983. The description is based on observation of photographs which provide insights regarding the fluid dynamics of the flame. Additionally a short description of some earlier work on aluminum powder-oxygen flames at Temple University during the mid-1950s is provided for comparative purposes.

4.1 Structure of the Flame of the Present TRS

Figure 15 is a schematic diagram of the TRS flame. The diagram was reproduced from photographs using the luminous boundry of the TRS flame as a guide. It may be divided into three zones which can be clearly distinguished in most photographs of the flames. The lowest zone, 1 in the figure, corresponds to a sharply angled expansion of the luminous region just above the TRS nozzle. Through recent measurements made during March and April of 1984, it seems clear that this apparent rapid expansion of the flame is pressure driven, and the aluminum-oxygen mixture is forced into the surrounding air. (17) The pressure measured at the mouth of the nozzle is about 30 psi and is caused by the rapid vaporization of liquid oxygen, partly from the sensible heat of the aluminum powder and partly from combustion.

It may be readily calculated that with 30 percent excess oxygen, the sensible heat in the aluminum powder above the boiling point of liquid oxygen (about 90°K) is sufficient to vaporize about two-thirds of the liquid oxygen. The heat of vaporization of liquid oxygen at its boiling temperature, 90.2°K, is 50.98 cal/g. (4) The sensible heat of aluminum above this temperature, assuming an initial temperature of 298°K (77°F) is 37.7 cal/g. Since in the present TRS the overall stoichiometry of the flame is 30 percent excess oxygen, the flame contains 1.16g of oxygen per gram of aluminum. Hence the ratio of the sensible heat in the aluminum powder to the heat of vaporization of oxygen is $37.7/(1.16 \times 50.98) = 0.638$.

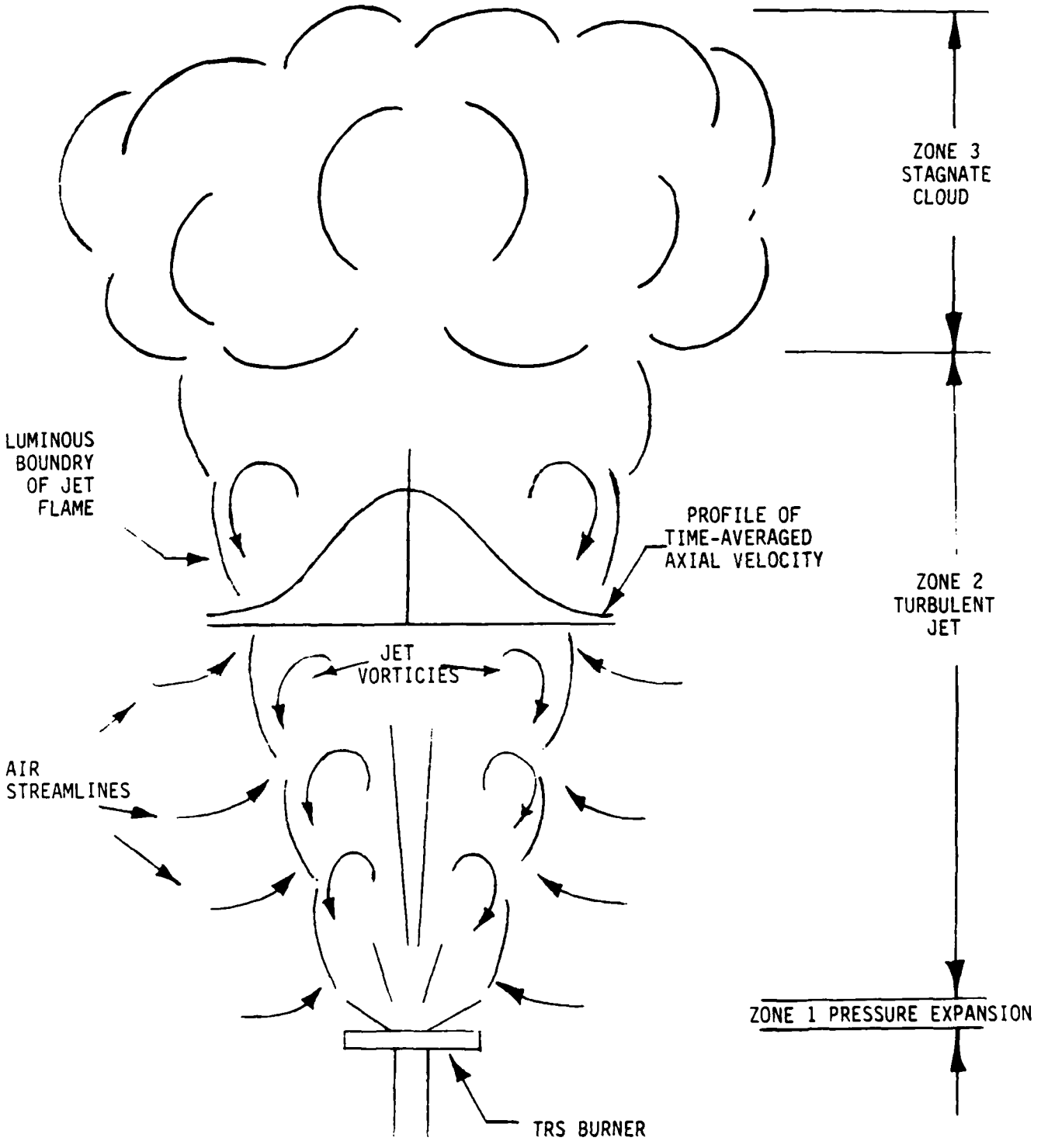

Figure 15. Flow characteristics in a TRS aluminum lox flame

The second zone extends to a height of 3 to 6 meters above the first, depending on the mass flow rate of aluminum and oxygen, and, as defined by the luminous boundary of the flame, expands from about 0.5 meters in diameter at the bottom to 2 to 3 meters at the top of this zone. The expansion characteristics of this zone are similar to those commonly observed in turbulent jet flames. The expansion is a result primarily of the entrainment of air.

The third zone is the large opaque cloud above the spreading jet. The entrainment of air in the second zone results in a decreased average velocity of the jet, and eventually sufficient air is entrained to reduce the upward velocity of the jet to a minimal value. Additionally, the entrained air lowers the temperature of the combustion products. The lowered temperature together with the high loading of particulate aluminum oxide results in a cloud with a neutral or negative buoyancy. The net result is the stagnation of the combustion products in what is observed as a relatively slowly expanding cloud above the TRS flame.

Most of the radiation from the TRS arises from the second zone of the flame. Stopped-down photographs of this region indicate a high degree of non-uniformity, with respect to luminosity, and calorimeter measurements indicate a decreasing level of radiative flux from the bottom to the top of the zone. (17) Although no other measurements have been made, these features together with the expansion, noted above, suggest a typical turbulent jet. In such jets, as is well known, the time averaged velocity in the axial direction decreases from the center to the periphery of the jet as shown schematically in Figure 15. (18) This region of velocity gradient, of course, is due to the entrainment of air as mentioned above, and constitutes a free shear-layer in which vorticity is being generated by the shearing action. Hence, if it were available, an instantaneous measurement of velocity would show a set of ring-like structures (vortex rings) surrounding the jet, containing mixtures of air and combustion products moving downward at the periphery relative to the average central flow. (19)

The implication of this dynamical behavior is that the hot regions of the jet flame are shielded by a relatively cold cloud of particulate aluminum oxide. Moreover, if the particles are small, the average opacity is expected to be high. However, because of turbulence and the circulation about the vortex rings, the thickness of the shield will appear to fluctuate as the appearance and disappearance of luminous regions. Time averaged, the entrainment of air and the lowered velocity result in a thickening of the cool particulate cloud from the bottom to the top and, as observed, a corresponding decreasing level of radiative flux from the bottom to the top.

This is an admittedly qualitative understanding of the TRS flame, and it is based on a minimum of quantitative measurements. However, the "picture" appears to be a reasonable working hypothesis in view of the detailed knowledge available for turbulent gas jets and flames, in general. Following this "picture", "cures" for the low performance of the present aluminum fueled TRS immediately suggest themselves and are discussed in Section 6.

4.2 Temple University Aluminum-Oxygen Torch

Under the sponsorship of the Navy, Army, and the Air Force, each at various times, Grosse and his colleagues at the Research Institute, Temple University, experimented with metal powder-oxygen flames. (20) Most of their work, described in published reports, dealt with aluminum powder. The flames were generated by metering aluminum powder into a flow of oxygen gas and igniting the mixture as it flowed from the end of a tube. The flame produced was similar to that of an ordinary Bunsen burner.

The metal powder was metered by a screw conveyer which in turn was fed by gravity from an inverted conical tank which held the powder. The screw conveyer discharged the powder into a stream of oxygen which entrained the powder. The burner consisted of a short length of pipe through which the metal powder-oxygen dispersion flowed. Ignition was accomplished at the mouth of the burner (the open end of the pipe) by a coaxial pilot flame consisting of a fuel gas such as propane, acetylene, hydrogen, or carbon

monoxide. Typically, the metal powder dispersion ignited within a short distance from the open end of the pipe, and a flame was produced with a "bright" zone and then a diffuse zone, further away. Figure 16 shows schematically the burner and the flame structure.

The burner diameters used ranged from 0.125 to 1.0 inch. The flow rates of metal powder ranged from 50 to 550 g/min. The flow of pilot flame fuel gas typically was about 14 l/min (about 0.25 g/sec when propane was used). Many metal powders were burned in this device including magnesium, iron, manganese, silicon, titanium, zirconium, and calcium, in addition to aluminum. Most of the experiments were performed with aluminum.

Typically the metal powder-oxygen dispersions ignited at the mouth of burner, although with some metals and at a high flow velocity, ignition appeared to be at a distance of up to 4 inches. The bright portion of the flame varied from 1 to 12 inches in length and its diameter from 0.5 to 3 inches, depending on the rate of feed of metal powder (and presumably therefore the velocity of the dispersion). A photograph of an aluminum-oxygen flame in Reference 19 indicates that a ratio of about 22 for the length of the bright flame zone to the burner diameter can be attained.

Grosse also determined the blow-off and flash-back velocities of aluminum powder-oxygen flames in his burner. At a pilot gas rate of 14 l/min, the flash-back velocity with Alcoa 10 aluminum powder (average particle size 17 to 24 microns) was 20 ft/sec (6.1 m/sec). With an aluminum powder of smaller size, Reynolds 400 (4 to 6 microns), the flash-back velocity was about 100 ft/sec (30.5 m/sec). The corresponding blow-off velcities were 300 ft/sec (91.5 m/sec) and 975 ft/sec (297.4 m/sec), respectively. The combustion efficiency was reported to be very poor for flames near the blow-off limits. As also would be expected, it was reported that the rate of flow of the pilot gas affects these limits but no quantitative data were presented.

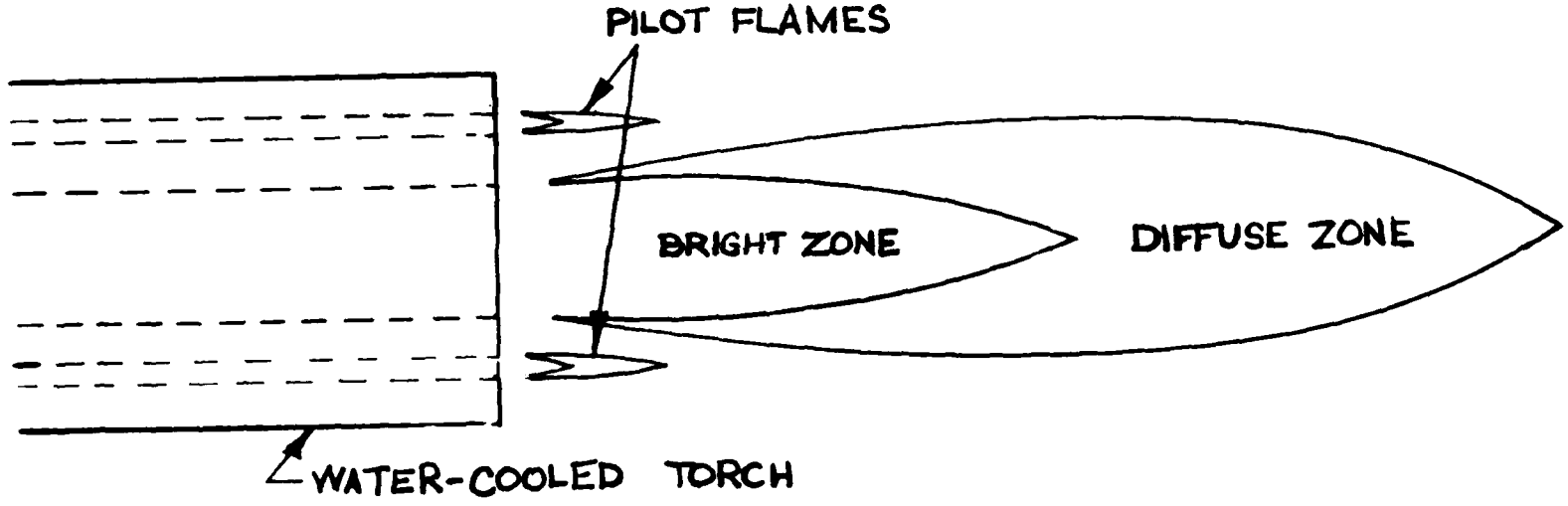

SOURCE: REFERENCE 20

Figure 16. Powder metal-oxygen flame burner

SECTION 5
THERMAL RADIATION FROM METAL POWDER FLAMES

This section presents a discussion of some measurements and certain theoretical aspects of the radiative properties of metal powder flames. The measurements consist primarily of reported data on various types of photoflash bulbs. The theory deals with the interrelationships between the radiative power and height of a flame on the one hand, and the size, concentration and emissivity of a flame's particulate matter and a flame's thickness and velocity, on the other hand.

5.1 The Radiative Properties of Photoflash Bulbs

Commercial photoflash bulbs are an inexpensive source of high color temperature radiation. Their purpose is to provide a source of visible radiation approximating the sun for photographic purposes. In this respect photoflash bulbs bear some similarity to a TRS.

More importantly, however, the commercial development of photoflash bulbs has led to the use of the combustion of aluminum and zirconium with oxygen. Although zirconium is more expensive than aluminum and produces about one third less light per unit weight of metal, it is a favored metal, partly because it provides a higher color temperature and partly because zirconium flash bulbs can operate properly at a lower pressure of oxygen.

The light-production characteristics of aluminum-filled photoflash bulbs have been studied in several investigations. (5, 21, 22, 23) Rautenberg and Johnson studied the spectral characteristics of aluminum ribbons at low total pressures of oxygen. (21) In both cases, strong emission from AlO was observed. However in flash bulbs, this emission which occurs initially, becomes submerged in a continuum spectrum as the intensity of the flash builds towards its peak. The duration of the flash typically is 10 to 20 millisec. Rautenberg and Johnson concluded that the flash closely approximates black body radiation over most of its

duration. Their principal evidence for this was a comparison of the brightness and color temperatures of standard aluminum-filled flash bulbs. They estimated the brightness as the average over the entire projected bulb area and found it to range between 3200 and 3450°K for General Electric bulbs. They believed that their estimates were low because high-speed, stopped-down movies of flash bulbs clearly show that the luminous reaction fills only about two-thirds of the projected area of the bulb. They estimated the color temperature to be about 3800°K, which at the time was the accepted value for the boiling temperature of aluminum oxide.

Bracco and Weisberger made definitive measurements of the color temperature of two types of aluminum-filled photoflash bulbs. (22) They measured the relative intensity of the total emitted radiation over the spectral range of 0.34 to 0.76 microns using special photographic emulsions. The relative intensities were fitted by a least squares proceedure to derive a "best-fit" effective black body temperature. The small Sylvania M-2 flash bulbs (output, 7500 lumen-seconds) had a color temperature of 4008 $\pm$ 76°K. The effective black body radiation at longer wave lengths was not determined.

According to Nijland and Schroder of the N.V. Philips Gloeilampenfabrieken, the reaction of aluminum with oxygen in photoflash bulbs can yield up to 680 lumens-seconds/mg of metal. (23) They also presented data for relating lumens of visible radiative power to the total radiative power from a black body. Assuming a black body temperature of 4000°K, the ratio is about 56 lumens per watt. Thus the total radiation from the combustion of aluminum with oxygen, during the useful period of the flash, is about (680/(56 x 4.18))1000 = 2900 cal/g. This is only about 75 percent of the 3800 cal/g predicted, based on Figure 1 (see the discussion in Section 3.2.). The difference may be the result of the use of less than a stoichiometric amount of oxygen in aluminum-filled flash bulbs.

The spectral and energy characteristics of zirconium filled photoflash bulbs also have been studied. (22, 23). In addition to aluminum-filled flash bulbs, Bracco and Weisberger also measured the color temperature of two zirconium flash bulbs using the same techniques. They obtained a value of 4447 $\pm$ 83°K for the M-3 bulb (output, 16,000 lumen-seconds) and 4480°K $\pm$ 142°K for the small AG1 (output, 7000 lumen-seconds). The authors noted that the zirconium measurements gave a greater dispersion and in particular a very high equivalent black body temperature of 6737°K was obtained for the region of 0.64 to 0.76 microns. They ascribed this dispersion of measurements to contributions of bands from the molecule ZrO.

Nijland and Schroder performed an extensive investigation of the energy available for radiation in a zirconium-filled flash bulb. (23) As the result of many measurements they determined that the maximum visible output is 450 lumen-seconds/mg of zirconium. They also concluded that the radiation from zirconium flash bulbs approximates that of a black body between 4000 and 5000°K, based on spectral measurements which were not described in Reference 20. Assuming a black body temperature of 4400°K, there are approximately 67 lumens per watt of total radiation. Hence the radiated energy form a zirconium flash bulb during its useful flash period is $(450/(67 \times 4.18))1000 \approx 1610$ cal/g, which is in excellent agreement with the value derived from Figure 3 (see the discussion in Section 3.2.

Pertinent to a HTRS, these authors point out that the net output of light depends on the surface area of the bulb per unit weight of zirconium in the bulb. As zirconium burns, zirconium oxide condenses on the cold glass wall of the bulb. This layer absorbs radiation form the remainder of the burning zirconium and thereby reduces the output to a value below the maximum (ie. 450 lumen-seconds/mg). An analogous mechanism will operate in a TRS when cold air mixes with the combustion products and results in the condensation of relatively cold particles of oxide.

The above described results, although on a small scale, strongly support the feasibility of a HTRS, that a high color temperature with corresponding high levels of radiative flux can be realized via the

combustion of aluminum and zirconium with oxygen. Nijland's results, especially, indicate that nearly the theoretical energy is radiated during the combustion of these metals, when the combustion is protected from other modes of energy dissipation.

5.2 Optical Properties of Dispersions of Metal Oxide Particles

As will be discussed in the following subsections, theoretical arguements and fundamental data support the data from photoflash bulbs and the projection of those data to large-scale combustion devices.

5.2.1 Absorbtion and Scattering Coefficients

The combustion of metals with oxygen produces radiation from a cloud of hot particles, and hence any portion of the metal-oxygen flame is a volume emitter. Because it is a volume emitter there are certain non-combustion related parameters which are important determinants of the radiative output. These include:

(1) Absorption coefficient in the TRS flame
(2) Scatter coefficient in the TRS flame
(3) Volume concentration of particles in the flame
(4) Dimensions of the flame volume
(5) Diameter of particulates in the flame.

The absorption and scatter coefficients are the quantities of radiation absorbed (or emitted) and scattered by a volume of differential thickness, normal to a pencil of radition. For large particles (with no negative curviture) such that $2\pi r/\lambda \geq 5$,, the absorption coefficient is

$$K_a = \varepsilon A_t/4 \quad , \qquad (17)$$

and the scatter coefficient is

$$K_s = \sigma A_t/4 \quad , \tag{18}$$

where A_t is the total particle surface area per unit volume (the product of the surface area of a particle and the number of particles per unit volume of the cloud), and ε and σ are the hemispherical material emissivity and reflectivity, respectively. (24) For smaller particles, the coefficients are complex functions of the radiation wave length, the complex index of refraction and the concentration and volume of the particles.

In a HTRS, temperatures of 3300 to 4500°K are of interest. The wave lengths corresponding to the median of the spectral energy distribution of a black (or grey body) at these temperatures are 1.24 microns and 0.91 microns, respectively. Assuming, then, that the wave length of interest is about 1.0 micron, a "large" particle for the purpose of radiation estimates is one whose diameter exceeds 1.6 microns. Combustion of aluminum may produce a substantial fraction of particles smaller than this size, whereas the combustion of zirconium will involve much larger particles as well. For the present, the validity of Equations (17) and (18) are assumed. The lack of optical data for molten oxides precludes the estimation of absorption and scattering coefficients for smaller particles.

5.2.2 Emissivities of Molten Oxides

According to Equations (17) and (18) important factors determining absorption and scattering coefficients are the particle emissivities and reflectivities. A search of the literature uncovered little quantitative information on these parameters for molten oxides. There are however data on total and spectral emissivities of solid oxides, including those of aluminum, magnesium, zirconium and titanium. The data for the spectral emissivities of solid slabs of oxide, at temperatures between 1000° and 2000°K are available in Reference (25). A notable feature of the data for the oxides of aluminum, zirconium and other white oxides is the low

emissivity in the wave length range of interest, one to two microns. As an example, Figure 17, shows this behavoir for aluminum oxide. On the other hand it is notable that the emissivity may increase as the level of impurities increases (Figure 17). The increase is even more dramatic when small amounts (eg. 1%) of a black oxide, such as nickel oxide, are added to aluminum oxide. A four-fold increase in emissivity results. It is likely that other black oxides such as ferrous oxide (FeO) would have the same effect. Although these are solid oxides, the same effects might prevail for the molten materials as well.

Carlson measured the emissivity of magnesia and alumina particles heated in a rocket exhaust. (26) The size distribution of the particles ranged from sub-micron to about 4 microns. For the alumina particles, the most numerous size was about 0.7 micron. In a temperature range of about 2000 to 2700°K, the emissivity (at λ = 0.59 micron) of the magnesia particles was about 0.4. This value is about three orders of magnitude geater than the value calculated by Mie theory for solid particles using index of refraction data at 1073°K. In the temperature range of the experiments, magnesia is a solid and the author ascribed the increase in emissivity to an unknown temperature effect.

His data for alumina are shown in Figure 18. Importantly, the emissivity of molten alumina was three orders-of-magnitude greater than solid alumina. Moreover, the measured emissivity was a strong function of temperature, increasing from about 0.01 at 2300°K to 0.1 at 2900°K. The reasons for the large increase upon melting and the strong temperature dependence are not known, but it was speculated that it is due to the increase in the number of conduction electrons. Other instances of a large increase in the emissivity associated with the melting of dielectric materials are known, but quantitative information is lacking. (26)

This result has been confirmed in other experimental work on alumina. Pendant drops of aluminum oxide, 2 to 5mm in diameter, were heated by a CO_2 laser and observed photographically and pyrometrically. (27) It was observed that the emissivity of the liquid was substantially greater than that of the solid. Unfortunately, no quantitative measurements were

Source: Reference 25

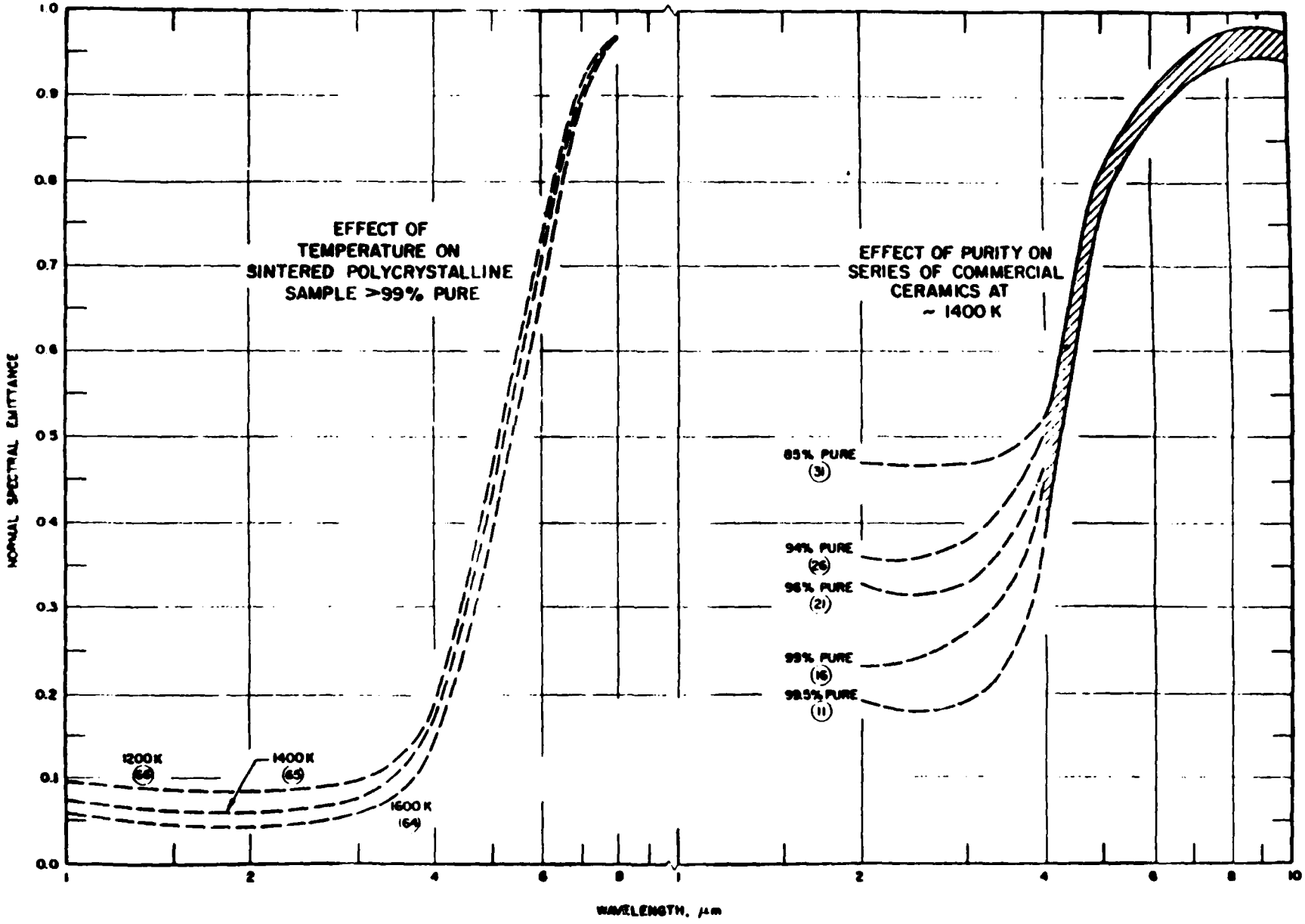

Figure 17. Analyzed · mal spectral emittance of aluminum oxide

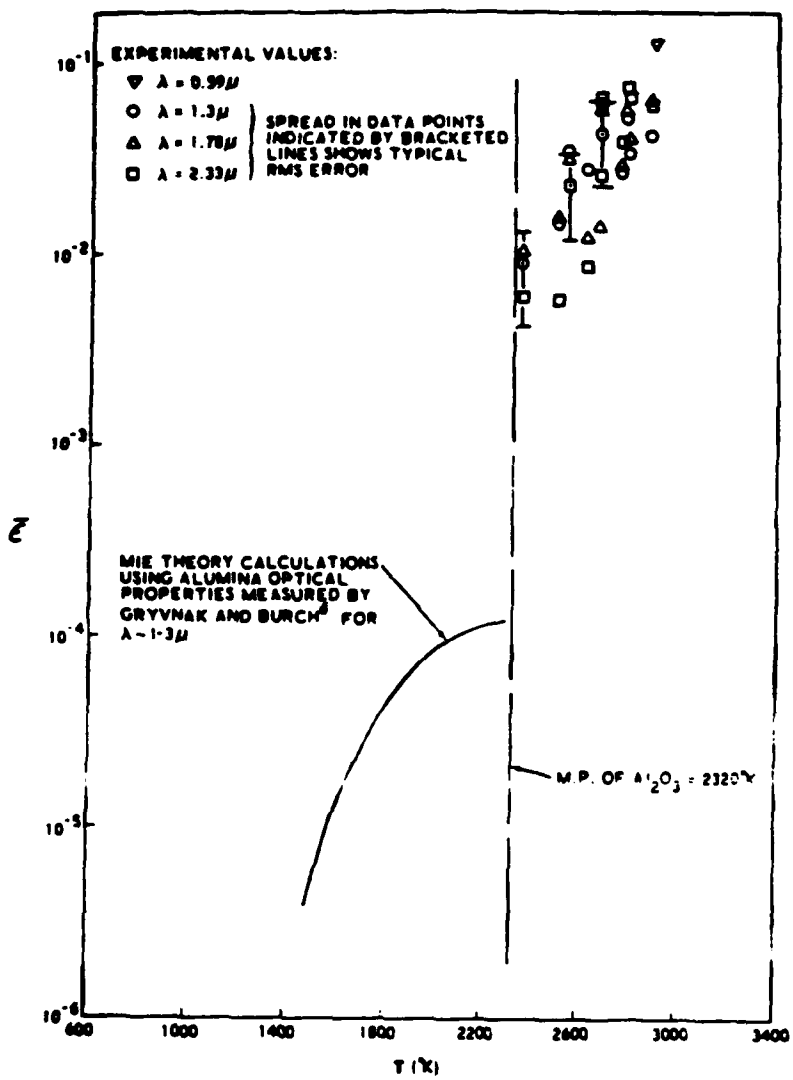

Source: Reference 26

Figure 18. Alumina emittance from rocket-engine experiments and MIE theory calculations

made. It was noted also that the emissivity of the molten oxide drops in an argon-atmosphere was about 37 percent higher than in an oxygen atmosphere. Upon cooling, the argon-atmosphere drop had a grey appearance whereas the oxygen-atmosphere drop was white. The authors ascribed the grey appearance to the formation of free aluminum metal at the surface of the argon-atmosphere drop.

In other work, aluminum oxide particles prepared with "several volume percent" of free aluminum were found to have an emissivity that is higher than that calculated by the Mie theory. (28) The author of this work concluded that it is the presence of unburned aluminum in the exhaust of rockets burning aluminum-fueled propellants which leads to IR radiation which is higher than calculated based on optical data for the pure oxide.

5.2.3 Optical Mean-Free-Path Lengths

The other factor in the Equations (17) and (18) is the total volumetric surface area of the particles, $A_t/4$, which has units of reciprocal length (particle surface area per unit volume). This quantity of course depends on the size of the particles and their volumetric concentration. An estimate of the range of its values in a TRS flame may be developed from the output of the theoretical combustion calculations described in Section 3.2. Figure 19 is a plot of the inverse of $A_t/4$, i.e. the mean absorption length for black particles, with ε=1 in Equation (17), as a function of temperature for two sizes of aluminum particles. The conditions selected are those of the products of combustion of aluminum with 30 percent excess oxygen in equilibrium at the indicated temperatures. The estimates assumed that all of the particles are of the same size and are uniformly distributed.

Not too suprisingly, Figure 19 shows that $A_t/4$ (and hence K_a and K_s as defined by Equations (17) and (18)) will vary both during combustion and as the flame gases cool. Above about 3900°K this variation is due primarily to the additional aluminum oxide which condenses from the vapor. Below about 3900°K the variation is due primarily to the decrease in gas volume with decreasing temperature. Also

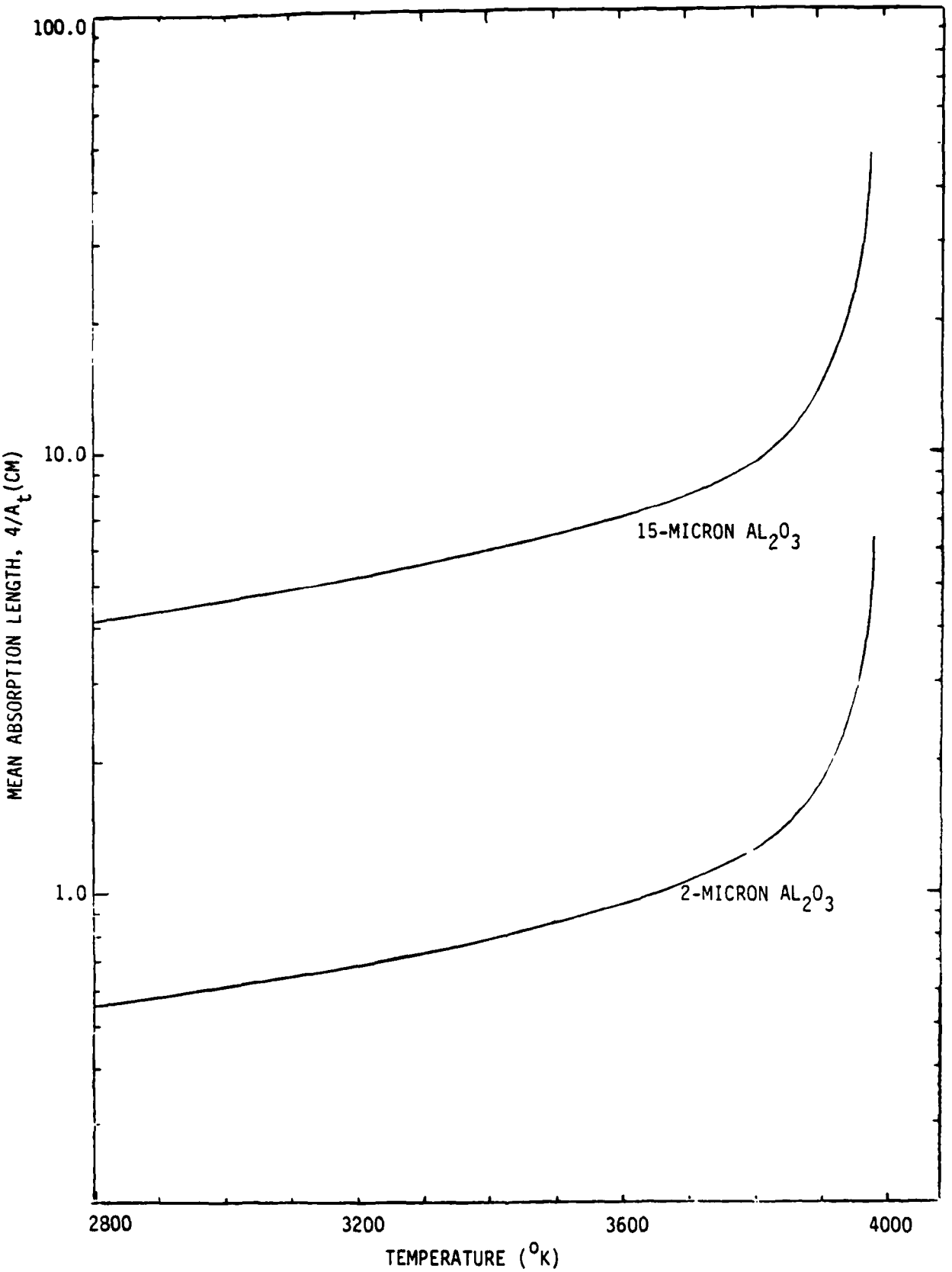

Figure 19. Estimates of mean optical absorption length in the products of combustion of aluminum with 30 percent excess oxygen

as expected, the value of $A_t/4$ decreases directly with particle diameter, since, for a given mass of particles per unit mass of flame gases, the number concentration of particles decreases inversely with the cube of particle diameter, whereas the area of a particle increases with the square of diameter.

Clearly, particle diameter is an important parameter of radiation output of an aluminum-oxygen flame. Figure 19 shows that if the particles of aluminum oxide are small and their emissivity is high (0.5, say), then only the outer edges of the flame are the effective radiators. For example, if the flame contains 2-micron particles of aluminum oxide and the edge of the flame is at 3300°K, Figure 19 and Equation (17) indicate that the optical thickness or mean absorption path length is $1/K_a$ = (1/0.5) (0.73) = 1.5 cm. The relatively high emissivity of 0.5 is suggested by an extrapolation of Carlson's measurements to above 3000°K. If the extrapolation is approximately correct, then the radiation from the flame arises from a relatively thin layer of particles whose temperature is somewhat above 3000°K.

As the outer layers cool to below 3000°K, the particle emissivity decreases to a value of 0.1 or less, and from Figure 19, assuming a temperature of 2900°K and 2-micron particles, $1/K_a$ = (1/0.1) (0.68) = 6.8 cm. Thus the outermost, cooler layers of the aluminum TRS flame tend to become transparent. Actually, as cooling proceeds, K_s may increase significantly, and transmission may occur primarily by scattering.

Thus it is concluded, tentatively, that the mean absorption path for radiation in the present aluminum TRS flame is very short, much less than the flame's characteristic radial dimension (see Section 4.1). This tends to create large radial temperature gradients within the flame, and the radiation is characteristic of a layer at a temperature intermediate between the cooler outside edge of the flame and its hot core. Radiation from the hotter core of the flame is effectively blocked out. The following subsection presents a theoretical calculation of the radiation and this "blockage" effect.

5.2.4 Estimated Radiative Power of an Ideal Aluminum-Oxygen Flame

Radiation from a cloud of hot particles was analyzed in order to:

- determine the effect of optical mean-free-path upon the level of radiative flux and
- determine the trends of the effects of cooling of the periphery of the cloud, as occurs around the present TRS flame because of mixing with ambient air (see Section 4.1).

To make the analysis tractable, but yet retain sufficient detail to illustrate the effects of particle size and cooling of the flame surface, a semi-infinite plane slab cloud was considered in the analysis. The half-thickness of the slab was assumed to be four optical mean-free-paths. This geometry is illustrated in the upper portion of Figure 20. A portion of a cross-section of the half-slab is shown at the top of the exhibit. The slab is divided into four layers, each with unity optical thickness, i.e. $K_a L=1$, where L is the width of the layer. Since optical thickness (at constant emissivity and particle size) is a conserved quantity, the mass and therefore the heat capacity associated with the combustion products of one unit of optical thickness are constant with respect to changes in temperature.

The emissivity of the particles was assumed to be 0.7, and their initial concentration was assumed to be 0.4 mg/cc, which is equivalent to conditions in an aluminum-oxygen flame that has 30 percent oxygen in excess of the stoichiometric amount. Scattering of radiation was neglected, an omission which does not produce severe errors over a few mean-free-paths at high values of particle emissivity.

Radiant flux from the surface of the slab cloud was calculated as a function of time for four assumed initial temperature profiles and two particles sizes. The temperature profiles also are shown in the upper portion of the exhibit. The results have been plotted in the figure as

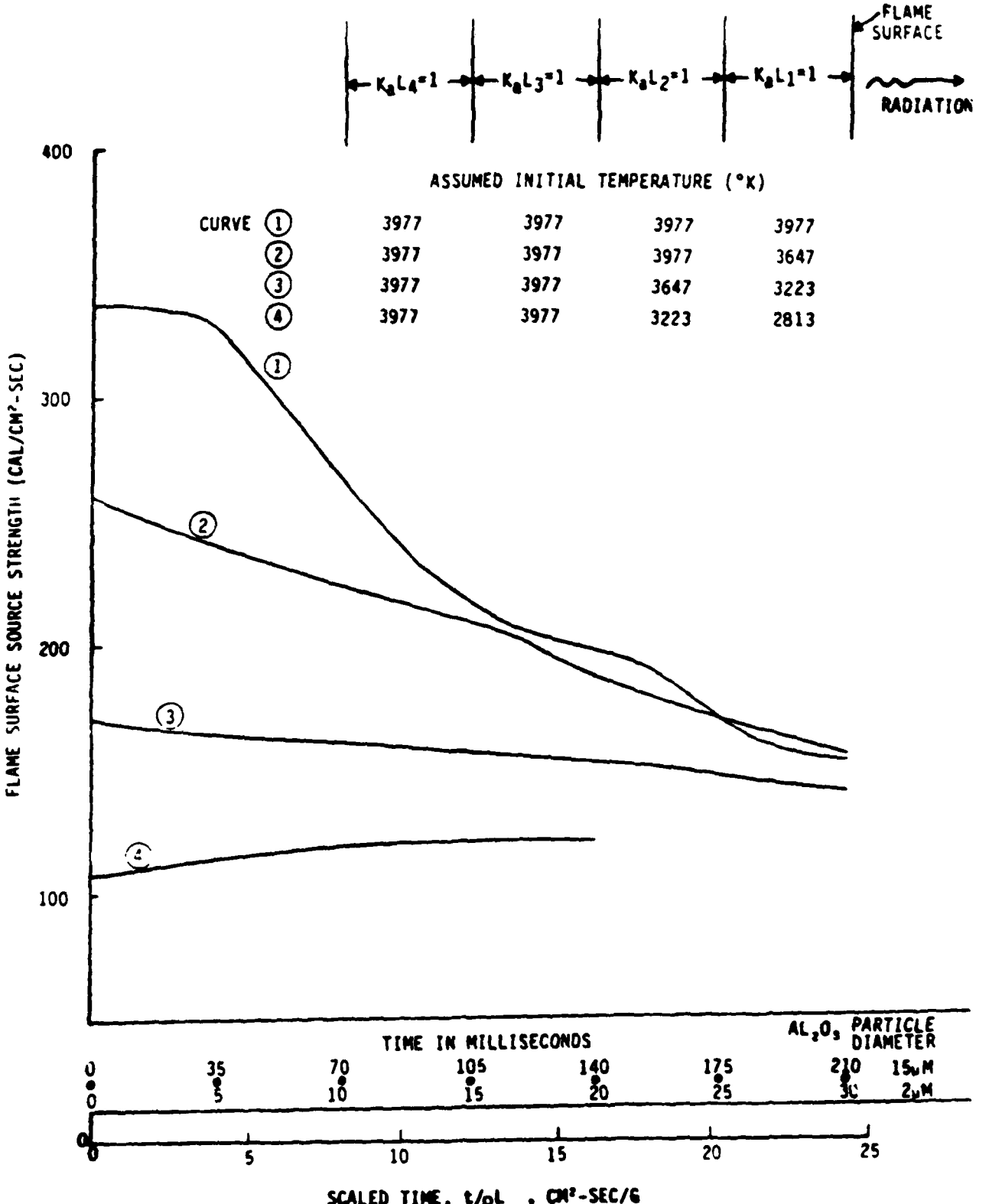

Figure 20. The effect of air dilution on radiation from slab flame of aluminum and oxygen of half-thickness of four optical mean free path-lengths (Grey, non-reflective particles)

four curves corresponding to each of the assumed temperature profiles. The particle size effect is shown as a change in the time scale. The initial temperature of 3977°K assumed for much of the cloud, is the adiabatic combustion temperature of aluminum with 30 percent excess oxygen. Combustion is assumed to be complete before radiation begins. This is an approximation which is justified because of the very short burning time, less than one millisecond, predicted for 15-micron particles.

The curve labeled 1 in the figure shows the radiative flux when the periphery of the cloud is not cooled by other mechanisms such as mixing with cold ambient air. The radiative flux exceeds 200 cal/cm^2-sec for about 20 milsec for 2-micron particles and 140 milsec for 15-micron particles. The reason the cloud with larger particles can maintain a higher flux for a longer period of time is simply a result of the fact that the longer optical path length allows more of the mass of the cloud to contribute to the radiation from the surface. The greater mass has a greater heat capacity and, hence, a greater capacity to sustain high levels of flux.

The other curves demonstrate the adverse impact of peripheral cooling of the cloud before and during combustion of the aluminum powder.

A calculated temperature history of the slab flame is shown in Figure 21. The temperature history corresponds to curve 1 in Figure 20, the uniform initial temperature profile. Figure 21 illustrates how quickly steep temperature gradients are developed by radiation at the periphery of a hot cloud of absorbing particles. This of course is responsible for the rapidly decreasing radiative flux as indicated in curve 1 of Figure 20.

This analysis assumed a luminous slab flame such that there is no mixing of combustion products between layers. As discussed in Section 4.1, the TRS flame is surrounded by a turbulent free shear layer with

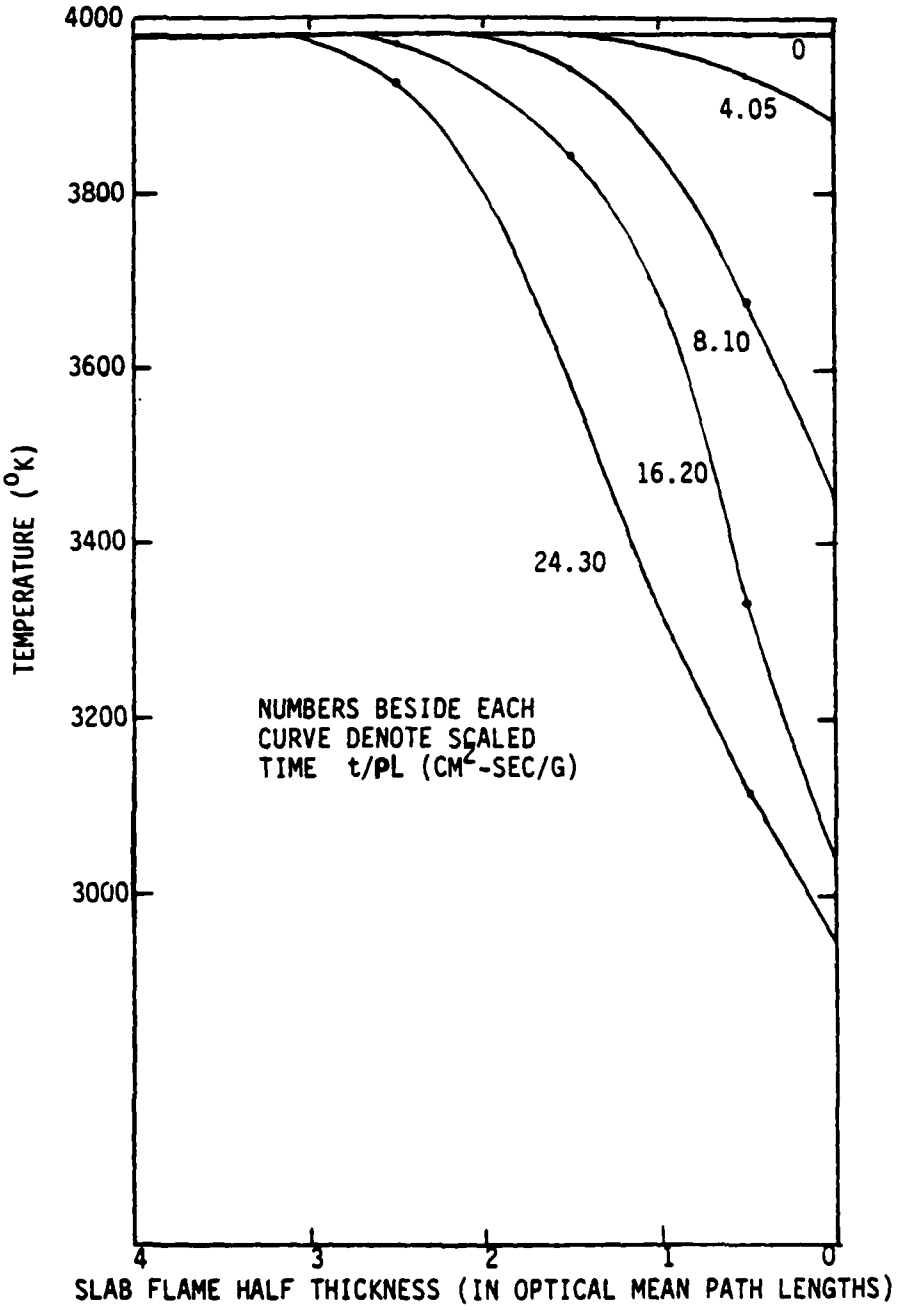

Figure 21. Temperature profiles in a theoretical aluminum-oxygen slab flame

large toroidal vorticies about the flame. These will, on the one hand, circulate hot material to the surface of the flame, tending to maintain a high surface temperature for a longer period time than is suggested in Figure 21. On the other hand, these same toroidal vorticies draw-in cold air and mix it with and cool the hot combustion products. Thus by the time the hot material is circulated to the "surface" of the flame it already has an established temperature gradient, perhaps as indicated in curves 2 through 4 in Figure 20. Hence, the net expected result of the turbulence is a decreased level of radiation.

5.2.5 The Height of a Metal Powder-Oxygen TRS Flame

The importance of the duration of the radiation (abscissa in Figure 20) stems from the usual need for a long or tall flame of uniform surface flux for a TRS. For a given level of flux, Q, the height h, of a TRS flame depends on the optical thickness, $1/K_a$, the velocity of the combustion products (in direction of h), v, the density of the combustion products, , and their decrease in specific enthalpy, ΔH. To a first approximation the interrelation of these quantities for a planar flame may be expressed in the simple equation

$$h = \frac{v \rho \Delta H}{K_a \dot{Q}} . \qquad (19)$$

This equation may be derived by equating the energy radiated over the height, h, to the decrease in enthalpy of the combustion products at a depth, $1/K_a$.

Thus, if the other values of the variables are constant, the flame height, h, can only be increased by increasing the velocity. However, v cannot be increased without limit; it cannot exceed the "blow-off" limit of the flame (see Section 4.2). Hence it is desirable to be able to decrease K_a (increase the optical mean free path) and/or increase ρ. For an aluminum-fueled TRS, the value of K_a might be decreased through encouraging the growth of larger particles of aluminum oxide. This, in turn, might be accomplished by preventing the mixing with cold ambient air, which favors high rates of nucleation and formation of small

particles of liquid oxide. Also, by burning a mixture of large and small aluminum particles, the rate of burning and therefore the rate of production of aluminum oxide is slowed, compared to the case for small aluminum particles alone. This will tend to cause the growth of larger oxide particles. For a zirconium-fueled TRS, K_a might be decreased simply by burning larger particles. Finally, the value of ρ may be increased somewhat, by reducing the oxygen-to-fuel ratio for example. However this approach is limited because of the obviously adverse effect on the flame temperature and hence ΔH and $\dot{Q}$.

SECTION 6
DEVELOPMENT OF A HTRS

The preceding discussion of the combustion characteristics of aluminum and zirconium, factors which control radiation from clouds of particles and the dynamics of jet flames suggest approaches for achieving the HTRS performance goals. These have been formulated into six techniques which are discussed in greater detail in the following paragraphs. The strategy of recommended experimental research to explore, develop and implement these techniques is discussed subsequently.

6.1 Six Techniques for a HTRS

The six techniques for increasing the radiative output of a HTRS are discussed in the order of their likely importance. The techniques are summarized in Table 7.

The first two techniques are alternative types of coaxial flows of gas around the TRS flame. Their purpose is to reduce or to eliminate the layer of cold particulate matter which blocks out the higher temperature radiation coming from the interior of the flame. The remaining techniques consist of chemical and physical alterations of the metal-oxygen flame itself, such as the use of zirconium powders as the fuel.

It is to be emphasized that the six techniques are not alternatives. Indeed they are, for the most part, mutually supporting. For example, it is likely that the use of a cold gas or a hot gas envelope will be essential. A cold oxygen envelope may be sufficient for a zirconium HTRS. Although a cold gas envelope is expected to be significantly beneficial for an aluminum TRS, a hot gas envelope is likely to be necessary for reaching the performance goals. The effects of mixture ratio and particle size on the emissivity and flame height of an aluminum TRS likely will be significant, but may not be discernible without a cold or hot gas envelope.

Table 7. Techniques for achieving the HTRS performance goals: color temperature 4000°K and radiative flux exceeding 160 CAL/CM^2 - SEC

TECHNIQUES	DESCRIPTION	EXPECTED BENEFITS
1. Cold Gas Envelope	The TRS flame is encircled by a wide stream of air or oxygen whose velocity matches, approximately, the velocity of the flame.	Shielding of radiation by cold particles at the surface of the flame is greatly reduced; also, a more slender and taller flame is expected.
2. Hot Gas Envelope	A fuel gas such as propane or cyanogen is burned in an oxygen envelope to heat it to 2200° to 4500°K.	Cooling of flow by cold ambient air is prevented and shielding of radiation by cold particles at the surface of the flame is prevented
3. Zirconium Powder Fuel	A powder of zirconium particles is burned with oxygen.	Flame with a color temperature exceeding 4200°K and a correspondingly high level of radiative flux is expected.
4. Fuel-Rich Mixtures	Mixtures, which have less oxygen than is stoichiometric for the metal oxide, are burned in the flame.	Possibly can produce aluminum and zirconium HTRS flames with improved optical characteristics.
5. Powder Particle Size	A powder with large and small particles is used as the fuel.	For the aluminum TRS, this may improve the optical properties of the flame by allowing the growth of larger oxide particles.
6. Additives	Iron or nickel, which form black oxides, and/or carbon monoxide, carbon dioxide or nitrogen are added to the fuel.	The emissivity of the particles of oxide in the TRS flame may be increased.

These six techniques are not the only ones for improving the overall performance and applicability of a TRS. There are others and two of these, a TRS that is focusable and whose radiative output can be arbitrarily shaped as a function of time, are mentioned in Section 6.2.3.

6.1.1 Cold Gas Envelope

In order to eliminate the accumulation of the slower moving sheath of cold oxide particles (see Section 4.1), a high-velocity envelope of air or oxygen could be employed to maintain the upward momentum of the periphery of the jet flame. This is illustrated in Figure 22. By matching the velocity of the gaseous envelope with that of the jet flame, the shear layer at the flame periphery could be essentially eliminated, and as a consequence, the rate of mixing of the flame combustion products with the ambient air could be minimized. This is expected to result in:

- a reduced rate of heat dissipation by entrainment of cold air
- a reduced rate of spreading of the jet flame
- and as a result of these, a flame which produces a higher flux and is taller.

The height to which the gaseous envelope may be expected to "protect" the flame is limited by its own loss of momentum as it entrains ambient air. This height will depend on the thickness of the envelope (true for turbulent jets as expected to be the general case here). (18) The relationship between protective height and the thickness of the envelope will have to be determined by experiment, but the height should be at least 8 to 10 times the width of the envelope's nozzle.

An advantage of using oxygen rather than air as the envelope gas is that mixing of the burning metal powder with nitrogen can be avoided. The presence of nitrogen can have adverse affects on the combustion of metal powders as discussed in Sections 3.3 and 3.4.

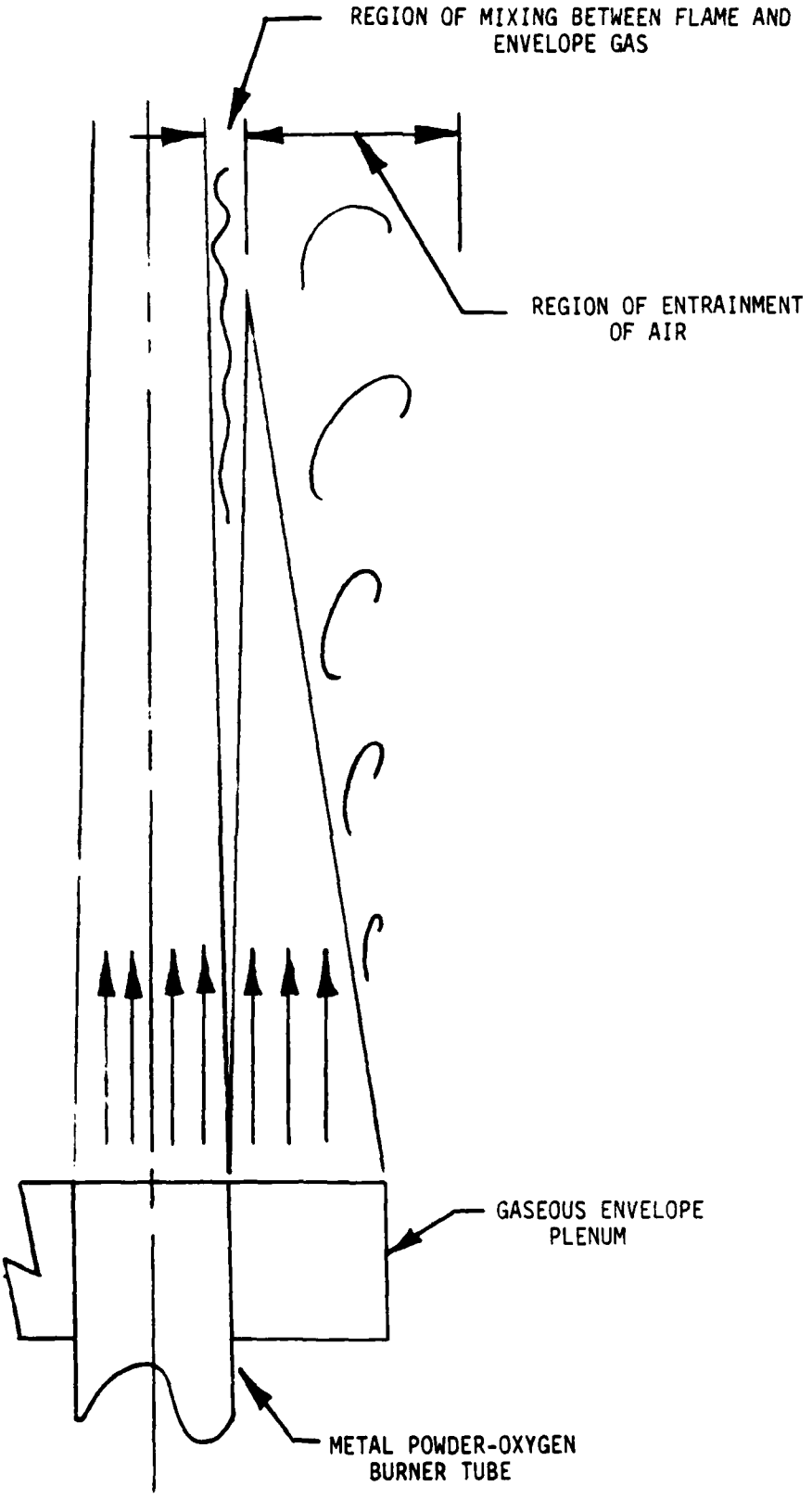

Figure 22. Diagram illustrating how a gaseous envelope can protect and reduce spreading of a TRS flame

6.1.2 Hot Gas Envelope

The gas envelope technique can be carried further by heating the air or oxygen envelope and thereby either reducing or eliminating the cooling of the flame periphery by mixing. The heating is easily accomplished by burning a fuel gas, e.g. carbon monoxide, methane, propane, etc., in the envelope. If air is used in the envelope, the maximum temperature achievable in this way will be about 2200°K, still considerably below the combustion temperature of aluminum and oxygen. Nevertheless, some beneficial effect should be observed. However, if the air is replaced with oxygen, then the temperature of the envelope can be increased to about 3200°K, and very little heat loss from the jet flame via mixing will result. Finally, the energy of the fuel can be increased still further by using a fuel gas such as cyanogen, and with oxygen, the temperature of the envelope may be boosted to over 4500°K. The use of cyanogen and similar gases may not be desirable however because of their cost (about $50/lb) and their toxicity.

Burning any of the above mentioned fuels produces essentially transparent combustion gases (except for some line absorption), and hence little or no dimming of the radiation from the TRS flame is expected by this mechanism.

6.1.3 Zirconium Fuel

The third technique is to use zirconium as the fuel. Although more costly than aluminum, and perhaps more difficult to handle, it does have the potential of achieving higher levels of both radiative flux and color temperature. Moreover, since much of the radiation arises from the burning particle itself, optical thickness and flame length are expected to be easier to control. However, as with aluminum, it probably is desirable to "protect" the zirconium-oxygen flame with an envelope of cool or perhaps hot oxygen. This has two purposes, first to prevent undue dissipation of combustion energy and second to prevent the shielding of radiation by a layer of zirconium oxide smoke, as in the case of aluminum flames.

Heating an oxygen envelope may not be as beneficial as for aluminum since, as shown in the single particle experiments, a high level of radiative flux is generated by zirconium particles burning in cold oxygen.

6.1.4 Fuel Rich Mixtures

The jet flame may be formulated to be fuel-rich. In this mode, the burning rate of the aluminum powder and/or the rate of condensation of metal oxide might be controlled to some extent, permitting the growth of larger aluminum oxide particles. This in turn could lead to increased flame height. Also, the emissivity of aluminum oxide particles may be enhanced if unburned aluminum condenses in the oxide (see Section 5.2.2).

6.1.5 Powder Particle Size

The fifth technique, also intended primarily for the aluminum TRS, is to use a wide size distribution of aluminum particles as the fuel. The intent is to reduce the overall burning rate and to encourage the growth of larger particles of aluminum oxide. As explained in Section 3.3 and 5.2.5, this is expected to increase the effective length of the radiative flame.

6.1.6 Additives

The sixth technique also is intended primarily for the aluminum TRS and involves trying the use of additives, such as iron and nickel, which form black oxides, and gases such as nitrogen, carbon monoxide and carbon dioxide. These techniques are aimed at increasing the emissivity of the molten oxide combustion product as described in Section 3.3 and 5.2.2. The need for such techniques to improve the emissivity of a zirconium-oxygen flame is yet to be determined.

6.2 Recommended Development Strategy

An experimental investigation of the radiative properties of metal powder-oxygen flames as a function of certain controllable parameters,

which together comprise the six techniques described above, is recommended. The effect of these parameters can be studied using a laboratory-scale, cylindrical jet flame of metal powder mixed with gaseous oxygen. This geometry is recommended for three reasons. The first is that it is similar to that of the present TRS, and hence the results obtained should be directly applicable to the present TRS. Second, such flames are the simplest to create. Third, they are symmetrical and are easily studied.

6.2.1 Concept for the Experimental Apparatus

The apparatus suggested for generating the cylindrical jet flames is described below. Metal powder would be transported, pneumatically, into the base of a vertical tube where it would be thoroughly mixed with the desired amount of oxygen gas. The mixture of powder and oxygen then would flow upward and out of the tube as a jet. As the jet leaves the tube it would be ignited by a pilot flame of oxygen and propane (or other suitable fuel) created by a thin annular burner which completely surrounds the jet at the end of the tube. A thicker annular plenum would surround both the pilot burner and the tube end, and the flow of air, oxygen and their mixtures with fuel would serve to create the protective envelopes that would be investigated. Care should be exercised in the design and operation of apparatus to ensure that pressures of the jet flame and the envelope gas are at atmospheric pressure in order to obtain a smooth flow. The oxygen-metal powder mixer should be designed to ensure that mixing is complete and that the degree of mixing is not a variable in the investigation.

The above concept of the experimental apparatus has much similarity to the current TRS and should make use of that technology as is appropriate and practical. The cylindrical burner tube has already been mentioned, but the major item of common experience is the pneumatic technique for metering and flowing the metal powder. One area of difference is that gaseous rather than liquid oxygen would be used. This is expected to simplify both the experimental procedures and the attainment of a uniform mixture of metal powder with oxygen. Mixing with liquid oxygen,

AD-A162 163 HIGH-TEMPERATURE THERMAL SIMULATOR(U) SCIENCE 2/2
APPLICATIONS INTERNATIONAL CORP MCLEAN VA
J A SIMMONS ET AL. 20 FEB 85 SAIC-84/1715 DNA-TR-84-312
UNCLASSIFIED DNA001-83-C-0224 F/G 20/13 NL

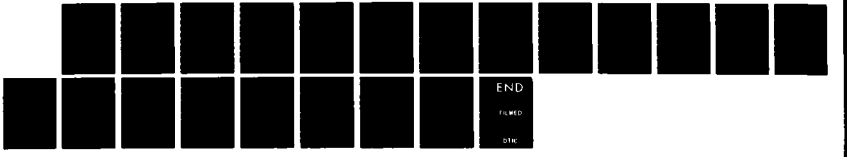

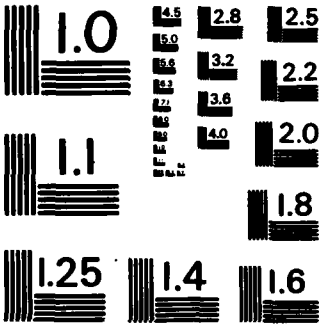

especially without a combustion chamber designed for the purpose, is difficult because the contact between the powder and liquid oxygen causes a portion of the latter to flash into vapor. This, in turn, tends to create a vapor barrier between impinging streams of metal powder and liquid oxygen and impedes their mixing.

The concept of the experimental apparatus also borrows from the work of Grosse and Conway whose work was discussed in Section 4.2. Their findings can be helpful in settling the final design of the experimental burners.

6.2.2 Parameters to Be Investigated

The parameters that should be investigated with the experimental burner described above include the following:

- Type of metal powder (aluminum and zirconium)
- Metal powder particle size
- Oxygen-powder mixture ratio
- Flame thickness (burner tube diameter)
- Powder-oxygen velocity
- Protective, gaseous envelope
  - Velocity (relative to the jet flame)
  - Thickness
  - Temperature
  - Composition
- Special Additives in the flame.

The six techniques for obtaining the HTRS performance goals should be be evaluated by varying these parameters over an appropriate range of values. Table 8 presents a matrix summarizing the variation of the parameters for each technique. The justification for the parameters and their range of values is discussed in the following paragraphs and is based on the discussions in Sections 3, 4 and 5.

The two fuels are selected on the basis of their high potential for achieving the performance goals. All of the planned testing with aluminum should be performed first before testing with zirconium. There are two reasons for this. First, zirconium, because its flames may be more optically thin than aluminum flames, may require larger diameter burners. It is desirable to gain experience with the small-diameter burners, i.e. those using aluminum, before proceeding to experiments with the larger burners. The second reason is that experience obtained with aluminum may be used to guide the more expensive (due to fuel costs) experiments with zirconium.

The particle size of the metal powders should be selected based primarily on burning rate. Based on the discussions in Sections 3 and 4, the nominal average size of the aluminum powders should range from 15 to 150 microns. Powders of the smaller size are expected to burn completely within less than one millisecond, or equivalently, within a few centimeters of the end of the burner tube, depending on flow velocities. This size would be used in most of the experiments especially those to investigate the effectiveness of the protective envelope. Powders containing larger particles would be used to investigate the effects of size including the possibility of increasing the size of the radiative oxide particles and height of the flame. For zirconium, it is anticipated that powders with a size ranging between 25 and 150 microns should be used. This choice reflects a compromise between attaining a satisfactory optical mean free path with reasonable burner diameters, 5 to 10 cm, and a sufficiently long burning time, 15 to 40 msec, for adequate flame length at reasonable jet flame velocities.

Table 8. Experimental variables for the evaluation of techniques to achieve HTRS performance goals

	APPROACHES TO PERFORMANCE GOALS					
	PROPOSED RESEARCH			FUTURE RESEARCH		
CONTROLLABLE PARAMETERS	1 COLD GAS GAS	2 HOT ENVELOPE GAS	3 ZIRCONIUM POWDER	4 MIXTURE RATIO	5 ADDITIVES	6 PARTICLE SIZE
TYPE OF METAL POWDER	Al	Al	Zr	Al	Al	Al
PARTICLE SIZE OF POWDER	15 m	15 m	25 - 75 m	15 m	15 - 150 m	15 - 150 m
OXYGEN-TO-POWDER MIXTURE RATIO	STOICH.	STOICH	50 - 130% OF STOICH.	BEST	BEST	BEST
FLAME THICKNESS (BURNER DIAMETER, D)	2.5 CM	2.5 CM	2.5	2.5 CM	5 CM	5 CM
POWDER-OXYGEN GASEOUS ENVELOPE	10 - 40 M/S	10 - 40 M/S	10-40 M/S	10 - 40 M/S	10 - 40 M/S	10 - 40 M/S
VELOCITY	75 - 150% Vf	75 - 150%Vf	BEST	BEST	BEST	BEST
THICKNESS	50 - 200%	50 - 200% D	BEST	BEST	BEST	BEST
TEMPERATURE	300°K	TO 3000°K	TO 3000°K	TO 4500°K	BEST	BEST
COMPOSITION	AIR, O_2	O_2	O_2	BEST	BEST	BEST
FUEL ADDITIVES	--	--	--	Fe, Ni, N_2, CO, CO_2	BEST	--

The mixture ratios of oxygen to metal powder that should be investigated are expected to be within the range of 50 to 130 percent of stoichiometric. Based on thermodynamics alone, the stoichiometric mixture should give both the highest color temperature and the highest radiative flux. However there are other factors which influence the radiative characteristics. The high end of the range of mixture ratios is used in the present TRS, and has been thought to be required to ensure complete combustion. On the other hand, substoichiometric ratios may have beneficial effects as mentioned in Section 5.2.2. In the case of aluminum, a substoichiometric ratio may favor the growth of larger particles of oxide and may enhance the emissivity of the oxide particles. In the case of zirconium powders with substoichiometric amounts of oxygen, the concentration of burning zirconium particles will be higher in the flame which will improve the optical thickness of small-diameter flames. Moreover, the additional oxygen needed for complete combustion may be supplied from an oxygen-containing protective envelope gas. A possible adverse consequence of substoichiometric mixtures in the jet flame is the enhancement of agglomeration of unburned particles through collisions, thereby decreasing the already low optical density in the case of zirconium.

At least two diameters of the burner should be used in the experiments, 2.5 cm and, 5 cm. Most of the experiments with aluminum would be performed with the smaller tube. This diameter is recommended based on the expectation that, for aluminum combustion, the optical thickness of a flame of this diameter will be slightly greater than unity (i.e. $K_a D > 1$). This choice also appears correct based on the fact that 2.5 cm is slightly larger than that of most commercial, aluminum-filled photoflash bulbs.(21) From an experimental point of view, it is desirable to make the burner tube as small as possible in order to minimize excessive requirements for materials.

The performance of aluminum jet flames also should be tested in a 5-centimeter tube, both to investigate the effect of diameter on optical thickness and to investigate the potential for increasing flame height through an increase in diameter alone.

For experiments with zirconium, the 5-centimeter burner tube probably should be used. The reason for this is expectation that the relatively large particles will require a relatively thick flame for satisfactory optical thickness. (This is in apparent contradiction to zirconium-filled photoflash bulbs which are small, e.g. one centimeter in diameter. However, in these bulbs, zirconium is burned in oxygen which initially is at a pressure of between 5 and 10 atm, depending on the type of bulb. The higher pressure permits a high loading of zirconium per unit volume in the bulb, and therefore provides the needed optical thickness(23)).

As noted in Section 5.2, the velocity of the jet flame is an important parameter in determining the height of the flame. The height over which the flame will emit radiation increases with velocity. However, there are factors which limit the velocity to a particular range. At the low end, the limit is the flashback velocity which, as noted in Section 4.2, will be in the neighborhood of 600 cm/sec for aluminum-oxygen flames. At the high end, the limit is the blow-off velocity, which is governed primarily by the strength of the ignitor flame and the use of flame holding devices. Velocities in the range of 1000 to 6000 cm/sec are recommended for exploration in the investigation. The lower limit is just above the expected flashback limit.

The upper limit for velocity is governed by experimental considerations and limitations for obtaining the needed flow-rate capacity for the oxygen gas that will be required for both the flame and the protective gas envelope. It is anticipated that velocity will not be effective in enhancing flame length unless entrainment of cold ambient air can be minimized. The flow of envelope gas required is proportional to the product of the width of the plenum, w_e, and the velocity of the envelope gas, v_e, which is approximately equal to the velocity of the flame. The thickness of the protective envelope required for a given flame height is directly proportional to the height. The flame velocity required to reach the given height also is proportional to the height (see Equation 19). Therefore the flow of envelope gas, m_e, required for protection is proportional to the square of the height:

$$m_e \propto w_e v_e \propto h^2. \qquad (20)$$

The experimental flame height may be estimated with Equation (19) in Section 5.2.5. For aluminum, with the 2.5 cm diameter burner, Q (flame surface radiative flux) may be approximately 240 cal/cm^2-sec, ΔH = 4960 cal/gm, K_a = 0.59 cm^{-1} (1.7 cm optical mean free path), and ρ= 5 x 10^{-4} g/cc in the jet flame, the expected height of the flame is:

$$h = \frac{(5\times10^{-4})\ (4960)v}{(0.59)\ (240)} = 0.0175v. \qquad (21)$$

For the selected velocity range, 1000 to 6000 cm/sec, h is expected to range from 18 to 105 cm. This estimate of course assumes the prevention of air entrainment by the protective gas envelope. A similar estimate for a zirconium powder flame has not been made because of a too high uncertainty of the appropriate value of K_a.

The effectiveness of the protective gas envelope will depend on the four variables listed above. It is recommended that the effect of velocity over the range of 50 to 150 percent of the velocity of the jet flame be investigated. In order to minimize shear and mixing with the jet flame, it is expected that most of the experiments will be performed with the velocity of the envelope gas adjusted to be nearly equal to the velocity of the jet flame.

The thickness of the envelope should be varied from approximately 50 to 200 percent of the burner diameter. In general, it is expected that the width would be as large as necessary to ensure a maximum height of the jet flame.

The effect of the envelope's temperature should be investigated, over the range from ambient to approximately 4500^{o}K. The effect of temperature is expected to be significant for aluminum-oxygen flames, but perhaps less so for zirconium-oxygen flames. The highest temperature would be produced by burning cyanogen in oxygen. Intermediate temperatures, 2000 to 3200^{o}K can be produced by burning substoichiometric and stoichiometric amounts of propane in an oxygen gas envelope.

The primary gas to be used in the envelope would be oxygen, for the various reasons as noted in the foregoing discussion. Because of its ready availability and the practicality of its use in the field, air also will be investigated as the envelope gas. When high temperatures must be generated in the envelope, part or all of the oxygen must be burned with a suitable fuel, and, as a consequence, the envelope gas will contain combustion products such as H_2O, N_2, CO and CO_2. As noted in Sections 3.3 and 3.4. these may affect the combustion of the metal powders. However, the presence of these gases is difficult to avoid if the envelope gas is to be heated by practical means. The effect of these contaminants should be examined along with the other additives.

The last parameter listed at the beginning of this section constitutes the additives to the metal powder to enhance the emissivity of the jet flame's particulate matter. For the reasons noted in Section 5.2.2, the effect of small percentages of iron and nickel would be investigated. Also, the presence of small amounts of N_2, CO and CO_2 contaminants may affect both the combustion of the powders and the emissivity of the oxides. These contaminants would be added to the jet flame via their use to pneumatically transport the metal powders to the burner.

6.2.3 Instrumentation

Since the objective of the investigation is to find means to enhance the radiative properties of oxygen-metal powder flames, the minimum recommended primary instrumentation consists of calorimeters to measure radiative flux and spectrometers to measure color temperature. As a minimum three calorimeters should be used to measure the flux versus time at three different heights along the jet flame:

- Near the base of the flame
- At the top of the radiative portion of the flame
- At an intermediate height.

The view of the calorimeters and the monochromators should be restricted to a narrow portion of the flame with collimating tubes. The data from the calorimeters can be converted to radiative flux from the flame surface using the known geometry and reflectivity of the tube materials.

The data from the spectrometers would be analyzed to derive an effective color temperature of the flame. The analysis could utilize a least squares fit of the intensity of the radiation at selected wavelengths relative to a reference wavelength. The latter should be selected near the peak intensity but not at a wavelength which obviously has a strong line radiation component.

The flux and color temperature data would serve as the primary gauge of how the metal powder-oxygen flames are affected by variations of the several parameters. For this purpose, flames both with and without the enhancement techniques should be studied for comparison.

In addition to this primary data, supporting data also should be gathered including:

- Effective flame emissivity derived from the flux and color temperature measurements
- Particle size and composition of the combustion products
- General shape and height of the flame recorded photographically
- Flow rates of oxygen gas, metal powder and envelope gas.

The combustion products can be sampled by passing a metal or graphite plate through the flame at selected heights. Molten particles of oxide and burning metal will impinge and stick to the plate. A qualitative appraisal of the particle size distribution of the combustion products may then be made through microscopic examination of the collected sample. The extent of combustion for selected samples can be determined via chemical analysis for the free metal.

6.3 Implementation of Techniques to Achieve the HTRS Performance Goals

The investigation outlined in the preceding subsection has a good potential of being highly successful in demonstrating a high color temperature and high level of radiative flux. The fact that a high performance can be obtained with metal powder-oxygen flames has already been demonstrated on a small scale in photoflash bulbs. Another anticipated result of the investigation is an understanding of how radiative performance is effected by the several controllable variables. At this point, implementation of the techniques to enhance the performance then can proceed. There are two options for this, one aiming at near-term applications and the other at longer-term applications.

Near-term applications would involve minor modifications of existing TRS hardware in order to obtain significant benefits in the current DNA testing programs. For example, an air curtain is being developed for a special TRS unit which is to be installed in a large blast and thermal simulation shock tube facility. The air curtain is intended to prevent the accumulation of TRS combustion products in the shock tube by surrounding the TRS flame with a high-velocity air stream and ejecting it out through a narrow opening in the top of the tube. Information developed in the above-mentioned investigation could be used to properly adjust the velocity and temperature of the curtain to achieve increased radiative performance from the TRS unit. The latter could be accomplished by burning a fuel gas, such as propane, in the air as it emerges from the plenums. In the same vein, an experimenter may require a higher level thermal radiation, than now is available, in a future DNA HE shot. Based on the results of the investigation, it might be possible to achieve the higher level of radiation simply by adding a field version of the air curtain.

Applications in the longer term are those that would require more significant modifications of TRS hardware. Some examples of these are:

- Development of an improved flow system and mixer for fuel and oxygen which will be optimum for implementation of techniques to achieve a high radiative output

- Development of a full-scale burner for zirconium powder fuel

- Development of an improved radiation system for studying the effects of thermal radiation on various surfaces and the creation of thermal layers in air

- Development of techniques to create focusable flames with a very intense radiative output.

The last could be an intriguing development since a focusable TRS flame could be used to drive certain types of high-energy lasers, as well as a useful tool for thermal simulation. In this instance what is desired is a long, small-diameter flame. As already mentioned in Section 6.1, the use of a gaseous envelope, which has the same velocity as the flame, has the potential for significantly reducing the angle of spread of the flame. By also applying an ejector system above the flame with a properly designed inlet, it may be possible to reduce the spreading of the jet flame still further. Hence a flame that can be focused to some degree may be created by these relatively simple technqiues.

A somewhat more complicated technique also might be used as an alternative. The central idea in this case is to swirl both the flame and the surrounding envelop gas about the longitudinal axis of the flame in order to create a strong centrifugal force field. In at least one experiment with a gas diffusion flame, this technique generated a very long vertical cylindrical flame with a temperature gradient at the flame boundary exceeding 1,000°F/cm.(29) The stabilization of such steep gradients is partly dependent on the flame gases having a low density compared with the surrounding air or gas. In the case of metal powder-oxygen flames, this technique may not be successful in all instances because the effective density of the burned mixture is increased by the condensed-phase combustion products.

Other techniques that might be used to help to form a focusable flame include burning larger particles (non-swirled flow) which are less susceptible to having their movement diverted by the turbulent motion of the surrounding gas. In addition, by formulating the jet flame to be fuel

rich and using oxygen as an envelope gas, the net flow of gas will be radially inward during burning. This is expected to keep spreading of the jet flame to a minimum. These techniques would be especially applicable to zirconium-oxygen flames in which large particles are desirable in order to obtain long burning times and long flames. In this case swirling the flame reactants might be detrimental.

LIST OF REFERENCES

1. Grosse, A.V. "The Production of High Temperatures by Chemical Means and Particularly by the Combustion of Metals", SRI High Temperature Symposium, Berkeley, California (1956).

2. Stull, D.R. and H. Prophet, JANNAF Thermochemical Tables, Second Edition, NSRDS-NBS37, U.S. Government Printing Office (1971); and Supplements appearing in J. Physical and Chemical Reference Data (1974), (1975), (1978) and (1982).

3. Gordon, S. and B.J. McBride, Computer Program of Calculation of Complex Chemical Equilibrium Compositions, Rocket Performance, Incident and Reflected Shocks, and Chapman Jouguet Detonations, National Aeronautics and Space Administration Report NASA SP-273 (1976).

4. Brewer, L., "The Thermodynamic Properties of the Oxides and their Vaporization Processes", Chem. Rev. 52, 1 (1953); National Bureau of Standards Technical Notes 270-3, 270-4, 270-5, 270-6, 270-7 and 270-8.

5. Brzustowski, T.A. and I. Glassman in Progress in Astronautics and Aeronautics, Volume 15, Heterogeneous Combustion, H.G. Wolfhard, I. Glassman, L. Green, Jr., Eds., Academic Press (1964), p.117, and Mellor, A.M., and I. Glassman, Ibid, p. 159.

6. Prentice, J.L., Aluminum Droplet Combustion: Rates and Mechanisms in Wet and Dry Oxydizers, Naval Weapons Center Report NWC TP 5569, April 1974.

LIST OF REFERENCES (Continued)

7. Macek, A. "Fundamentals of Combustion of Single Aluminum and Beryllium Particles" in Eleventh Symposium (International) on Combustion, The Combustion Institute (1967).

8. Wilson, R.P. and F.A. Williams, "Experimental Study of the Combustion of Single Aluminum Particles in O_2/Ar", Thirteenth Symposium (International) on Combustion, The Combustion Institute (1971).

9. Brzustowski, T.A. and I. Glassman, in Progress in Astronautics and Aeronautics, Volume 15, Heterogenerous Combustion, H.G. Wolfhard, I. Glassman, L. Green, Jr., Eds., Academic Press (1964), p. 75.

10. Prentice, J.L. (Ed.), Metal Particle Combustion Progress Report, 1 July 1965 - 1 July 1967, Naval Weapons Center Report NWC TP 4435, August 1968.

11. Charagundla, S.R., and G.L. Pellett, "Transient Processes in Metal Droplet Combustion", 19th JANNAF Combustion Meeting, October 1982.

12. Nelson, L.S., H.S. Levine, D.E. Rosner, and S.C. Karzius, "Combustion of Zirconium Droplets", High Temp. Science, 2, 343-75 (1970).

13. Nelson, L.S., "Combustion of Metal Droplets Ignited by Flash Heating", Eleventh Symposium (International) or Combustion, The Combustion Institute (1967).

14. Nelson, L.S., D.E. Rosner, S.C. Kurzius, and H.S. Levine, "Combustion of Zirconium Droplets in Oxygen/Rare Gas Mixtures - Kinetics and Mechanism", Twelfth Symposium (International) on Combustion, The Combustion Institute (1969).

LIST OF REFERENCES (Continued)

15. Myer, R.J. and L.S. Nelson, "The Role of Nitrogen in the Formation of Microbubles During the Explosive Combustion of Zirconium Droplets in N_2/O_2 Mixtures", High Temp. Science, 2, 35-57 (1970).

16. Carslaw, H.S. and J.C. Jaeger, Conduction of Heat in Solids, Second Ed., Oxford University Press (1959), p. 242.

17. Dishon, J., Science Applications, Inc., In-House Data (1984).

18. Hinze, J.O., Turbulence, McGraw-Hill Book Company (1959), pp. 404-431.

19. Brown, G.L., and A. Roshko, "On Density Effects and Large Structures in Turbulent Mixing Layers", J. Fluid Mech, 64, 775-816 (1974).

20. Grosse, A.V., and Conway, J.B., "Combustion of Metals in Oxygen", Ind. Eng. Chem, 50, (1958) pp. 663-672.

21. Rautenberg, T.H., and P.D. Johnson, "Light Production in the Aluminum-Oxygen Reaction", J. Optical Soc. Amr., 50, 602-606 (1960).

22. Bracco, D.J., and S. Weisberger, "Determination of the Spectral Emission of Commercial Flashbulbs By Emission Spectrographic Techniques", Applied Optics, 5, 1275-1279 (1966).

23. Nijland, L.M., and J. Schroder, "The Generation of Light by Chemical Reactions in Flash Lamps", Twelfth Symposium (International) on Combustion, The Combustion Institute (1969).

24. Hottel, H.C. and A.F. Sarofin, Radiative Transfer, McGraw-Hill Book Company (1967).

LIST OF REFERENCES (Concluded)

25. Touloukian, Y.S. and D.P. DeWitt, Thermal Radiative Properties, Nonmetalic Solids, Thermophysical Properties of Matter, Volume 8, IFI, Pelenum (1972).

26. Carlson, D.J., "Emittance of Condensed Oxides in Solid Propellant Combustion Products", Tenth Symposium (International) on Combustion, The Combustion Institute (1965).

27. Nelson, L.S., N.L. Richardson, K. Keil, and S.R. Skaggs, "Effects of Oxygen and Argon Atmospheres on Pendant Drops of Aluminum Oxide Melted with Carbon Dioxide Laser Radiation", High Temp. Science, 5, 138-154 (1973).

28. Rieger, T.J., "On the Emission of Alumina - Aluminum Composite Particles", J. Spacecraft and Rockets, 16, 438-9 (1979).

29. Emmons, H.W. and S. Ying, "The Fire Whirl", Eleventh Symposium (International) on Combustion, The Combustion Institute (1967).

DISTRIBUTION LIST

DEPARTMENT OF DEFENSE

Asst to the Secy of Defense, Atomic Energy
ATTN: Executive Assistant

Commander in Chief, Atlantic
ATTN: J7

Defense Advanced Rsch Proj Agency
ATTN: Dir, Strat Tech Off
ATTN: H. Winsor
ATTN: NMRO
ATTN: PMO

Defense Communications Agency
ATTN: Code 510

Defense Electronic Supply Center
ATTN: DEFC-ESA

Defense Intelligence Agency
ATTN: DB-4C, Rsch, Phys Vuln Br
ATTN: RTS-2A, Tech Lib
ATTN: RTS-2B

Defense Nuclear Agency
ATTN: NASF
ATTN: NAWE
ATTN: RAAE
ATTN: SPAS
ATTN: SPSS
ATTN: SPTD
ATTN: STNA
ATTN: STRA
ATTN: STSP
4 cy ATTN: STTI-CA

Defense Technical Information Center
12 cy ATTN: DD

Deputy Under Secy of Defense, Cmd Contl, Comm & Intell
ATTN: Principal DASD, C3I, H. Van Trees

Field Command, DNA, Det 2
Lawrence Livermore National Lab
ATTN: FC-1

Field Command, DNA
ATTN: FCPR
ATTN: FCT
ATTN: FCTEI
ATTN: FCTT
ATTN: FCTXE

Field Command Test Directorate
ATTN: FCTC

Interservice Nuclear Weapons School
ATTN: TTV

Joint Chiefs of Staff
ATTN: GD50, J-5 Force Plng & Prog Div
ATTN: J-5 Nuclear Div/Strat Div
ATTN: SAGA

Under Secy of Defense for Rsch & Engrg
ATTN: Engr Tech, J. Persh
ATTN: Strat & Space Sys (OS)

DEPARTMENT OF DEFENSE (Continued)

Joint Strat Tgt Planning Staff
ATTN: JLK, DNA Rep
ATTN: JLKC
ATTN: JLKS
ATTN: JPST

DEPARTMENT OF THE ARMY

US Army Electronics R & D Command
ATTN: DELAS-EO

BMD Advanced Technology Center
ATTN: 1CRDABH-X

BMD Program Office
ATTN: DACS-BMT
ATTN: DACS-BMZ

BMD Systems Command
ATTN: BMDSC-HW

Harry Diamond Laboratories
ATTN: DELHD-DTSO
ATTN: DELHD-NW-P
ATTN: DLEHD-TA-L, Tech Lib

US Army Armament Material Readiness Command
ATTN: MA Library

US Army Armament Rsch Dev & Cmd
ATTN: DRDAR-LCW

US Army Ballistic Research Lab
ATTN: DRDAR-BLA-S, Tech Lib
ATTN: DRDAR-BLT

US Army Chemical School
ATTN: ATZN-CM-TPR

US Army Cold Region Res Engr Lab
ATTN: Technical Director

US Army Comm-Elec Engrg Instal Agency
ATTN: Tech Library

US Army Communications Command
ATTN: CC-OPS-PD
ATTN: Technical Reference Division

US Army Communications R&D Command
ATTN: DRDCO-COM

US Army Corps of Engineers
ATTN: DAEN-RDL

US Army Electronics R&D Command
ATTN: DELET-ER

US Army Engineer Ctr & Ft Belvoir
ATTN: ATZA-DTE-ADM
ATTN: DT-LRC

US Army Engineer Div Huntsville
ATTN: HNDED-SR

DEPARTMENT OF THE ARMY (Continued)

US Army Engineer Div Ohio River
ATTN: ORDAS-L, Tech Lib

US Army Engr Waterways Exper Station
ATTN: Library
ATTN: WESSE
ATTN: WESSS

US Army Foreign Science & Tech Ctr
ATTN: DRXST-SD

US Army Material Command
ATTN: DRCDE-D
ATTN: DRXAM-TL, Tech Lib

US Army Mobility Equip R&D Command
ATTN: DRDME-WC, Tech Lib

US Army Nuclear & Chemical Agency
ATTN: Library
ATTN: MONA-OPS
ATTN: MONA-WE

US Army Tank Automotive R&D Command
ATTN: DRDTA-UL, Tech Lib

US Army TRADOC Sys Analysis Actvy
ATTN: ATAA-TDC

US Army Training and Doctrine Comd
ATTN: ATCD-T
ATTN: ATORI-OP

US Army White Sands Missile Range
ATTN: STEWS-FE-R
ATTN: STEWS-TE-AN
ATTN: STEWS-TE-N

USA Missile Command
ATTN: DRSMI-MSM
ATTN: DRSMI-RH

DEPARTMENT OF THE NAVY

David Taylor Naval Ship R & D Center
ATTN: Tech Info Ctr Code 522.1

Naval Air Systems Command
ATTN: AIR-360G JP-2

Naval Electronic Systems Command
ATTN: PME 117-21

Naval Facilities Engineering Command
ATTN: Code 04B

Naval Material Command
ATTN: MAT 08T-22

Naval Research Laboratory
ATTN: Code 2627, Tech Lib
ATTN: Code 4700
ATTN: Code 4720
ATTN: Code 5584
ATTN: Code 5584
ATTN: Code 6770
ATTN: Code 7780

Naval Surface Weapons Center
ATTN: Code E21
ATTN: Code X211, Tech Lib

DEPARTMENT OF THE NAVY Continued)

Naval Surface Weapons Center
ATTN: Tech Library & Info Svcs Br

Naval Weapons Center
ATTN: Code 266
ATTN: Code 3263
ATTN: Code 343, FKA6A2, Tech Svcs

Naval Weapons Evaluation Facility
ATTN: Code 10, Tech Lib

Ofc of the Deputy Chief of Naval Ops
ATTN: NOP 654, Strat Eval & Anal Br

Office of Naval Research
ATTN: Code 474

Strategic Systems Project Office
ATTN: NSP-43, Tech Lib

DEPARTMENT OF THE AIR FORCE

Aeronautical Systems Division
ATTN: ASD/ENSSA

Air Force
ATTN: INT

Air Force Armament Laboratory
ATTN: DLYV

Air Force Institute of Technology
ATTN: Library

Air Force Weapons Laboratory
ATTN: DEX
ATTN: NTE
ATTN: NTED
ATTN: NTES-C
ATTN: NTES-G
ATTN: SUL

Asst Chief of Staff, Intelligence
ATTN: IN

Ballistic Missile Office/DAA
ATTN: ENSN
ATTN: SYM

Deputy Chief of Staff, Rsch, Dev & Acq
ATTN: AFRD

Foreign Technology Division
ATTN: NISS Library
ATTN: SDBF

Sacramento Air Logistics Center
ATTN: MMEAE

Space Division
ATTN: YGD, L. Doan

Strategic Air Command
ATTN: DOCSD
ATTN: DOWE
ATTN: INAO
ATTN: NRI/STINFO
ATTN: XPFS

DEPARTMENT OF ENERGY

Department of Energy
Albuquerque Operations Office
ATTN: Technical Library

Department of Energy
Nevada Operations Office
ATTN: Doc Con for Tech Library

OTHER GOVERNMENT AGENCIES

Central Intelligence Agency
ATTN: OSWR/NED

Department of Commerce
ATTN: Sec Ofc for R. Levine

Federal Emergency Management Agency
ATTN: Ofc of Rsch/NP, D. Bensen

OTHER

Brookhaven National Laboratory
ATTN: P. Levy

DEPARTMENT OF ENERGY CONTRACTORS

University of California
Lawrence Livermore National Lab
ATTN: L-14
ATTN: L-47
ATTN: Technical Info Dept Library

Los Alamos National Laboratory
ATTN: Librarian
ATTN: MS P364 Reports Library
ATTN: MS/410
ATTN: MS218

Sandia National Laboratories
ATTN: Library & Sec Class Div

Sandia National Laboratories
ATTN: Div 1531, P. Adams
ATTN: Div 6222
ATTN: Div 7111
ATTN: Org J, E. Bear
ATTN: Org 2330
ATTN: Org 7110
ATTN: Org 7112
ATTN: Tech Lib 3141

DEPARTMENT OF DEFENSE CONTRACTORS

Aerospace Corp
ATTN: Library Acquisition M1/199

AVCO Systems Division
ATTN: Library A830

BDM Corp
ATTN: Corporate Lib

Boeing Co
ATTN: Aerospace Library
ATTN: M/S 85/20

California Research & Technology, Inc
ATTN: F. Sauer

Charles Stark Draper Lab, Inc
ATTN: Tech Library

University of Denver
ATTN: Sec Officer for J. Wisotski

DEPARTMENT OF DEFENSE CONTRACTORS (Continued)

EG&G Wash Analytical Svcs Ctr, Inc
ATTN: Library

Georgia Institute of Technology
ATTN: EES/EMSL/Solar Site, C. Brown

IIT Research Institute
ATTN: Documents Library

Kaman Sciences Corp
ATTN: Library

Kaman Tempo
ATTN: DASIAC

Kaman Tempo
ATTN: DASIAC

Lockheed Missiles & Space Co, Inc
ATTN: Tech Info Ctr D/Coll, D/90-11, B/106

Merritt CASES, Inc
ATTN: Library

Mission Research Corp
ATTN: Tech Library

National Academy of Sciences
ATTN: Natl Materials Advisory Board

University of New Mexico
ATTN: Technical Library

Pacific-Sierra Research Corp
ATTN: H. Brode, Chairman SAGE

Pacifica Technology
ATTN: Tech Library

Physics International Co
ATTN: Tech Library

R & D Associates
ATTN: P. Haas
ATTN: Technical Info Center

Rockwell International Corp
ATTN: Library

S-CUBED
ATTN: Library

Science & Engrg Associates, Inc
ATTN: B. Chambers III

Science Applications Intl Corp
ATTN: G. Binninger

Science Applications Intl Corp
ATTN: K. Sites

Science Applications Intl Corp
ATTN: Technical Library
ATTN: W. Plows

Science Applications Intl Corp
ATTN: Technical Library

Tetra Tech, Inc
ATTN: Library

DEPARTMENT OF DEFENSE CONTRACTORS (Continued)

Science Applications Intl Corp
ATTN: J. Cockayne
ATTN: M. Knasel
ATTN: R. Sievers
ATTN: W. Chadsey
ATTN: W. Koechner
ATTN: W. Layson
2 cy ATTN: J. Simmons
2 cy ATTN: M. McDonnell

DEPARTMENT OF DEFENSE CONTRACTORS (Continued)

Teledyne Brown Engineering
ATTN: D. Ormond
ATTN: F. Leopard
ATTN: J. Ravenscraft
ATTN: MS-12 Technical Library

END

FILMED

1-86

DTIC